COMMUNICATION SCIENCES INSTITUTE

"BLIND MULTIUSER RECEIVERS FOR DS-CDMA IN FREQUENCY-SELECTIVE FADING CHANNELS"

by

Sau-Hsuan Wu

CSI-07-03-01

USC Viterbi School of Engineering
Ming Hsieh Department of
Electrical Engineering
Los Angeles, CA 90089-2565

BLIND MULTIUSER RECEIVERS FOR DS-CDMA IN FREQUENCY-SELECTIVE FADING CHANNELS

by

Sau-Hsuan Wu

A Dissertation Presented to the
FACULTY OF THE GRADUATE SCHOOL
UNIVERSITY OF SOUTHERN CALIFORNIA
In Partial Fulfillment of the
Requirements for the Degree
DOCTOR OF PHILOSOPHY
(Electrical Engineering)

December 2003

Dedication

Dedicated with love to my family.

Acknowledgements

Back to the early morning on Aug. 3rd three years ago in 2000, I had just packed my luggage in to my 93's Camry and started warming up the engine in preparation for a long trip from east to west coast. I took a deep breath of the fresh air of Texas morning and looked around the small town where I had stayed for the first year of my graduate study. I wondered if I was moving on the right track towards an unpredictable future.

I had been vacillating for the whole summer between continuing at the Texas A&M University, a place that I had just gotten familiar with, or transferring to the University of Southern California (USC), a whole new restart of my graduate study. Finally, I made a phone call to Prof. J.H. Chou to seek for a second opinion. Prof. Chou was the graduate advisor of my master thesis. Whenever I am perplexed or irresolute, I can always find some help from him, even thought he usually does not make definite suggestions to me. I felt much more confident after talking with him and made another phone call to Prof. C.-C. Jay Kuo at USC to see if he still wanted

to take me as his student. He gave me a simple yet solid answer: "call me when you arrive in Los Angeles".

I could not have thanked Prof. Kuo more. He gave me a chance to pursue my Ph.D degree at USC and took me into the breadth of signal processing area. He maintains a large research group that provides a fertile bed where thoughts and ideas can sprout and grow. He takes care of more than thirty Ph.D students, and still can memorize each student's characteristic and explore their potentials. I could barely learn a little piece of his abundant knowledge, endless energy for doing research and his solid attitude. He finds every chance to help his students. Even at the last stage of my doctoral study, he still helps me on my career development and job hunting.

My research at USC started with a class offered by Prof. Urbashi Mitra. Since then she have led me to explore many interesting fields in wireless communications. I could not have gone this far without her guidance. She showed me how to stimulate creativity, draw concepts and realize plans. I am deeply influenced by her enthusiasm on academics, her passionate yet rigorous attitudes on pursuing solutions as well as her sincere support to students. Through countless discussions and cross-validations, raw ideas gradually evolved into concrete results. This really makes my graduate study a wonderful adventure.

I would like to take this opportunity to express my gratitude to all my colleagues in Prof. Kuo's research group. Working with them broadens my scope of research and makes my staying at USC a wonderful journey. Special thanks are extended to

members in the communication subgroup. The fruitful discussions with them clarify many important aspects of my research.

Finally, there is nothing enough for me to show my appreciation to my family in Taiwan. I especially thank my parents for everything they have done for me. It is their spirit and their continuing support that makes me achieve one of my most important milestones. Thank you all very much.

Contents

List of Tables

List of Figures

Abstract

Two types of blind multiuser detection schemes are proposed in this research for direct-sequence (DS) code-division multiple-access (CDMA) systems in frequency-selective fading channels. One features low-complexity reduced-rank linear receivers, the other aims at pursuing high-performance low bit error probabilities based on the expectation maximization (EM) algorithm.

In the first part, a class of multistage implementations of the minimum mean square error, minimum output energy, maximum likelihood and best linear unbiased estimator filter banks is developed based on the concept of the multistage Wiener filtering. These filter banks are shown to share a common multistage structure for interference suppression. Based on this finding, a framework is proposed for blind multiuser detection of DS-CDMA in frequency-selective fading channels.

In the second part, the performance of the detection schemes constructed under this framework is studied for multipath Rayleigh fading channels. A generic bit error rate (BER) formula is provided for detectors of any possible number of stages. The output signal-to-interference plus noise ratios (SINRs) are shown to be monotonically

increasing with the number of stages, and are upper bounded by the number of resolvable paths in the desired user's channel. The condition for asymptotically achieving the upper bound is provided; this condition serves as a test of the existence of a BER floor for coherent detection. The channel mismatch due to differential detection is also analyzed to determine the BER floor for non-coherent multiuser detection. Based on the analysis, a simple, yet effective rule for choosing the number of stages is provided.

In the third part, we aim at solving a challenging problem in blind multiuser detection, *i.e.* joint channel estimation, symbol detection and multiple-access interference suppression in multipath fading channels. A low-complexity Kalman-like filter is proposed for blind channel tracking based on the recursive EM and the non-coherent BCJR algorithms. By exploiting the property of discrete random phase ambiguity of the channel estimate using the EM algorithm, the proposed scheme can track channel phase even in deep fading.

Chapter 1

Introduction

1.1 Significance of the Research

After the pioneering research on optimum multiuser detection (MUD) for direct-sequence code-division multiple-access (DS-CDMA) systems in the 80's [25], a significant amount of efforts has been made to bring this theoretical framework into practice. Since the complexity of optimum detection schemes grows exponentially with the number of users in the system, linear detection methods, *e.g.* the decorrelating detector [16] and the minimum mean square error (MMSE) detector [17], have been widely considered as effective receivers to alleviate the implementation complexity as well as to bridge the gap between practical considerations and theoretical soundness. Moreover, in view of the time-varying characteristics of system parameters and/or channel statistics, adaptive linear detection schemes have been examined to combat multiple access interference (MAI) under a generalized MMSE criterion [20, 11]. To improve the system performance in time-varying fast fading

environments, it is important to track channel coefficients on-line, either by regularly inserting pilot symbols or using blind detection schemes [24]. The performance of the estimation scheme under either scenario is subject to the size of the processing block, the fading speed and the overhead of training symbols. All of them are related to the time-varying characteristics of a fading channel to some extent. In this thesis, a sequence of results are derived for multiuser receiver designs for DS-CDMA systems under this hostile wireless communication environment.

1.2 Reduced-rank Filtering via Multistage Filter Banks

Reduced-rank schemes have been proposed with an objective to improve the tracking performance under the time-varying fast fading channel condition. Under the reduced-rank signal processing approach, the number of samples required for approximating accurate channel statistics can be drastically reduced. Furthermore, the strength of noise or MAI can be mitigated by rejecting dimensions in which interference overwhelms, thus making the estimates capture the true channel statistics of the desired signal better. In the first part of this thesis, we focus on the reduced-rank filtering approach.

1.2.1 Related Work

A few blind subspace detection schemes based on the reduced-rank idea have been published *e.g.* [26, 22]. Partly due to the complexity of on-line singular value decomposition (SVD) and partly due to the difficulty in finding an accurate estimate of the signal subspace, the eigen-decomposition approach does not offer much performance improvement. Moreover, on-line subspace tracking is in general a challenging task, which makes the overall system performance uncertain and difficult to analyze, especially in frequency-selective fading channels. Thus, an efficient blind adaptive algorithm based on reduced-rank interference suppression for frequency-selective fading channels is still under intensive research study.

As a result of the research on multistage Wiener filtering (MSWF) [8] and its application to adaptive multiuser detection [10], there arises a new subspace MMSE approach featuring no SVD and successive interference suppression. Based on the MSWF concept, a common multistage structure for a class of MMSE-based filter banks, including the MMSE, the minimum output energy (MOE), the best linear unbiased estimator (BLUE) and the maximum likelihood detector (ML), has been developed in [29, 28].

To exploit the full diversity offered by a frequency-selective fading channel without resorting to complicated joint channel estimation and symbol detection schemes, Miller *et al*, [21], proposed a differential MMSE receiver to perform multiuser detection (MUD) based on noncoherent equal gain combining (EGC). In this approach,

the product of the channel coefficients and the transmitted symbol is estimated by an MMSE/MOE receiver. By multiplying two consecutive outputs of the same filter, the diversity combining of a receiver, often referred to as the maximum ratio combining (MRC), is implicitly performed, if differential encoding is employed. Being motivated by this receiver structure and the reduced-rank MSWF receiver in [10], which was originally proposed for additive white Gaussian (AWGN) channels, we investigate the design and analysis of reduced-rank multistage receivers for multipath fading channels. On one hand, the most appealing features for the reduced-rank MSWF are its simple procedure for implementation and very fast convergency of the output signal-to-interference plus noise ratio (SINR) with respect to the number of applying stages. On the other hand, the mathematical formulation for multistage interference suppression in a multipath fading channel (or, more precisely, the multistage reduced-rank estimation in a general linear Gaussian model) was nevertheless lacking during the early stage of our study.

1.2.2 Outline of the Proposed Solution

In an effort to explore a more general multistage filter, we derive a unified structure for the reduced-rank implementation of the MMSE, MOE, BLUE and ML filter banks (FBs). These filter banks are shown to share a common multistage structure for interference suppression, modulo distinctive scaling matrices at each filter's output [29, 28]. Base on this finding, a framework is proposed, as shown in Fig. 1.1, for

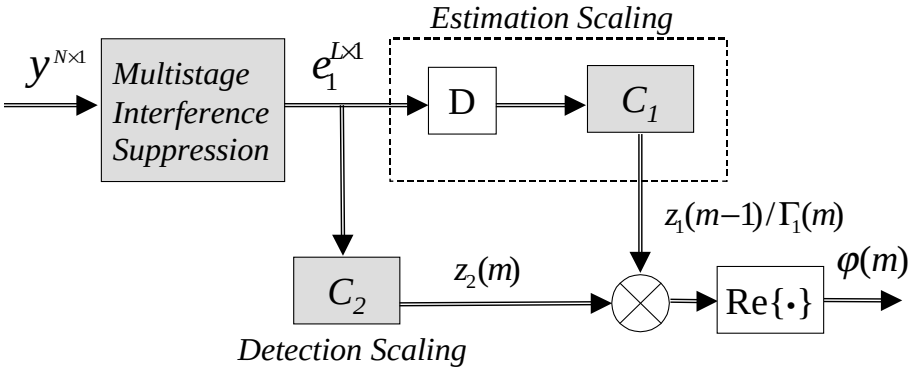

Figure 1.1: Illustration of the common framework for MRC and EGC detectors in multi-path fading channels, where estimation scaling is replaced by true channel coefficient Γ_1 for MRC, and C_1 and C_2 are scaling matrices of MMSE/MOE/BLUE/ML-FB.

symbol detection and channel estimation of blind multiuser detection in multipath fading channels. With this common platform, a number of adaptive reduced-rank detection schemes can be implemented and evaluated using a unified procedure without resorting to SVD. Moreover, by making use of the recursive structure of the multistage implementation, a thorough performance analysis in terms of bit error rates (BER) and output SINRs can be conducted [32, 31]. This helps provide insights into the relationship and the tradeoff between reduced-rank filtering algorithms and their detection performance. Furthermore, we show that linear receivers using differential EGC are subject to performance limitations due to the non-exact MRC with channel coefficients belonging to the previous symbol interval. The degree of degradation depends on the fading speed or, in order words, the autocorrelation value of a fading process.

1.3 Joint Channel Estimation and Symbol Detection via EM Algorithm

The performance of a linear receiver is highly constrained by its available dimensions for suppressing interference. To conquer these two difficulties, we consider joint channel estimation and symbol detection based on the expectation maximization (EM) algorithm [6] in the second part of the thesis.

1.3.1 Related Work

The EM algorithm has found many applications in estimation and detection for wireless channels since the work of Kaleh and Vallet [13]. In [13], the EM algorithm was used for joint parameter estimation and maximum *a posteriori* (MAP) symbol detection for static channels by treating transmitted symbols as missing data. Georghiades and Han [7] later applied EM for blind maximum likelihood (ML) sequence detection (MLSD) over flat fading channels by viewing unknown channel coefficients as missing data. This approach has been extended to blind MLSD over frequency-selective fading channels in many aspects, *e.g.* the per-survivor processing (PSP) for noncoherent sequence detection in [18]. A common drawback of this approach is the complexity of PSP. For every survived path, a Kalman filter is employed for channel estimation, using data symbols along the survived path. On the other hand, the approach in [13] was extended for joint channel estimation and MUD

for multipath CDMA channels in [2, 30]. In [2], a non-casual recursive approach was proposed for channel tracking with a complexity exponentially growing with the number of users.

Zamiri-Jafarian and Pasupathy [33] developed the EM algorithm into a recursive fashion of optimization extended from the second-order sequentially stochastic optimization scheme [15]. It was shown in [33] that the EM algorithm is essentially a common framework under which a number of receivers can emerge automatically, ranging from the recursive least square (RLS) estimator using the Frequentist approach to the Kalman filter derived with the Bayesian approach.

1.3.2 Outline of the Proposed Solution

For the practical implementation, we propose a sliding-window batch method for channel tracking with complexity proportional to the number of users. Based on the recursive EM algorithm developed in [33], we develop a stochastic Kalman-like estimator for blind channel estimation. It is shown that both the stochastic ML estimator [13] and the RLS [14] are special cases of our results. Through the multistage filtering structure, we also show that the difference between the BLUE/ML estimators of the frequentist approach and the MMSE/MOE filters obtained with the Bayesian method is only at their distinct scaling matrices to the same output of the common interference suppressor as shown in Fig. 1.1. It is further derived that a Kalman-like algorithm or the RLS estimator can be given under the same framework

of EM, and their difference lies in how missing data are assigned for different design criteria.

1.4 Contributions of the Research

Contributions of this research are summarized below.

- In this research, a common structure for the multistage MMSE/MOE/BLUE/ML filter banks is proposed. These filter banks have distinctive properties, *e.g.* some with a lower variance and some bearing unbiasedness. The tradeoff in performance among these filter banks can be compared and evaluated using a unified approach offered by the common structure.

- Although being with quite different characteristics, the MMSE/MOE/BLUE/ML filter banks can only be differentiated by their unique output scaling matrices under the proposed multistage implementation. Based on this important fact, a platform is constructed for both the reduced-rank coherent MRC and the non-coherent differential EGC detection schemes for DS-CDMA in multipath fading channels. A receiver can choose to maximize the output SINR, maintain the unbiasedness, or take the advantage from the mixture of them (for EGC schemes) at almost no additional cost.

- With the common implementation, the output SINRs analysis of theses filter banks can be conducted using an unified mathematical approach. Along this

direction, analytic formulas for MRC filter banks are derived, and the condition to make the output SINRs of these filter banks equal is established. As a very special and interesting result, their output SINRs are identical in flat fading channels. Moreover, the output SINRs of MRC schemes are shown to be monotonically increasing with the number of stages, and upper bounded by a number equal to the resolvable paths of the target user's channel. The saturation of the output SINR in the high SNR regime is linked to the BER floor of MRC detectors.

- Based on the common framework of the multistage implementation of coherent MRC and non-coherent EGC schemes as shown in Fig. 1.1, a generic closed-form BER formula is derived for both detectors of DS-CDMA. As a result, BERs in each class of combings are shown to be equal to each other for flat Rayleigh fading channels. This coincides with the results for the output SINR analysis of MRC filter banks. In addition, analytic formulas make it possible to further analyze the tradeoff between the performance bound and the dimension of reduced-rank filtering.

- The condition for achieving the output SINR upper bound is given for MRC schemes, which leads to a test condition for the existence of BER floors of MRC schemes. The channel mismatch due to differential combining is also analyzed to form BER floors for EGC schemes. In junction with the output SINR analysis, the relationship between the ranks of filters, the dimensions of

MAI and channel mismatch is studied to understand the phenomemon of BER floors in both MRC and EGC schemes. Performance bounds are given for EGC schemes as functions of the autocorrelation value of Rayleigh fading channels, even though MAI can be suppressed efficiently. Based on this analysis, the impact of reduced-rank filtering on the performance limit of detection schemes is better understood. That is, even though a full-rank output SINR can be nearly achieved via reduced-rank filtering, there can be significant degradation in the BER performance for a reduced-rank detection scheme.

- A stochastic batch ML estimator as well as a stochastic Kalman-like estimator for blind channel estimation of DS-CDMA systems are derived based on the EM algorithm. It is shown that the ML estimator and the RLS are only special instances of our results, if the transmitted symbols are given. The stochastic batch ML is also a special case of the stochastic Kalman-like estimator when the window size is equal to one.

- A low-complexity sliding-window scheme is proposed for channel tracking based on the EM algorithm and a noncoherent maximum *a posteriori* probability (MAP) multi-user detector. Most data blind implementations of the EM algorithm suffer from the channel phase ambiguity, in spite of a reasonable estimation of channel gains. The problem of inherent phase ambiguity is eliminated using the stochastic Kalman filter in conjunction with the noncoherent BCJR

algorithm [4] to evaluate the posterior properties under phase errors. The proposed filter can track and adjust the channel estimate automatically even if the channel is in deep fade.

1.5 Outline of the Dissertation

The rest of this thesis is organized as follows. Chapter 2 reviews the Bayesian and the Frequentist statistic approaches for detection and estimation with emphasis on asynchronous DS-CDMA in multipath fading channels. A class of reduced-rank multistage MMSE-based filter banks and their adaptive implementations of the blind reduced-rank multiuser detector are given in Chapter 3. The performance and the structure of output SINRs, BER formulas as well as performance limits are given in Chapter 4. The joint channel estimation and symbol detection scheme using the EM algorithm is proposed in Chapter 5. Concluding remarks and possible future research direction are described in Chapter 6.

Chapter 2

Background Review: Linear Estimators and Detectors

This chapter presents some background material for the research work to be presented in Chapters 3 and 4 of this thesis proposal. A linear Gaussian model can be expressed as

$$\mathbf{y} = \mathbf{H}\Theta + \mathbf{n}, \tag{2.1}$$

where $\mathbf{y}^{N\times 1}$ is the received signal vector, $\mathbf{H}^{N\times L}$ is a matrix that characterizes the system behavior, $\Theta^{L\times 1}$ is the vector of system parameters of interest and $\mathbf{n}^{N\times 1}$ is a Gaussian noise vector with covariance matrix $\mathbf{C}^{N\times N}$. All variables in this model are complex. Our goal is to estimate or detect system parameters Θ given that $\mathbf{y}$ and $\mathbf{H}$ are available. Traditionally, there are two classes of estimators widely used, *i.e.* the Bayesian approach and the Frequentist approach. They will be examined in Sections 2.2 and 2.2, respectively. Then, the system model of blind multiuser detection for asynchronous DS-CDMA in a multipath fading channel environment

will be derived and shown to be equal to a linear Gaussian model with colored noise in Section 2.3.

2.1 Linear Bayesian Estimators

2.1.1 MMSE Estimators

The most commonly used criterion for multiuser detection is the MMSE estimation. The cost function for this criterion is of the form

$$\hat{\omega} = \arg\min_{\omega} E\|\Theta - \omega^H \mathbf{y}\|^2. \tag{2.2}$$

If $\mathbf{H}$ is a constant matrix and Θ is a random vector with zero mean and covariance matrix $\mathbf{C}_\Theta = E(\Theta\Theta^H)$, then the solution is

$$\omega_{mmse} = \mathbf{R}^{-1}E(\mathbf{y}\Theta^H) = \mathbf{R}^{-1}\mathbf{H}\mathbf{C}_\Theta, \tag{2.3}$$

where $\mathbf{R} = E(\mathbf{y}\mathbf{y}^H)$ is the autocorrelation matrix of $\mathbf{y}$. Consider a digital communication system with the binary phase shift keying (BPSK) modulation, in which the transmitted symbol of the target user (user no. 1) is $b_1 \in \{-1,\ 1\}$. By letting $\Theta = b_1$ and $\mathbf{\Sigma}_1 = 1$, the MMSE multiuser detector for a DS-CDMA system was developed in [17].

One main difficulty in applying the MMSE criterion to received signals in a fading channel directly is that the fading coefficient Γ_1 of the target user is involved in matrix $\mathbf{H}$ such that $E(\mathbf{y}\Theta^H) = E(\mathbf{H}) = \mathbf{0}$. To get around this problem, the system parameter is modified into $\Theta = \Gamma_1 b_1$ so that $\mathbf{H}$ is now independent of the fading coefficients and can be viewed as a constant matrix. The modified MMSE receiver is of the form

$$\omega_{mmse} = \mathbf{R}^{-1}\mathbf{H}, \tag{2.4}$$

where $\mathbf{C}_\Theta = E(\Gamma_1\Gamma_1^H) = \mathbf{I}$ for the BPSK modulation.

However, with the above modification, the estimated parameter becomes $\Gamma_1 b_1$, but not the desired b_1. To obtain the desired user's symbol b_1, we need to solve the coupling problem of Γ_1 and b_1. If the desired user's symbol b_1 is known, by setting $\Theta = \Gamma_1$ we can immediately obtain the estimate of channel coefficients Γ_1 based on the MMSE estimation. For the case of extremely slow fading, this problem can be solved by sending a preamble for channel estimation, which is however not effective for most fading channels. Thus, we need other techniques to solve this problem. The most simple and effective way is to use differential encoding, which serves the main foundation of this proposal. Starting from this point, a class of reduced-rank receivers will be discussed in detail in the following chapters. To continue our discussion on other detection methods, it is still assumed that $\Theta = \Gamma_1 b_1$ in the following.

2.1.2 MOE Detectors

One variation of the MMSE multiuser receiver is the minimum output energy (MOE) receiver for the AWGN channel as proposed in [11]. The filter was claimed to be more robust than the original MMSE receiver and extended to the more general case of the multipath fading channel in [21]. The basic idea of the MOE receiver is to design a linear filter of the form

$$\omega = \mathbf{H} + \mathbf{H}_{\perp}, \quad \mathbf{H}^H \mathbf{H}_{\perp} = \mathbf{0}. \tag{2.5}$$

Obviously, the column space of the matrix $\mathbf{H}$ is the space in which the system parameter vector Θ is embedded. By taking a constrained minimization of the form

$$\hat{\omega} = \arg\min_{\omega} E\|\omega^H \mathbf{y}\|^2, \quad \text{s.t.} \quad \omega^H \mathbf{H} = \mathbf{H}^H \mathbf{H}, \tag{2.6}$$

interferences reside in the subspace spanned by the column space of $\mathbf{H}_{\perp}$ will be minimized, and the overall quality of the target user's signal can be improved. It can be shown that the MOE receiver has the solution in form

$$\omega_{moe} = \mathbf{R}^{-1}\mathbf{H}(\mathbf{H}^H \mathbf{R}^{-1} \mathbf{H})^{-1} \mathbf{H}^H \mathbf{H}. \tag{2.7}$$

2.2 Linear Frequentist Estimators

For the MMSE and MOE receivers, the vector of system parameters, Θ, is treated as a random vector with zero mean and a covariance matrix $\mathbf{C}_\Theta$. On the other hand, this vector can be treated as a deterministic unknown. By minimizing the variance of estimation with filter ω or maximizing the probability density function (PDF) of $\mathbf{y}$ with respect to Θ, an estimator can be obtained with different meanings. In this section, we will examine the best linear unbiased estimator (BLUE) for channel estimation and the maximum likelihood detector (ML) for symbol detection. They both belong to the family of linear Frequentist estimators.

2.2.1 BLUE Estimators

With Θ being treated as a deterministic unknown vector, we may design a filter such that the variance of the estimation can be minimized. Thus, the optimization problem can be written as

$$\hat{\omega} = \arg\min_{\omega} E\|\Theta - \omega_1^H \mathbf{y}\|^2 \quad \text{s.t.} \quad E(\omega_1^H \mathbf{y}) = \Theta, \tag{2.8}$$

and the minimizing filter is given by

$$\omega_{blue} = \mathbf{C}^{-1}\mathbf{H}(\mathbf{H}^H\mathbf{C}^{-1}\mathbf{H})^{-1}. \tag{2.9}$$

Note that, for the linear Gaussian model, the BLUE estimator is equivalent to the minimum variance unbiased estimator (MVU) and the ML estimator for parameter Θ

2.2.2 ML Detectors

For the linear Gaussian model, the probability density function for the received signal $\mathbf{y}$ is of the form

$$\begin{aligned} \mathcal{P}(\mathbf{y}) &= \frac{1}{(2\pi)^N \det(\mathbf{C})} \exp\left\{-(\mathbf{y}-\mathbf{H}\Theta)^H \mathbf{C}^{-1}(\mathbf{y}-\mathbf{H}\Theta)\right\} \\ &= \frac{1}{(2\pi)^N \det(\mathbf{C})} \exp\left\{-(\mathbf{y}-\mathbf{H}\Gamma_1 b_1)^H \mathbf{C}^{-1}(\mathbf{y}-\mathbf{H}\Gamma_1 b_1)\right\}. \end{aligned} \tag{2.10}$$

To minimize the bit error probability, the maximum likelihood (ML) symbol detector can be obtained via hypothesis testing. That is, the detected symbol is of the following form

$$\hat{b}_1 = \mathrm{sgn}\{Re[\Gamma_1^H \mathbf{H}^H \mathbf{C}^{-1}\mathbf{y}]\}, \tag{2.11}$$

while the ML filter bank is

$$\omega_{ml} \equiv \mathbf{C}^{-1}\mathbf{H}. \tag{2.12}$$

Note that this ML detector should not be confused with the ML estimator described in the last paragraph of Section 2.2.1 for the BLUE estimator.

2.3 Receiver Model for DS-CDMA Systems

In the section, we will derive a receiver model for the DS-CDMA communication system and show how this model can fit into the linear Gaussian linear model described above.

Let us consider a standard model for asynchronous DS-CDMA communication systems. The baseband representation of the transmitted signal for the kth user can be written as

$$x_k(t) = A_k \sum_{n=-\infty}^{\infty} b_k(n) s_k(t - nT_s - \tau_k), \tag{2.13}$$

where T_s is the symbol duration, and $b_k(n)$, A_k and τ_k are the symbol stream, amplitude and relative delay with reference to the base station, respectively, for the kth user. The transmitted symbols $b_k(n)$ are identically and independently distributed (i.i.d.) random variables taking a binary value of 1 and -1. The spreading waveform is given by $s_k(t) = \sum_{i=0}^{N-1} c_k(j)\psi(t - jT_c)$, where $c_k(i) \in \{-1, 1\}$ is the signature sequence for the kth user and is fixed with a period of N, $\psi(t)$ is a normalized chip pulse shaping function of duration T_c. The spreading gain N is the ratio of T_s and T_c, *i.e.* $N = T_s/T_c$.

The kth user's signal $x_k(t)$ propagates through a multipath fading channel with the complex impulse response

$$g_k(t) = \sum_{l=0}^{L_k-1} g_{kl}(t)\delta(t - \eta_{kl}), \tag{2.14}$$

where L_k is the number of the paths for user k, η_{kl} is the delay time for the lth tap of a tap-delay-line channel model and $g_{kl}(t)$ is the fading process corresponding to the tap.

The received signal at the base station from the kth user is given by

$$r_k(t) = x_k(t) * g_k(t) = A_k \sum_{n=-\infty}^{\infty} b_k(n) \sum_{j=0}^{N-1} \sum_{l=0}^{L_k-1} g_{kl}(t)\psi(t - nT_s - jT_c - \tau_{kl}), \quad (2.15)$$

where $\tau_{kl} \equiv \tau_k + \eta_{kl}$. The overall received signal at the base station is given by

$$r(t) = \sum_{k=1}^{K} r_k(t) + n(t), \quad (2.16)$$

where K is the number of users and $n(t)$ is a complex zero-mean white Gaussian noise.

For simplicity, it is assumed that the maximum delay spread is less than the symbol duration for all users, *i.e.*

$$|\max_l\{\tau_{kl}\} - \min_l\{\tau_{kl}\}| < T_s, \quad \forall k, l. \quad (2.17)$$

Thus, the delay time $\tau_{k1} < T_s$ for the first path of every user, and $\tau_{kl} < 2T_s$, for $l \geq 2$. For cases where the delay spread is larger than T_s, the detection window can be simply extended for more than one symbol duration to cover the longest delay symbols among all users. Without loss of generality, user 1 is chosen to be the target

user. It is assumed that the delay time for each path of the target user is known and that the receiver's clock is synchronized with the reception of the first path of the desired user, *i.e.* $\tau_{11} = 0$ and $\tau_{1l} < T_s$, for $l \geq 2$.

Let us define

$$\lfloor \frac{\tau_{kl}}{T_s} \rfloor = m_{kl}, \quad m_{kl} \in \{0, 1\}, \tag{2.18}$$

where $\lfloor x \rfloor$ denotes the closest integer less or equal to x. Furthermore, if the notation $a \mid b$ means the remainder of b divided by a, we can introduce several parameters below:

$$\begin{aligned} \Delta_{kl} &= T_s \mid \tau_{kl}, & (2.19)\\ i_{kl} &= \lfloor \frac{\Delta_{kl}}{T_c} \rfloor, \quad 0 \leq i_{kl} < N - 1, & (2.20)\\ \delta_{kl} T_c &= T_c \mid \Delta_{kl}, \quad 0 \leq \delta_{kl} < 1. & (2.21) \end{aligned}$$

For the convenience of expression, we also define the following:

$$\begin{aligned} \mathbf{c}_k^L(i_{kl}) &= [0 \cdots 0, c_k(0) \cdots c_k(N - i_{kl} - 1)], & (2.22)\\ \mathbf{c}_k^R(i_{kl}) &= [c_k(N - i_{kl}) \cdots c_k(N - 1), 0 \cdots 0], & (2.23)\\ \mathbf{s}_{kl}^+ &= (1 - \delta_{kl})\mathbf{c}_k^L(i_{kl}) + \delta_{kl}\mathbf{c}_k^L(i_{kl} + 1), & (2.24)\\ \mathbf{s}_{kl}^- &= (1 - \delta_{kl})\mathbf{c}_k^R(i_{kl}) + \delta_{kl}\mathbf{c}_k^R(i_{kl} + 1). & (2.25) \end{aligned}$$

The parameters $g_{kl}(t)$ of the fading process are assumed to be constant in one symbol interval and can be modeled by a discrete-time fading process $a_{kl}\gamma_{kl}(m)$, where a_{kl} is a time-invariant gain and $\gamma_{kl}(m)$ is a complex zero-mean Gaussian process satisfying

$$E\{\gamma^*_{k_1l_1}(m)\gamma_{k_2l_2}(m)\} = \delta(k_1 - k_2)\delta(l_1 - l_2), \tag{2.26}$$

with the auto-correlation of two adjacent symbols defined by

$$\rho = E[\gamma^*_{k_1l_1}(m)\gamma_{k_1l_1}(m-1)], \quad 0 \leq |\rho| < 1. \tag{2.27}$$

The received signal is match-filtered by the chip pulse shaping function $\psi(t - mT_s - iT_c)$ and sampled at the chip rate. The discrete time signal vector $\mathbf{y}$ obtained by collecting N consecutive samples of the matched filter output is given by [21]

$$\mathbf{y}(m) = \sum_{k=1}^{K}\sum_{l=1}^{L_k} A_{kl}\gamma_{kl}(m) \cdot [\mathbf{s}^+_{kl}b_k(m - m_{kl}) + \mathbf{s}^-_{kl}b_k(m - m_{kl} - 1)] + \mathbf{n}(m), \tag{2.28}$$

where $A_{kl} = A_k a_{kl}$. The filtered noise vector $\mathbf{n}(m)$ is complex Gaussian distributed with covariance matrix $N_0\mathbf{I}$, which is denoted by $\mathcal{N}(\mathbf{0}, N_0\mathbf{I})$. Note that $m_{1l} = 0$. For the convenience of analysis, the received signal $\mathbf{y}(m)$ is rewritten of the form of

$$\mathbf{y}(m) = \mathbf{S}_{1+}\mathbf{A}_1\Gamma_1(m)b_1(m) + \mathbf{I}_1(m), \tag{2.29}$$

where

$$\mathbf{A}_1^{L\times L} = \text{diag}([A_{11},\ldots,A_{1L_1}]), \tag{2.30}$$

$$\mathbf{S}_{1+}^{N\times L} = [\mathbf{s}_{11}^{+},\ldots,\mathbf{s}_{1L_1}^{+}], \tag{2.31}$$

$$\Gamma_1^{L\times 1} = [\gamma_{11},\ldots,\gamma_{1L_1}]^T, \tag{2.32}$$

and

$$\mathbf{I}_1(m) = \sum_{k=2}^{K}\sum_{l=1}^{L_k} A_{kl}\gamma_{kl}(m)\cdot\mathbf{s}_{kl}^{+}b_k(m-m_{kl}) + \sum_{k=1}^{K}\sum_{l=1}^{L_k} A_{kl}\gamma_{kl}(m)\mathbf{s}_{kl}^{-}b_k(m-m_{kl}-1) + \mathbf{n}(m), \tag{2.33}$$

which is the aggregated form of the inter symbol interference (ISI), the multiple access interference (MAI) and the AWGN noise to the target user's signal.

Since fading coefficient γ_{kl} is zero-mean and complex Gaussian distributed, $b_1 \in \{-1,1\}$ and $\mathbf{s}_{kl}^{+}$ and $\mathbf{s}_{kl}^{-}$ are fixed, it is clear that $\mathbf{I}_1$ is also complex Gaussian distributed with zero mean. Then, by checking the expression given in (2.1), we see that the multiuser detection problem in the receiver end of the DS-CDMA system as expressed by (5.4) is essentially a linear Gaussian model.

Chapter 3

Blind Adaptive Multistage MMSE-Based Receivers

In this chapter, a class of multistage implementations of the minimum mean square error (MMSE), minimum output energy (MOE), maximum likelihood (ML) and best linear unbiased estimator (BLUE) filter banks is developed based on the concept of the multistage Wiener filter (MSWF) introduced by Goldstein *et al.* [8]. All these filter banks share a common multistage structure modulo a distinctive scaling matrix at each filter's output. Based on this feature, four types of adaptive reduced-rank detection schemes, including MMSE, MOE, BLUE and ML, are proposed and evaluated for coherent and non-coherent blind multiuser detections for DS-CDMA communication systems with multipath fading channels.

3.1 Multistage MMSE Filter Bank

Assuming that the steering matrix $\mathbf{S}_{1+}^{N\times L}$ is of full column rank, it can be factored by the Gram-Schmidt process into

$$\mathbf{S}_{1+} = \mathbf{H}_1^{N\times L}\mathbf{U}_1^{L\times L}, \tag{3.1}$$

where the column space of $\mathbf{H}_1$, formed by the column vectors of $\mathbf{H}_1$ and denoted as $\mathcal{H}_1$, is an orthonormal space spans the column space of $\mathbf{S}_{1+}$. Thus, $\mathbf{H}_1^H\mathbf{H}_1 = \mathbf{I}$. Now, we choose an unitary matrix $\mathbf{T}^{N\times N}$ of the form

$$\mathbf{T} \equiv \left[\mathbf{H}_1 \mid \mathbf{B}_1^H\right]^H, \tag{3.2}$$

where $\mathbf{B}_1$ is of dimension $(N-L)\times N$, and $\mathbf{B}_1\mathbf{H}_1 = \mathbf{0}$, denoted as $\mathbf{B}_1^H \perp \mathbf{H}_1$. Thus, $\mathbf{B}_1$ is often referred to as the blocking matrix of $\mathbf{S_{1+}}$ and can be obtained via the QR factorization of $\mathbf{S_{1+}}$.

By exploiting the invariance of MSE under an unitary transform of $\mathbf{y}$, we can estimate $b_1\Gamma_1$ via

$$\min_{\omega} E\|b_1\Gamma_1 - \omega^H\mathbf{y}\|^2 = \min_{\omega} E\|b_1\Gamma_1 - \omega^H\mathbf{T}\mathbf{y}\|^2. \tag{3.3}$$

The solution to (3.3) is given by

$$\omega_{mmse}^{N\times L} = \arg\min_{\omega} E\|b_1\Gamma_1 - \omega^H\mathbf{T}\mathbf{y}\|^2 = (\mathbf{T}\mathbf{R}\mathbf{T}^H)^{-1}\mathbf{T}\mathbf{S}_{1+}\mathbf{A}_1. \tag{3.4}$$

The invariance can be easily verified, *i.e.*

$$\mathbf{A}_1\mathbf{S}_{1+}^H\mathbf{T}^H(\mathbf{T}\mathbf{R}\mathbf{T}^H)^{-1}\mathbf{T}\mathbf{y} = \mathbf{A}_1\mathbf{S}_{1+}^H\mathbf{R}^{-1}\mathbf{y}, \tag{3.5}$$

where the unitary property of T is used. The objective of choosing such a matrix $\mathbf{T}$ is to separate signal components of $\mathbf{y}$ in subspace $\mathcal{H}_1$ from those lying in $\mathcal{H}_1$'s orthogonal complement $\mathcal{B}_1$ spanned by the column space of $\mathbf{B}_1^H$. Then, the projected signal $\mathbf{B}_1\mathbf{y}$ is used to suppress the multiple access interference (MAI) in subspace $\mathcal{H}_1$. This concept will be justified rigorously later in this section following the derivation of MS-MMSE-FB.

By substituting (3.2) into (3.4) and applying the Matrix Inversion Lemma [14] to $(\mathbf{T}\mathbf{R}\mathbf{T}^H)^{-1}$, the MMSE filter bank ω_{mmse} becomes

$$\begin{aligned}
\omega_{mmse} &= \left(\left[\begin{array}{c}\mathbf{H}_1^H\\ \hline \mathbf{B}_1\end{array}\right]\mathbf{R}\left[\begin{array}{c|c}\mathbf{H}_1 & \mathbf{B}_1^H\end{array}\right]\right)^{-1}\left[\begin{array}{c}\mathbf{H}_1^H\\ \hline \mathbf{B}_1\end{array}\right]\mathbf{S}_{1+}\mathbf{A}_1 \\
&= \left(E\left[\begin{array}{c|c}\mathbf{d}_1\mathbf{d}_1^H & \mathbf{d}_1\mathbf{y}_1^H\\ \hline \mathbf{y}_1\mathbf{d}_1^H & \mathbf{y}_1\mathbf{y}_1^H\end{array}\right]\right)^{-1}\left[\begin{array}{c}\mathbf{U}_1\\ \hline \mathbf{0}\end{array}\right]\mathbf{A}_1
\end{aligned}$$

$$
\begin{aligned}
&\equiv \left(\left[\begin{array}{c|c} \mathbf{R}_{\mathbf{d}_1} & \boldsymbol{\Upsilon}^H_{\mathbf{y}_1\mathbf{d}_1} \\ \hline \boldsymbol{\Upsilon}_{\mathbf{y}_1\mathbf{d}_1} & \mathbf{R}_{\mathbf{y}_1} \end{array}\right]\right)^{-1} \left[\begin{array}{c} \mathbf{U}_1 \\ \hline \mathbf{0} \end{array}\right] \mathbf{A}_1 \\
&= \left[\begin{array}{c|c} \mathbf{E}_1^{-1} & -\mathbf{E}_1^{-1}\boldsymbol{\Upsilon}^H_{\mathbf{y}_1\mathbf{d}_1}\mathbf{R}^{-1}_{\mathbf{y}_1} \\ \hline -\mathbf{R}^{-1}_{\mathbf{y}_1}\boldsymbol{\Upsilon}_{\mathbf{y}_1\mathbf{d}_1}\mathbf{E}_1^{-1} & \Delta \end{array}\right] \left[\begin{array}{c} \mathbf{U}_1 \\ \hline \mathbf{0} \end{array}\right] \mathbf{A}_1 \\
&= \left[\begin{array}{c} \mathbf{I} \\ \hline -\mathbf{R}^{-1}_{\mathbf{y}_1}\boldsymbol{\Upsilon}_{\mathbf{y}_1\mathbf{d}_1} \end{array}\right] \mathbf{E}_1^{-1}\mathbf{U}_1\mathbf{A}_1, \qquad (3.6)
\end{aligned}
$$

where $\mathbf{d}_1^{L\times 1} \equiv \mathbf{H}_1^H\mathbf{y}$, $\mathbf{y}_1^{(N-L)\times 1} \equiv \mathbf{B}_1\mathbf{y}$, $\mathbf{R}_{\mathbf{d}_1}$ and $\mathbf{R}_{\mathbf{y}_1}$ are auto-correlation matrices of $\mathbf{d_1}$ and $\mathbf{y_1}$, respectively, $\boldsymbol{\Upsilon}_{\mathbf{y}_1\mathbf{d}_1} \equiv E(\mathbf{y}_1\mathbf{d}_1^H)$ is the cross-correlation matrix of $\mathbf{y}_1$ and $\mathbf{d}_1$, and

$$
\mathbf{E}_1 \equiv (\mathbf{R}_{\mathbf{d}_1} - \boldsymbol{\Upsilon}^H_{\mathbf{y}_1\mathbf{d}_1}\mathbf{R}^{-1}_{\mathbf{y}_1}\boldsymbol{\Upsilon}_{\mathbf{y}_1\mathbf{d}_1}) = E[(\mathbf{d}_1 - \omega_1^H\mathbf{y}_1)(\mathbf{d}_1 - \omega_1^H\mathbf{y}_1)^H]. \qquad (3.7)
$$

The soft output of the filter can be obtained via

$$
\begin{aligned}
\mathbf{z} &= \omega^H_{mmse}\mathbf{T}\mathbf{y} = \mathbf{A}_1\mathbf{U}_1^H\mathbf{E}_1^{-1}\left[\mathbf{I}\,\middle|\, -\boldsymbol{\Upsilon}^H_{\mathbf{y}_1\mathbf{d}_1}\mathbf{R}^{-1}_{\mathbf{y}_1}\right]\left[\begin{array}{c} \mathbf{H}_1^H \\ \hline \mathbf{B}_1 \end{array}\right]\mathbf{y} \\
&= \mathbf{A}_1\mathbf{U}_1^H\mathbf{E}_1^{-1}[\mathbf{d}_1 - \omega_1^H\mathbf{y}_1], \qquad (3.8)
\end{aligned}
$$

where

$$
\omega_1^{(N-L)\times L} \equiv \mathbf{R}^{-1}_{\mathbf{y}_1}\boldsymbol{\Upsilon}_{\mathbf{y}_1\mathbf{d}_1} \qquad (3.9)
$$

is the MMSE filter bank that minimizes $E\|\mathbf{d}_1 - \omega_1^H \mathbf{y}_1\|^2$. Note that $\mathbf{E}_1$ is the outer product of the estimation error. Thus, by choosing another unitary matrix $\mathbf{T}_1^{(N-L)\times(N-L)} \equiv \left[\mathbf{H}_2 \mid \mathbf{B}_2^H\right]^H$ with $\mathbf{\Upsilon}_{\mathbf{y}_1\mathbf{d}_1} = \mathbf{H}_2^{(N-L)\times L}\mathbf{U}_2^{L\times L}$ and $\mathbf{B}_2^{(N-2L)\times(N-L)} \perp \mathbf{H}_2^H$, we have

$$E\|\mathbf{d}_1 - \omega_1^H \mathbf{y}_1\|^2 = E\|\mathbf{d}_1 - \omega_1^H \mathbf{T}_1 \mathbf{y}_1\|^2. \tag{3.10}$$

The same procedure from (3.3) to (3.8) in calculating ω_{mmse} can also be applied to ω_1. This results in

$$\omega_1^H \mathbf{T}_1 \mathbf{y_1} = \mathbf{U}_2^H \mathbf{E}_2^{-1}[\mathbf{d}_2 - \omega_2^H \mathbf{y}_2], \tag{3.11}$$

where $\mathbf{d}_2^{L\times 1} = \mathbf{H}_2^H \mathbf{y}_1$, $\mathbf{y}_2^{(N-2L)\times 1} = \mathbf{B}_2 \mathbf{y}_1$, $\mathbf{E}_2 = E[(\mathbf{d}_2 - \omega_2^H \mathbf{y}_2)(\mathbf{d}_2 - \omega_2^H \mathbf{y}_2)^H]$ and $\omega_2^{(N-2L)\times L} = \mathbf{R}_{\mathbf{y}_2}^{-1} \mathbf{\Upsilon}_{\mathbf{y}_2\mathbf{d}_2}$.

Recursively applying the above steps to $\omega_2^{(N-2L)\times L}$ and the forthcoming $\omega_3^{(N-3L)\times L}$, $\omega_4^{(N-4L)\times L}$, $\cdots$ until the dimension N is exhausted, a multistage implementation of the MMSE-FB can be constructed as shown in Fig. 3.1. It is straightforward to see that MS-MMSE-FB reduces to MSWF in the flat fading channel case, where the rank of both $\mathbf{H}_1$ and L is equal to one.

Before turning our attention to the multistage implementation of MOE-FB, we examine the physical meaning of the filter bank ω_1 in (3.9). Let us rewrite the received signal $\mathbf{y}$ as

$$\mathbf{y}(m) = \mathbf{S}_{1+}\mathbf{A}_1 \Gamma_1(m) b_1(m) + \mathbf{I}_1(m), \tag{3.12}$$

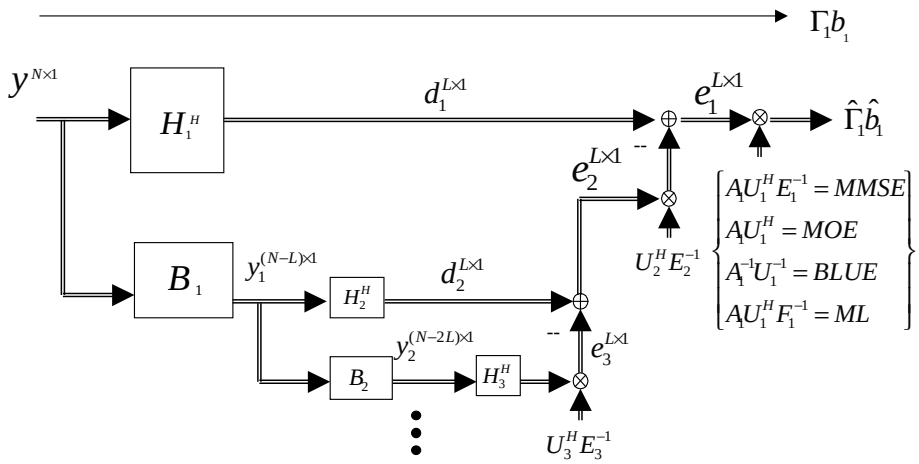

Figure 3.1: The structure of the MS-MMSE/MOE/BLUE/ML-FBs for channel estimation and multiuser detection in multi-path fading channels, where the output scaling matrix is $\mathbf{A}_1\mathbf{U}_1^H\mathbf{E}_1^{-1}$ for MS-MMSE-FB, $\mathbf{A}_1\mathbf{U}_1^H$ for MS-MOE-FB, $\mathbf{A}_1^{-1}\mathbf{U}_1^{-1}$ for MS-BLUE-FB and $\mathbf{A}_1\mathbf{U}_1^H\mathbf{F}_1^{-1}$ for MS-ML-FB and our object is $\Gamma_1 b_1$ for channel estimation.

where $\mathbf{I}_1(m)$ is the interference to the target user's signal given by

$$\mathbf{I}_1(m) \equiv \sum_{k=2}^{K}\sum_{l=1}^{L_k} A_{kl}\gamma_{kl}(m)\cdot\mathbf{s}_{kl}^{+}b_k(m-m_{kl})+\sum_{k=1}^{K}\sum_{l=1}^{L_k} A_{kl}\gamma_{kl}(m)\mathbf{s}_{kl}^{-}b_k(m-m_{kl}-1)+\mathbf{n}(m). \tag{3.13}$$

The filter bank ω_1 can be rewritten as

$$\omega_1 = \mathbf{R}_{\mathbf{y}_1}^{-1}\boldsymbol{\Upsilon}_{\mathbf{y}_1\mathbf{d}_1} = \mathbf{R}_{\mathbf{y}_1}^{-1}E(\mathbf{B}_1\mathbf{y}\mathbf{y}^H\mathbf{H}_1), \tag{3.14}$$

where

$$\mathbf{B}_1\mathbf{y} = \mathbf{B}_1(\mathbf{S}_{1+}\mathbf{A}_1\Gamma_1 b_1 + \mathbf{I}_1) = \mathbf{B}_1\mathbf{I}_1 \tag{3.15}$$

and

$$\mathbf{H}_1^H \mathbf{y} = \mathbf{U}_1 \mathbf{A}_1 \Gamma_1 b_1 + \mathbf{H}_1^H \mathbf{I}_1. \tag{3.16}$$

Thus, we have

$$\begin{aligned} E(\mathbf{B}_1 \mathbf{y}\mathbf{y}^H \mathbf{H}_1) &= E[(\mathbf{B}_1 \mathbf{I}_1)(\mathbf{U}_1 \mathbf{A}_1 \Gamma_1 b_1 + \mathbf{H}_1^H \mathbf{I}_1)^H] = \mathbf{B}_1 E(\mathbf{I}_1 \mathbf{I}_1^H) \mathbf{H}_1, \quad (3.17) \\ \mathbf{R}_{\mathbf{y}_1}^{-1} &= E(\mathbf{B}_1 \mathbf{I}_1 \mathbf{I}_1^H \mathbf{B}_1^H), \quad (3.18) \end{aligned}$$

where the last equality in (3.17) holds since $\mathbf{I}_1$ and b_1 are uncorrelated. Then, the filter bank ω_1 is equivalent to the one obtained by

$$\omega_1 = \arg \min_{w_1} \|\mathbf{H}_1^H \mathbf{I}_1 - \omega_1^H \mathbf{B}_1 \mathbf{I}_1\|^2 = [E(\mathbf{B}_1 \mathbf{I}_1 \mathbf{I}_1^H \mathbf{B}_1^H)]^{-1} E(\mathbf{B}_1 \mathbf{I}_1 \mathbf{I}_1^H \mathbf{H}_1). \tag{3.19}$$

In the above form, ω_1 can be interpreted as the filter bank that takes the interference projected on subspace $\mathcal{B}_1$ to suppress interferences residing in the signal subspace $\mathcal{H}_1$ using the MMSE criterion.

By following a similar procedure, the term $\mathbf{E}_1$ in (4.6) can be manipulated via

$$\mathbf{E}_1 = (\mathbf{R}_{\mathbf{d}_1} - \boldsymbol{\Upsilon}_{\mathbf{y}_1 \mathbf{d}_1}^H \mathbf{R}_{\mathbf{y}_1}^{-1} \boldsymbol{\Upsilon}_{\mathbf{y}_1 \mathbf{d}_1}) = \mathbf{U}_1 \mathbf{A}_1^2 \mathbf{U}_1^H + E[(\mathbf{H}_1^H \mathbf{I}_1 - \omega_1^H \mathbf{B}_1 \mathbf{I}_1)(\mathbf{H}_1^H \mathbf{I}_1 - \omega_1^H \mathbf{B}_1 \mathbf{I}_1)^H], \tag{3.20}$$

where $\mathbf{U}_1 \mathbf{A}_1^2 \mathbf{U}_1^H = \mathbf{H}_1^H \mathbf{S}_{1+} \mathbf{A}_1^2 \mathbf{S}_{1+}^H \mathbf{H}_1$ is the auto-correlation matrix of the target user's signal in signal subspace $\mathcal{H}_1$. Thus, matrix $\mathbf{E}_1$ can be interpreted as the

desired user's signal power plus the covariance matrix of the residual interference in subspace $\mathcal{H}_1$.

3.2 Multistage MOE Filter Bank

Next, let us extend the multistage concept to the MOE filter bank. Recall from (3.3) that the multistage Wiener filter differs from the original one by using the transformed received signal $\mathbf{Ty}$ (instead of $\mathbf{y}$) to form the MMSE filter bank. Motivated by this observation, The MOE criterion in (2.6) can be reformulated as

$$\hat{\omega} = \arg\min_{\omega} E\|\omega^H \mathbf{Ty}\|^2 \quad \text{s.t.} \quad \omega^H \mathbf{TS}_{1+}\mathbf{A}_1 = \mathbf{A}_1 \mathbf{S}_{1+}^H \mathbf{T}^H \mathbf{TS}_{1+}\mathbf{A}_1. \tag{3.21}$$

Let $\mathbf{R}_T = \mathbf{TRT}^H$ and $\mathbf{S}_T = \mathbf{TS}_{1+}$. The optimal filter bank is given by

$$\omega_{moe} = \mathbf{R}_T^{-1}\mathbf{S}_T(\mathbf{S}_T^H \mathbf{R}_T^{-1}\mathbf{S}_T)^{-1}\mathbf{S}_T^H \mathbf{S}_T \mathbf{A}_1. \tag{3.22}$$

It is clear that the filter's soft output is still invariant under unitary transformation $\mathbf{T}$. Using the same transformation matrix $\mathbf{T}$ as given in (3.2) and applying the Matrix Inversion Lemma to $\mathbf{R}_T^{-1}$ as given in (3.6), it is straightforward to show that

$$(\mathbf{S}_T^H \mathbf{R}_T^{-1}\mathbf{S}_T)^{-1} = \mathbf{U}_1^{-1}\mathbf{E}_1\mathbf{U}_1^{-H}. \tag{3.23}$$

By plugging this result into (3.22) and following the same derivation procedure from (3.6) to (3.8) for handling the term $\mathbf{R}_T^{-1}\mathbf{S}_T$, it is straightforward to show that MOE-FB in (3.22) is equal to

$$\omega_{moe}^H = \mathbf{A}_1\mathbf{U}_1^H \left[\mathbf{I} \mid -\boldsymbol{\Upsilon}_{\mathbf{y}_1\mathbf{d}_1}^H \mathbf{R}_{\mathbf{y}_1}^{-1}\right]. \tag{3.24}$$

The filter's soft output is given by

$$\mathbf{z} = \omega_{moe}^H \mathbf{T}\mathbf{y} = \mathbf{A}_1\mathbf{U}_1^H[\mathbf{d}_1 - \omega_1^H \mathbf{y}_1]. \tag{3.25}$$

Note that an important point revealed by this formula is that MS-MMSE-FB in (3.6) and MS-MOE-FB in (3.24) differ only in matrix $\mathbf{E}_1^{-1}$ of (3.20), which is a scaling matrix at the filter's output. The multistage implementation of MOE-FB is also shown in Fig. 3.1.

3.3 Observations on Detection and Combining

If the channel vector Γ_1 is available, the decision statistic via maximal ratio combining (MRC) is given by

$$\varphi(m) = Re[\Gamma^H(m)\mathbf{z}(m)], \tag{3.26}$$

where $\mathbf{z}(m)$ is the soft output of the MMSE-based estimator for $b_1\Gamma_1$. For BPSK, symbol detection is achieved via $\hat{b_1}(m) = \text{sgn}\{\varphi(m)\}$. In contrast, if the channel vector is unknown, differentially encoded BPSK (DBPSK) coupled with equal gain combining can be employed to yield $\varphi(m) = Re[\mathbf{z}^H(m-1)\mathbf{z}(m)]$. In the ideal case, we have $\mathbf{z}(m) = b_1(m)\Gamma_1(m)$ and therefore $Re[\mathbf{z}^H(m-1)\mathbf{z}(m)] \simeq b_1(m-1)b_1(m)\|\Gamma_1\|$. One interpretation of the EGC for DBPSK is that $\mathbf{z}(m-1)$ plays the role of the estimated channel vector required by MRC. It is however important to notice that, conditioned on the channel vector and the data, the MMSE and MOE estimators are biased. That is,

$$E[\mathbf{z}_{mmse}|\Gamma_1 b_1] = \mathbf{A}_1\mathbf{S}_{1+}^H\mathbf{R}^{-1}\mathbf{S}_{1+}\mathbf{A}_1\Gamma_1 b_1, \tag{3.27}$$

and

$$E[\mathbf{z}_{moe}|\Gamma_1 b_1] = \mathbf{A}_1\mathbf{S}_{1+}^H\mathbf{S}_{1+}\mathbf{A}_1\Gamma_1 b_1. \tag{3.28}$$

We also observe that the bias of the MMSE estimator is a function of system loading through its dependence on $\mathbf{R}$. Furthermore, when multistage implementations are employed, the mean values of MS-MMSE and MS-MOE estimators become, respectively,

$$E[\mathbf{z}_{mmse}|\Gamma_1 b_1] = \mathbf{A}_1\mathbf{S}_{1+}^H\mathbf{T}^H(\mathbf{T}\mathbf{R}\mathbf{T}^H)^{-1}\mathbf{T}\mathbf{S}_{1+}\mathbf{A}_1\Gamma_1 b_1, \tag{3.29}$$

$$E[\mathbf{z}_{moe}|\Gamma_1 b_1] = \mathbf{A}_1\mathbf{S}_{1+}^H\mathbf{T}^H\mathbf{T}\mathbf{S}_{1+}\mathbf{A}_1\Gamma_1 b_1. \tag{3.30}$$

As will be shown in Section 3.6, $\mathbf{T}$ is no longer an unitary matrix such that $\mathbf{T}^H\mathbf{T} \neq \mathbf{I}$ in reduced-rank implementations. The bias will also change with the rank of the transform. To eliminate the bias effect, we consider alternative approaches in estimating $\Gamma_1 b_1$ below.

3.4 Multistage BLUE Filter Bank

In this section, let us treat $b_1\Gamma_1$ as a deterministic unknown vector and combine MAI, inter symbol interference (ISI) and the complex Gaussian noise in (5.4) together as an interference vector $\mathbf{I}_1$ as given in (3.12) with covariance matrix $\mathbf{C}_1 = E[\mathbf{I}_1(m)\mathbf{I}_1^H(m)]$. The best linear unbiased estimator (BLUE) [14] for $b_1\Gamma_1$ can be obtained according to the following criterion:

$$\hat{\omega}(m) = \arg\min_{\omega} E\|\theta_1(m) - \omega_1^H\mathbf{y}(m)\|^2 \quad \text{s.t.} \quad E(\omega_1^H\mathbf{y}(m)) = \theta_1(m), \tag{3.31}$$

where we write $\theta_1(m) = b_1(m)\Gamma_1(m)$ as a function of m to emphasize time dependency and the difference of the current approach from the MMSE/MOE approach, where $b_1\Gamma_1$ is a random vector. The estimate of $\theta_1(m)$ can be written as

$$\hat{\theta}_1(m) = [\mathbf{A}_1^H\mathbf{S}_{1+}^H\mathbf{C}_1^{-1}\mathbf{S}_{1+}\mathbf{A}_1]^{-1}\mathbf{A}_1^H\mathbf{S}_{1+}^H\mathbf{C}_1^{-1}\mathbf{y}(m). \tag{3.32}$$

Under our assumptions about the fading process, data and spreading codes, the interference vector $\mathbf{I}_1(m)$ is a zero-mean, complex-Gaussian distributed vector due

to the fact that $\mathbf{s}_{kl}^{+}$ and $\mathbf{s}_{kl}^{-}$ are deterministic, and Γ_k is a complex Gaussian vector. Thus, (3.12) is a linear Gaussian model for $\mathbf{y}$. The ML estimator for $\theta_1(m)$ is also given by the same formula in (3.32) and achieves the Cramer-Rao Lower Bound (CRLB) [14].

Now, let us consider the multistage implementation of the BLUE filter bank. By projecting the received signal $\mathbf{y}(m)$ onto the space spanned by unitary matrix $\mathbf{T}$ given in (3.2), we obtain

$$\mathbf{Ty} = \mathbf{TS}_{1+}\mathbf{A}_1\Gamma_1(m)b_1(m) + \mathbf{TI}_1(m). \tag{3.33}$$

Let $\mathbf{C}_T = \mathbf{TC}_1\mathbf{T}^H$ and $\mathbf{S}_T = \mathbf{TS}_{1+}$. Then, the BLUE/ML estimator for $\theta_1(m)$ is given by

$$\begin{aligned}\hat{\theta}_1(m) &= [\mathbf{A}_1\mathbf{S}_T^H\mathbf{C}_T^{-1}\mathbf{S}_T\mathbf{A}_1]^{-1}\mathbf{A}_1\mathbf{S}_T^H\mathbf{C}_T^{-1}\mathbf{Ty}(m) \\ &= [\mathbf{A}_1\mathbf{S}_{1+}^H\mathbf{C}_1^{-1}\mathbf{S}_{1+}\mathbf{A}_1]^{-1}\mathbf{A}_1\mathbf{S}_{1+}^H\mathbf{C}_1^{-1}\mathbf{y}(m). \end{aligned}\tag{3.34}$$

The equality can be easily verified since $\mathbf{T}^H = \mathbf{T}^{-1}$. Like the case of MMSE-FB and MOE-FB, a unitary transformation does not change the estimation result. By applying the Matrix Inversion Lemma [14] to $(\mathbf{TCT}^H)^{-1}$, we have

$$(\mathbf{TC}_1\mathbf{T}^H)^{-1} = \left(\left[\begin{array}{c}\mathbf{H}_1^H \\ \hline \mathbf{B}_1\end{array}\right]\mathbf{C}_1\left[\begin{array}{c|c}\mathbf{H}_1 & \mathbf{B}_1^H\end{array}\right]\right)^{-1} = \left(\left[\begin{array}{c|c}\mathbf{K}_{\mathbf{I}_{H1}} & \boldsymbol{\Upsilon}_{\mathbf{I}_{B1}\mathbf{I}_{H1}}^H \\ \hline \boldsymbol{\Upsilon}_{\mathbf{I}_{B1}\mathbf{I}_{H1}} & \mathbf{K}_{\mathbf{I}_{B1}}\end{array}\right]\right)^{-1}$$

$$= \left[\begin{array}{c|c} \mathbf{F}_1^{-1} & -\mathbf{F}_1^{-1}\boldsymbol{\Upsilon}^H_{\mathbf{I}_{B1}\mathbf{I}_{H1}}\mathbf{K}^{-1}_{\mathbf{I}_{B1}} \\ \hline -\mathbf{K}^{-1}_{\mathbf{I}_{B1}}\boldsymbol{\Upsilon}_{\mathbf{I}_{B1}\mathbf{I}_{H1}}\mathbf{F}_1^{-1} & \Delta \end{array}\right], \tag{3.35}$$

where $\mathbf{I}_{H1} \equiv \mathbf{H}_1^H\mathbf{I}_1$, $\mathbf{I}_{B1} \equiv \mathbf{B}_1\mathbf{I}_1$; $\mathbf{K}_{\mathbf{I}_{H1}}$ and $\mathbf{K}_{\mathbf{I}_{B1}}$ are auto-covariance matrices of $\mathbf{I}_{H1}$ and $\mathbf{I}_{B1}$, respectively, $\boldsymbol{\Upsilon}_{\mathbf{I}_{B1}\mathbf{I}_{H1}} \equiv E(\mathbf{I}_{B1}\mathbf{I}_{H1}^H)$ is the cross-covariance matrix of $\mathbf{I}_{B1}$ and $\mathbf{I}_{H1}$, and

$$\mathbf{F}_1 \equiv (\mathbf{K}_{\mathbf{I}_{H1}} - \boldsymbol{\Upsilon}^H_{\mathbf{I}_{B1}\mathbf{I}_{H1}}\mathbf{K}^{-1}_{\mathbf{I}_{B1}}\boldsymbol{\Upsilon}_{\mathbf{I}_{B1}\mathbf{I}_{H1}}). \tag{3.36}$$

By inserting (3.35) into (3.34), we can simplify the BLUE receiver to be

$$\begin{aligned} \hat{\theta}_1(m) &= [\mathbf{A}_1\mathbf{U}_1^H\mathbf{F}_1^{-1}\mathbf{U}_1\mathbf{A}_1]^{-1}\mathbf{A}_1\mathbf{U}_1^H\mathbf{F}_1^{-1}[\mathbf{H}_1^H - \boldsymbol{\Upsilon}^H_{\mathbf{I}_{B1}\mathbf{I}_{H1}}\mathbf{K}^{-1}_{\mathbf{I}_{B1}}\mathbf{B}_1]\mathbf{y}(m) \\ &= \mathbf{A}_1^{-1}\mathbf{U}_1^{-1}[\mathbf{H}_1^H - \boldsymbol{\Upsilon}^H_{\mathbf{I}_{B1}\mathbf{I}_{H1}}\mathbf{K}^{-1}_{\mathbf{I}_{B1}}\mathbf{B}_1]\mathbf{y}(m) \\ &= \mathbf{A}_1^{-1}\mathbf{U}_1^{-1}[\mathbf{d}_1 - \boldsymbol{\Upsilon}^H_{\mathbf{I}_{B1}\mathbf{I}_{H1}}\mathbf{K}^{-1}_{\mathbf{I}_{B1}}\mathbf{y}_1], \end{aligned} \tag{3.37}$$

where $\mathbf{d}_1 \equiv \mathbf{H}_1^H\mathbf{y}$ and $\mathbf{y}_1 \equiv \mathbf{B}_1\mathbf{y}$. Since $\mathbf{B}_1^H \perp \mathbf{H}_1$, we have

$$\begin{aligned} \mathbf{K}_{\mathbf{I}_{B1}} &= E(\mathbf{B}_1\mathbf{I}_1\mathbf{I}_1^H\mathbf{B}_1^H) = E[\mathbf{B}_1(\mathbf{S}_{1+}\mathbf{A}_1\Gamma_1 b_1 + \mathbf{I}_1)(\mathbf{S}_{1+}\mathbf{A}_1\Gamma_1 b_1 + \mathbf{I}_1)^H\mathbf{B}_1^H] \\ &= E(\mathbf{B}_1\mathbf{y}\mathbf{y}^H\mathbf{B}_1^H) \equiv \mathbf{R}_{\mathbf{y}_1}. \end{aligned} \tag{3.38}$$

Based on similar arguments, we can get

$$\begin{aligned} \boldsymbol{\Upsilon}_{\mathbf{I}_{B1}\mathbf{I}_{H1}} &= E(\mathbf{B}_1\mathbf{I}_1\mathbf{I}_1^H\mathbf{H}_1) = E[\mathbf{B}_1\mathbf{y}(\mathbf{y} - \mathbf{S}_{1+}\mathbf{A}_1\Gamma_1 b_1)^H\mathbf{H}_1] \\ &= E(\mathbf{y}_1\mathbf{d}_1^H) - \mathbf{B}_1E(\mathbf{y})b_1^*\Gamma_1^H\mathbf{A}_1\mathbf{S}_{1+}^H\mathbf{H}_1 \equiv \boldsymbol{\Upsilon}_{\mathbf{y}_1\mathbf{d}_1}. \end{aligned} \tag{3.39}$$

The above derivation is based on the fact that

$$\mathbf{B}_1 E(\mathbf{y}) = \mathbf{B}_1 \mathbf{S}_{1+} \mathbf{A}_1 \Gamma_1 b_1 = \mathbf{B}_1^H \mathbf{H}_1 \mathbf{U}_1 \mathbf{A}_1 \Gamma_1 b_1 = 0, \tag{3.40}$$

and

$$\mathbf{R}_{\mathbf{d}_1} = \mathbf{U}_1 \mathbf{A}_1^2 \mathbf{U}_1^H + \mathbf{K}_{\mathbf{I}_{H1}}. \tag{3.41}$$

By inserting these expressions into (4.6), we have

$$\mathbf{F}_1 = \mathbf{K}_{\mathbf{I}_{H1}} - \mathbf{\Upsilon}_{\mathbf{y}_1\mathbf{d}_1}^H \mathbf{R}_{\mathbf{y}_1}^{-1} \mathbf{\Upsilon}_{\mathbf{y}_1\mathbf{d}_1} = \mathbf{E}_1 - \mathbf{U}_1 \mathbf{A}_1^2 \mathbf{U}_1^H. \tag{3.42}$$

By using (3.37), (3.38) and (3.39), the BLUE estimate can be expressed as

$$\hat{\theta}_1(m) = \mathbf{A}_1^{-1} \mathbf{U}_1^{-1} [\mathbf{d}_1 - \mathbf{\Upsilon}_{\mathbf{y}_1\mathbf{d}_1}^H \mathbf{R}_{\mathbf{y}_1}^{-1} \mathbf{y}_1], \tag{3.43}$$

where $\omega_1 \equiv \mathbf{R}_{\mathbf{y}_1}^{-1} \mathbf{\Upsilon}_{\mathbf{y}_1\mathbf{d}_1}$ is the MMSE filter bank that minimizes $E\|\mathbf{d}_1 - \omega_1^H \mathbf{y}_1\|^2$.

Recall that, in the multistage implementation of the MMSE/MOE filter banks, the filter bank ω_1 is exactly the same as that in (3.9). Thus, the multistage implementation of the BLUE filter bank has the same structure as that of MMSE/MOE-FBs modulo a constant matrix $\mathbf{A}_1^{-1} \mathbf{U}_1^{-1}$. The implementation is also shown in Fig. 3.1.

Now, we have the MS-BLUE-FB as an unbiased channel estimator for $\Gamma_1 b_1$. It is not difficult to show that covariance matrices for MS-MMSE/MOE/BLUE-FBs conditioned on $\Gamma_1 b_1$ are given by

$$Cov[z_{mmse}|\Gamma_1 b_1] = \mathbf{A}_1\mathbf{U}_1^H\mathbf{E}_1^{-1}\mathbf{U}_1\mathbf{A}_1 - (\mathbf{A}_1\mathbf{U}_1^H\mathbf{E}_1^{-1}\mathbf{U}_1\mathbf{A}_1)^2. \quad (3.44)$$

$$Cov[z_{moe}|\Gamma_1 b_1] = \mathbf{A}_1\mathbf{U}_1^H\mathbf{E}_1\mathbf{U}_1\mathbf{A}_1 - (\mathbf{A}_1\mathbf{U}_1^H\mathbf{U}_1\mathbf{A}_1)^2. \quad (3.45)$$

$$Cov[z_{blue}|\Gamma_1 b_1] = \mathbf{A}_1^{-1}\mathbf{U}_1^{-H}\mathbf{E}_1\mathbf{U}_1^{-H}\mathbf{A}_1^{-1} - \mathbf{I}, \quad (3.46)$$

Perform the singular value decomposition (SVD) for $\mathbf{A}_1\mathbf{U}_1^H\mathbf{E}_1^{-1}\mathbf{U}_1\mathbf{A}_1$, such that $\mathbf{A}_1\mathbf{U}_1^H\mathbf{E}_1^{-1}\mathbf{U}_1\mathbf{A}_1 = \mathbf{Q}\Lambda\mathbf{Q}^H$, and invoke the positive definiteness of a covariance matrix. With (3.44), it is straightforward to show that $\mathbf{0} \leq \Lambda \leq \mathbf{I}$. Thus, we have

$$\begin{aligned} Cov[z_{blue}|\Gamma_1 b_1] - Cov[z_{mmse}|\Gamma_1 b_1] &= \mathbf{Q}(\Lambda^2 - \Lambda - \mathbf{I} + \Lambda^{-1})\mathbf{Q}^H \\ &= \mathbf{Q}[\Lambda^{-1}(\Lambda + \mathbf{I})(\Lambda - \mathbf{I})^2]\mathbf{Q}^H \geq \mathbf{0}. \end{aligned} \quad (3.47)$$

As a result, the variance of the BLUE estimator is larger than that of the MMSE estimator, although it is unbiased. The use of these estimators depends on the sensitivity of a particular application is to the bias or the variance effect. Both these effects will be studied via computer simulation in Section 4.3 in the context of adaptive coherent detection for BPSK and non-coherent detection for DBPSK.

3.5 Differential Equal Gain Combining of Blind ML-FB

For non-coherent equal gain combining, we need another filter bank to serve as a multiuser detector. Although BLUE-FB can also be viewed as a detector for MS MMSE/MOE FBs, it is worthwhile to examine a multistage implementation for the ML multiuser detector, since the ML detector maximizes the output SINR conditioned on the channel vector Γ_1 [9].

Consider the blind ML multiuser detection where, the aggregation of MAI, ISI and AWGN channel noise is modeled as a Gaussian distributed interference vector $\mathbf{I}$ as given in (3.13). Furthermore, $\Gamma_1 b_1$ is treated as a deterministic unknown vector. The probability density function for the received signal $\mathbf{y}$ is of the form

$$\mathcal{P}(\mathbf{y}) = \frac{1}{(2\pi)^N \det(\mathbf{C}_1)} \exp\left\{-(\mathbf{y} - \mathbf{S}_{1+}\mathbf{A}_1\Gamma_1 b_1)^H \mathbf{C}_1^{-1}(\mathbf{y} - \mathbf{S}_{1+}\mathbf{A}_1\Gamma_1 b_1)\right\}. \quad (3.48)$$

The maximum likelihood symbol detector is given by

$$\hat{b}_1(m) = \text{sgn}\{Re[\Gamma_1^H(m)\mathbf{A}_1\mathbf{S}_{1+}^H\mathbf{C}_1^{-1}\mathbf{y}(m)]\} \equiv \text{sgn}\{Re[\Gamma_1(m)^H\omega_{ml}^H(m)\mathbf{y}(m)]\}. \quad (3.49)$$

Similarly, for the transformed signal $\mathbf{Ty}$, the soft output of the ML filter bank is given by

$$\mathbf{z}_{ml} = \mathbf{A}_1\mathbf{S}_{1+}^H\mathbf{T}^H(\mathbf{T}\mathbf{C}_1\mathbf{T}^H)^{-1}\mathbf{T}\mathbf{y} = \mathbf{A}_1\mathbf{U}_1^H\mathbf{F}_1^{-1}[\mathbf{d}_1 - \boldsymbol{\Upsilon}_{\mathbf{y}_1\mathbf{d}_1}^H\mathbf{R}_{\mathbf{y}_1}^{-1}\mathbf{y}_1], \quad (3.50)$$

where results from Eqs (3.35) to (4.7) are used in the above simplification steps, and $\mathbf{F}_1 = (\mathbf{E}_1 - \mathbf{U}_1\mathbf{A}_1^2\mathbf{U}_1^H)^{-1}$, [*cf.* (4.7)]. The same multistage structure for MMSE-FB also applies to the blind ML detector by replacing the output scaling matrix $\mathbf{E}_1$ with $\mathbf{F}_1$. It is interesting to point out the differences between the MS MMSE/MOE/ML multiuser detectors and the BLUE channel estimator/detector. The soft outputs for their multistage implementations are given by

$$\mathbf{z}_{mmse} \equiv \omega_{mmse}^H\mathbf{T}\mathbf{y} = \mathbf{A}_1\mathbf{U}_1^H\mathbf{E}_1^{-1}[\mathbf{d}_1 - \boldsymbol{\Upsilon}_{\mathbf{y}_1\mathbf{d}_1}^H\mathbf{R}_{\mathbf{y}_1}^{-1}\mathbf{y}_1] \quad (3.51)$$

$$\mathbf{z}_{moe} \equiv \omega_{moe}^H\mathbf{T}\mathbf{y} = \mathbf{A}_1\mathbf{U}_1^H[\mathbf{d}_1 - \boldsymbol{\Upsilon}_{\mathbf{y}_1\mathbf{d}_1}^H\mathbf{R}_{\mathbf{y}_1}^{-1}\mathbf{y}_1] \quad (3.52)$$

$$\mathbf{z}_{ml} \equiv \omega_{ml}^H\mathbf{T}\mathbf{y} = \mathbf{A}_1\mathbf{U}_1^H\mathbf{F}_1^{-1}[\mathbf{d}_1 - \boldsymbol{\Upsilon}_{\mathbf{y}_1\mathbf{d}_1}^H\mathbf{R}_{\mathbf{y}_1}^{-1}\mathbf{y}_1] \quad (3.53)$$

$$\mathbf{z}_{blue} \equiv \omega_{blue}^H\mathbf{T}\mathbf{y} = \mathbf{A}_1^{-1}\mathbf{U}_1^{-1}[\mathbf{d}_1 - \boldsymbol{\Upsilon}_{\mathbf{y}_1\mathbf{d}_1}^H\mathbf{R}_{\mathbf{y}_1}^{-1}\mathbf{y}_1]. \quad (3.54)$$

These four filter banks can only be distinguished by their output scaling matrix. The BLUE estimator is essentially the minimum variance unbiased estimator as well as the ML estimator for the Gaussian linear system model, whether matrix $\mathbf{T}$ is

unitary, full-rank or not. Together with the ML multiuser detector, we propose a non-coherent multiuser detector with the decision statistic given by

$$\varphi(m) = Re\{\mathbf{z}_{blue}(m-1)^H \mathbf{z}_{ml}(m)\}. \tag{3.55}$$

The receiver scheme is referred to as the equal gain combining of the ML filter banks (EGC-ML-FB). The implementation of this scheme is just to replace the matrices $\mathbf{C}_1$ and $\mathbf{C}_2$ in Fig. 1.1 with $\mathbf{A}_1^{-1}\mathbf{U}_1^{-1}$ and $\mathbf{A}_1\mathbf{U}_1^H\mathbf{F}_1^{-1}$, respectively. In contrast with the EGC MMSE/MOE/BLUE filter banks where two consecutive outputs of the same filter bank are combined with equal gain, EGC-ML-FB results in a heterogenous combining of two different filter banks' outputs.

3.6 Reduced-Rank Multistage Filter Banks

3.6.1 Multistage MRC/EGC Filter banks for Coherent/ Non-Coherent Detection

To improve the tracking performance and reduce the variance of the estimation error [14], reduced-rank implementations are often used. The subspace spanned by reduced-rank MSWF was studied in [12]. Later, the performance of MSWF was shown to be independent of the choice of the block matrix $\mathbf{B}_1$ in [3]. For multistage filter banks presented in this work, the reduced-rank implementations follow the

same rule as MSWF by keeping the first D stages of multistage filter banks. The subspaces spanned by the reduced-rank MS filter banks are the same, since these filter banks share a common structure. The common subspace is given by Proposition 1, and the proof is given in Appendix A.1. The subspace can be considered as a generalized version of the subspace spanned by MSWF given in [12].

Proposition 1 *The subspace for the multistage MMSE/MOE/BLUE/ML filter banks is characterized by the following properties.*

1. If the block matrix $\mathbf{B}_i$ *at each stage* i *as shown in Fig. 3.1 is taken to be* $\mathbf{B}_i^{N\times N} \equiv \mathbf{I} - \mathbf{H}_i\mathbf{H}_i^H$*, the matched filter banks* $\mathbf{H}_i^{N\times L}$ *at each stage* i *is given by*

$$\begin{aligned} \mathbf{H}_i^{N\times L}\mathbf{U}_i^{L\times L} &= E(\mathbf{y}_{i-1}\mathbf{d}_{i-1}^H) = \mathbf{B}_{i-1}E(\mathbf{y}_{i-2}\mathbf{y}_{i-2}^H)\mathbf{H}_{i-1} \\ &= \prod_{j=(i-1)}^{1}(\mathbf{I}-\mathbf{H}_j\mathbf{H}_j^H)\mathbf{R}\mathbf{H}_{i-1}, \quad i = 2\ldots D \\ \mathbf{H}_1\mathbf{U}_1 = \mathbf{S}_{1+}\mathbf{A}_1 \quad & \textit{and} \quad \mathbf{H}_i^H\mathbf{H}_i = \mathbf{I}, \quad \mathbf{H}_i \perp \mathbf{H}_j,\ i \neq j, \quad i = 1\ldots D, \end{aligned} \tag{3.56}$$

where $\mathbf{y}_i = \mathbf{B}_i\mathbf{y}_{i-1}$, $\mathbf{d}_i = \mathbf{H}_i^H\mathbf{y}_{i-1}$, *and* $\mathbf{y}_0 = \mathbf{y}$.

2. The subspace $\mathcal{T}_{LD}$ *spanned by the reduced-rank filter banks of* D *stages is equal to the row space of the transformation matrix,* $\mathbf{T}_{LD} : (N \times DL)$*, given by*

$$\mathcal{T}_{LD}\ \textit{span}\ \mathbf{T}_{LD}^H = \left[\mathbf{H}_1|\ \mathbf{B}_1\mathbf{H}_2|\ \ldots\ |\prod_{i=1}^{D-1}\mathbf{B}_i\mathbf{H}_D\right] = [\mathbf{H}_1|\ \mathbf{H}_2|\ \ldots\ |\ \mathbf{H}_D]\,. \tag{3.57}$$

The reduced-rank implementations of MS MMSE/MOE/BLUE/ML filter banks are equivalent to replacing the transformation matrix $\mathbf{T}$ in (3.4), (3.22), (3.34) and (3.50) by $\mathbf{T}_{LD}$.

3.6.2 Multistage Pre-Combining Filters for Coherent Detection

If the target user's channel parameter Γ_1 is available, then coherent MRC can be employed for symbol detection. For MS-MOE and MS-BLUE filter banks, Equations (3.25) and (3.43) can be further simplified by merging the channel parameter Γ_1 with the output scaling matrix by using the fact that $\mathbf{A}_1$ and $\mathbf{U}_1$ are constant matrices as given below.

$$z_{moe} = \Gamma_1^H \mathbf{A}_1 \mathbf{U}_1^H \left[\mathbf{d}_1 - \boldsymbol{\Upsilon}_{\mathbf{y}_1\mathbf{d}_1}^H \mathbf{R}_{\mathbf{y}_1}^{-1} \mathbf{y}_1\right] = [d_{11} - \underline{\omega}_{11}^H \mathbf{y}_1], \tag{3.58}$$

$$z_{blue} = \Gamma_1^H \mathbf{A}_1^{-1} \mathbf{U}_1^{-H} \left[\mathbf{d}_1 - \boldsymbol{\Upsilon}_{\mathbf{y}_1\mathbf{d}_1}^H \mathbf{R}_{\mathbf{y}_1}^{-1} \mathbf{y}_1\right] = [d_{12} - \underline{\omega}_{12}^H \mathbf{y}_1], \tag{3.59}$$

where $d_{11} \equiv \Gamma_1^H \mathbf{A}_1 \mathbf{U}_1^H \mathbf{H}_1^H \mathbf{y}$, $d_{12} \equiv \Gamma_1^H \mathbf{A}_1^{-1} \mathbf{U}_1^{-H} \mathbf{H}_1^H \mathbf{y}$, $\underline{\omega}_{11} \equiv \mathbf{R}_{\mathbf{y}_1}^{-1} E(\mathbf{y}_1 d_{11}^*)$ and $\underline{\omega}_{12} \equiv \mathbf{R}_{\mathbf{y}_1}^{-1} E(\mathbf{y}_1 d_{12}^*)$. The MRC MOE/BLUE filter banks with the steering matrix $\mathbf{H}_1$ are equivalent to filters obtained by using the pre-combining (PC) steering vectors $\Gamma_1^H \mathbf{A}_1 \mathbf{U}_1^H \mathbf{H}_1^H$ and $\Gamma_1^H \mathbf{A}_1^{-1} \mathbf{U}_1^{-H} \mathbf{H}_1^H$ of dimension $N \times 1$, respectively. They are referred to as the pre-combining (PC) MOE/BLUE filters. Their multistage implementations are shown in Fig. 3.2.

Based on a similar procedure in proving Proposition 1, it is straightforward to show that the subspaces, defined by $\mathcal{T}^H_{L+D-1}$, spanned by the reduced-rank PC MOE/BLUE filters of D stages are given by

$$\begin{aligned}
\mathcal{T}_{L+D-1} \quad \text{span} \quad & \mathbf{T}^H_{L+D-1} = [\mathbf{H}_1|\ \mathbf{h}_2|\ \dots\ |\ \mathbf{h}_D] \\
\mathbf{h}_i^{N\times 1}\delta_i \quad = \quad & E(\mathbf{y}_{i-1}d^*_{i-1}) = \mathbf{B}_{i-1}E(\mathbf{y}_{i-2}\mathbf{y}^H_{i-2})\mathbf{h}_{i-1} \\
= \quad & \prod_{j=(i-1)}^{2}(\mathbf{I}-\mathbf{h}_j\mathbf{h}_j^H)(\mathbf{I}-\mathbf{H}_1\mathbf{H}_1^H)\mathbf{R}\mathbf{h}_{i-1}, \quad i=2\dots D \\
\text{and} \quad & \mathbf{h}_i^H\mathbf{h}_i = 1, \quad \mathbf{h}_i \perp \mathbf{H}_1,\ \forall\ i,\ \&\ \mathbf{h}_i \perp \mathbf{h}_j,\ i\neq j,
\end{aligned} \tag{3.60}$$

where $\mathbf{B}_1 = (\mathbf{I}-\mathbf{H}_1\mathbf{H}_1^H)$ and $\mathbf{B}_i = (\mathbf{I}-\mathbf{h}_i\mathbf{h}_i^H),\ i=2,\cdots D$. Note that the subspaces for these two filters differ in the second stage, since the steering vector is equal to $\mathbf{h}_1\delta_1 = \mathbf{H}_1\mathbf{U}_1\mathbf{A}_1\Gamma_1$ and $\mathbf{h}_1\delta_{blue} = \mathbf{H}_1\mathbf{U}_1^{-1}\mathbf{A}_1^{-1}\Gamma_1$ for PC-MOE and PC-BLUE filters, respectively. The rank for each vector $\mathbf{h_i},\ i=2\dots D$ is one. The total rank of the PC MOE/BLUE filters becomes $L+D-1$ instead of LD as for the MRC MOE/BLUE FBs.

For the case of MMSE/ML filter banks, the output scaling matrices are $\mathbf{E}_1$ in (4.6) for the MMSE filter bank, and $\mathbf{F}_1$ in (4.7) for the ML filter bank. Both of them are functions of $\mathbf{R}$ and the number of stages applied, which is translated into the rank of $\mathbf{T}$. Therefore, the pre-combining (PC) MMSE/ML filters are different from the MRC MMSE/ML FBs. The PC-MMSE filter is exactly the MSWF proposed in [8] with the steering vector equal to $\mathbf{h}_1\delta_1 = \mathbf{S}_{1+}A_1\Gamma_1$. The PC-ML filter is

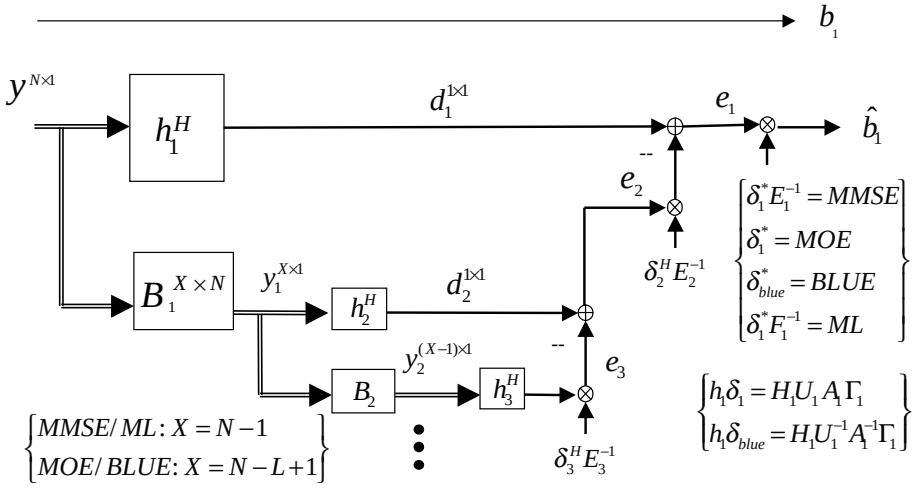

Figure 3.2: The structure of the pre-combining (PC) MMSE/MOE/ML/BLUE filters, where $\mathbf{h}_1\delta_1 = \mathbf{S}_{1+}\mathbf{A}_1\Gamma_1$ for the PC MMSE/MOE/ML filters and $\mathbf{h}_1\delta_{blue} = \mathbf{H}_1\mathbf{U}_1^{-1}\mathbf{A}_1^{-1}\Gamma_1$ for the PC-BLUE filter. The dimension of the blocking matrix $\mathbf{B}_1$ is $(N-1)\times N$ for the PC MMSE/ML filters and $(N-L+1)\times N$ for the PC MOE/BLUE filters. The output scaling value is $\delta_1^*\mathbf{E}_1^{-1}$ for the PC-MMSE filter, δ_1^* for the PC-MOE, δ_{blue}^* for the PC-BLUE and $\delta_1^*\mathbf{F}_1^{-1}$ for the PC-ML filter. The object for channel estimation is b_1.

equal to the MSWF by replacing the output scaling $\mathbf{F}_1$ with $\mathbf{E}_1$. Their multistage implementations are also shown in Fig. 3.2. The subspace $\mathcal{T}_D$ spanned by the D-stage implementations is given in [12], as

$$\mathcal{T}_D \ \text{ span } \ \mathbf{T}_D^H = [\mathbf{h}_1|\ \mathbf{h}_2|\ \ldots\ |\ \mathbf{h}_D]\,,\ \mathbf{h}_1\delta_1 = \mathbf{S}_{1+}A_1\Gamma_1. \tag{3.61}$$

The total rank of the reduced-rank PC MMSE/ML filters is D. The extra dimensions for the reduced-rank PC MOE/BLUE filters are used to meet the constraints for optimization. As a result, with the knowledge of the target user's fading coefficients Γ_1, the ranks of the MRC MMSE/ML filters and the MRC MOE/BLUE filters

drastically reduce from LD to D and $L+D-1$, respectively, without affecting the receiver's steady state performance. More importantly, the output SINRs of the pre-combining filters converge faster than that of the MRC filter banks as will be shown in simulation results. This will enhance receivers' performance in non-stationary fading channels and/or system loadings.

3.7 Simulation Results

Simulations have been conducted to study the performance of the multistage MRC MMSE/MOE/BLUE/ML FBs for coherent detection of BPSK modulated DS-CDMA systems and the performance of the multistage EGC MMSE/MOE/BLUE/ML FBs for non-coherent detection of DBPSK modulated systems. A short-code DS-CDMA system with spreading gains $N = 31$ or $N = 64$ is adapted. The signature sequences are either randomly generated for investigating the average output SINRs, or randomly chosen from a set of Gold codes to demonstrate BER performance. The simulation channel for each user is a 3-path (i.e. $L = 3$) Rayleigh fading channel with the normalized Doppler shift $f_d T_s = 5 \times 10^{-3}$. The path delay τ_{kl} for each user is randomly generated with uniform distribution over $[0, 2T_s)$ subject to the constraint that the delay spread $|\max_l\{\tau_{kl}\} - \min_l\{\tau_{kl}\}| < \tau_{max}$, where $\tau_{max} \leq T_s$ is defined as the maximum allowable delay spread for all users and serve as an experimental parameter for investigating detectors' performance. The sensitivities of

the output SINRs to different amount of maximum delay spreads τ_{max} are investigated by simulations and presented in the following results. There are a total of 10 users in the system and all are assumed to have the same received power with E_b/N_0 equal to 20dB in all simulation studies for output SINRs. Finally, the adaptive autocorrelation matrix of $\mathbf{R}$ is learned by $\widehat{\mathbf{R}}(m) = \lambda\widehat{\mathbf{R}}(m-1) + \mathbf{y}(m)\mathbf{y}^H(m),\ \lambda = 0.995$.

One important feature for the multistage MMSE-based filters is the fast convergence of output SINRs to steady-state values. With more ranks applied to their reduced-rank implementations, the output SINRs are expected to achieve higher level of steady-state values, but with slower convergence, on the contrary. As have been shown in Section 3.6.2, if the parameter vector Γ_1 of a fading channel is given, it can be somehow combined with the steering matrix $\mathbf{H}_1$ to form the PC MMSE/MOE/BLUE/ML filters. The ranks of the D-stage implementations of the MRC MMSE/ML FBs drop from $D \times L$ to D for the PC MMSE/ML filters, and it also drops to $D+L-1$ for the PC MOE/BLUE filters. Fig. 3.3 shows the convergence of the output SINRs for the adaptive reduced-rank MRC MMSE/MOE/BLUE/ML FBs of 6 stages ($D = 6$) versus the convergence of their pre-combining counterparts of the same stages. The spreading gain N is equal to 64, and the spreading sequences are randomly generated for each Monte-Carlo run to eliminate the performance dependence on a specific spreading code. The convergence of the PC filters are obviously faster than that of the MRC filter banks. However, the steady-state SINRs are the same for these two types of filters as shown in Section 3.6.2.

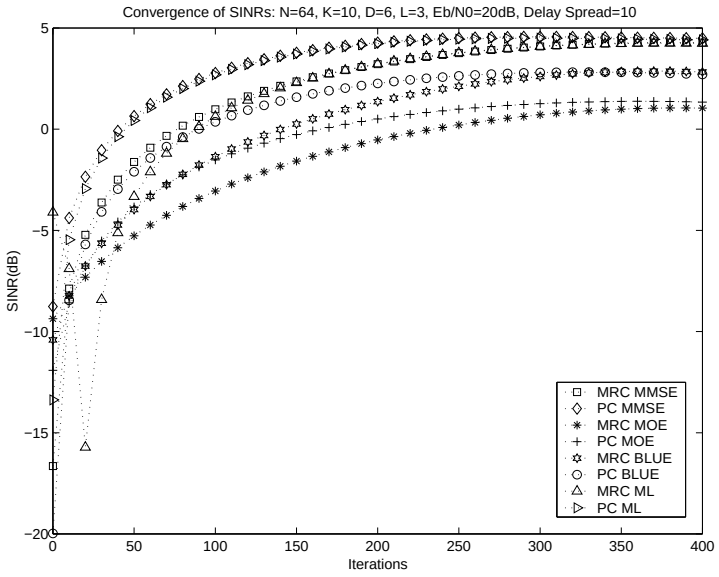

Figure 3.3: Convergence characteristics of the output SINRs of MRC schemes with respect to the number of samples for BPSK modulated signal over a Rayleigh fading channel with $L = 3$ and $f_d T_s = 5 \times 10^{-3}$. The maximum allowable delay spread $\tau_{max} = 10$ chips for all users and K=10. $D = 6$ for all reduced-rank filter banks.

The steady-state output SINRs with respect to the number of stages for the reduced-rank implementations of the MMSE/MOE/BLUE/ML FBs are also studied by simulations for both the cases of BPSK and DBPSK. The spreading gain $N = 31$, and the spreading sequences are also randomly generated for each Monte-Carlo run. Fig. 3.4 shows the steady-state output SINRs of the MRC MMSE/MOE/BLUE/ML FBs for coherent detection of BPSK vs. the number of stages. The channel coefficient vector Γ_1 is assumed given, and the maximum allowable delay $\tau_{max} = 10$ chips. The total rank is equal to $D \times L$, $D = 11$ actually corresponds to the full-rank implementation ($N = 31$). It is obvious that MMSE/ML FBs perform equally well and much better than the other two, since they both, as detectors, maximize the

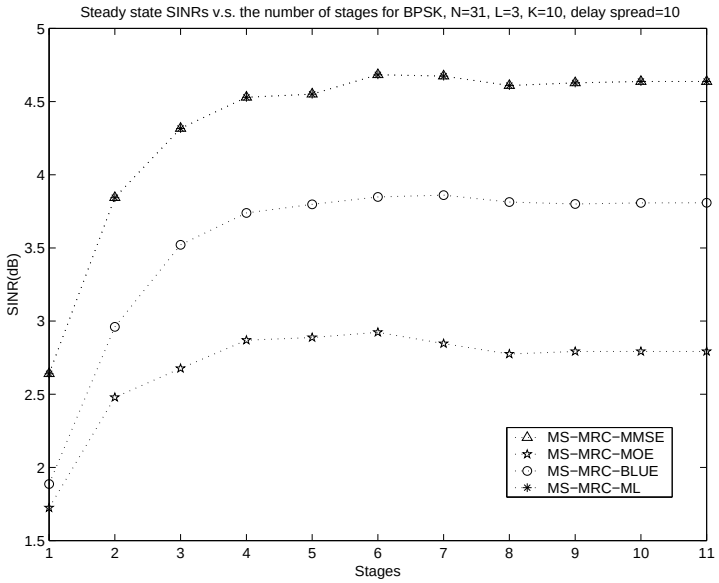

Figure 3.4: Steady state output SINRs of the adaptive reduced-rank MRC filter banks vs. the number of stages for BPSK modulated signals over a Rayleigh fading channel with $L = 3$ and $f_d T_s = 5 \times 10^{-3}$. Stage 11 in the plot actually corresponds to the full-rank (N=31) SINRs. $\tau_{max} = 10$ chips for all users and K=10.

output SINR. The full-rank SINRs can virtually be attained by 6-stage reduced-rank implementations.

The output SINRs of the EGC MMSE/MOE/BLUE/ML FBs for non-coherent detection of DBPSK vs. the number of stages are shown in Fig. 3.5. The simulation setup is the same as that for BPSK. In this case, the soft outputs of the previous symbol interval play the role of the channel estimators for $\Gamma_1 d_1$, and the current outputs serve as the symbol detectors. In contrast to the MRC-MMSE-FB, the output SINR of the EGC-MMSE-FB performs worst among the EGC filter banks. The output SINR degrades by 4.6 dB than its MRC counterpart and ,however,

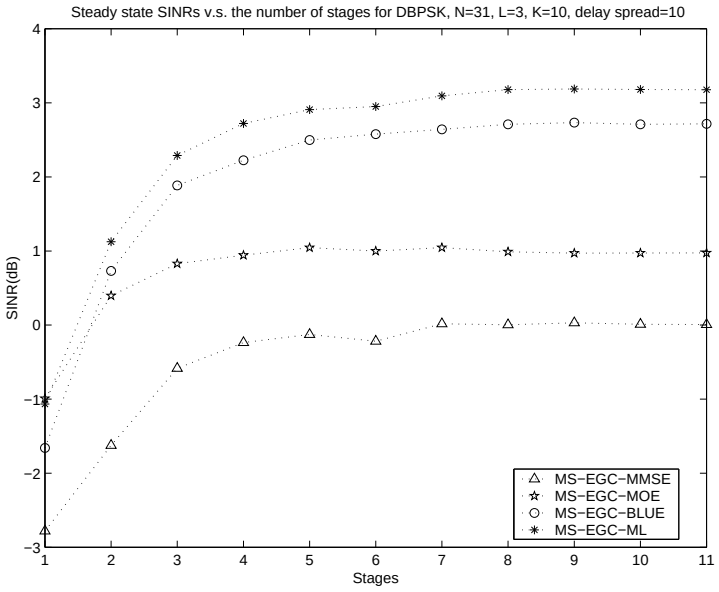

Figure 3.5: Steady state output SINRs of the adaptive reduced-rank EGC filter banks vs. the number of stages for DBPSK modulated signals over a Rayleigh fading channel with $L = 3$ and $f_d T_s = 5 \times 10^{-3}$. Stage 11 in the plot actually corresponds to the full-rank (N=31) SINRs. $\tau_{max} = 10$ chips for all users and K=10.

the output SINR of the EGC-ML-FB degrades by only 1.4 dB than the MRC-ML-FB which performs equally well as the MRC-MMSE-FB. Due to the fact that the variance of the MMSE estimator Γ_1 is smaller than that of the BLUE estimator [cf. (3.47)], this simulation result reveals that the detection performance in multipath fading channel is more sensitive to the bias of the channel estimates rather than variance. The EGC BLUE/ML FBs, both with unbiased BLUE estimator for $\Gamma_1 d_1$, suffer much less performance degradation than do the EGC MMSE/MOE FBs.

To evaluate the impact of delay spreads or , in other words, the strength of ISI on the performance of one-shot detection, the sensitivities of the full-rank output SINRs to the maximum allowable delay τ_{max} are characterized via simulation studies. For

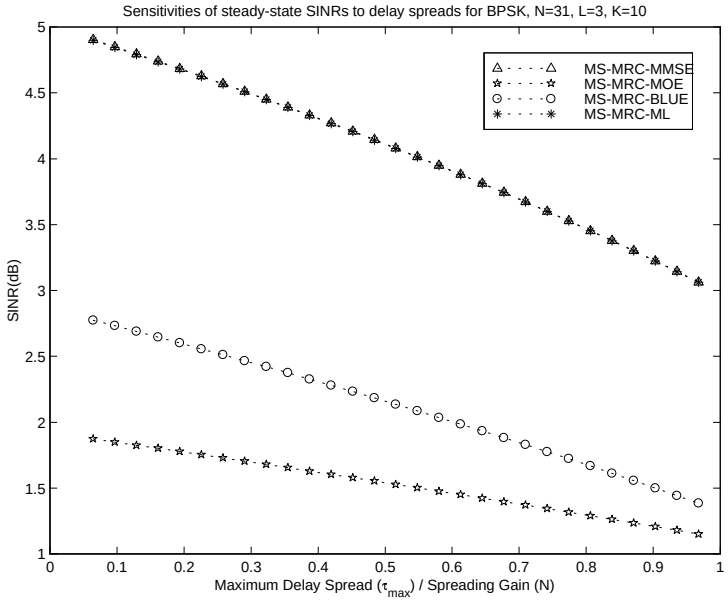

Figure 3.6: Steady state output SINRs of the adaptive full-rank MRC filter banks vs. the maximum allowable delay spread for BPSK modulated signal over a Rayleigh fading channel with $L = 3$ and $f_d T_s = 5 \times 10^{-3}$. τ_{max} ranges from 2 to N chips times.

each Monte-Carlo run of each value of τ_{max}, the spreading sequences are randomly generated with $N = 31$, and the path delay for each user is also randomly generated for each run. The maximum allowable delay spread τ_{max} ranges from 2 to 30 chips in simulations.

Fig. 3.6 shows the result of the full-rank output SINRs for BPSK. The level of the SINRs seems to degrade linearly with respect to τ_{max} in logarithmic scale . The sensitivities of the output SINRs to τ_{max} for DBPSK is also presented in Fig. 3.7. Both results show that MS ML/BLUE FBs are more robust to delay spreads. Note that the maximum delay spread has to be greater than $(L-1)T_c$ to maintain the full column-rank (L) of $\mathbf{S}_{1+}$.

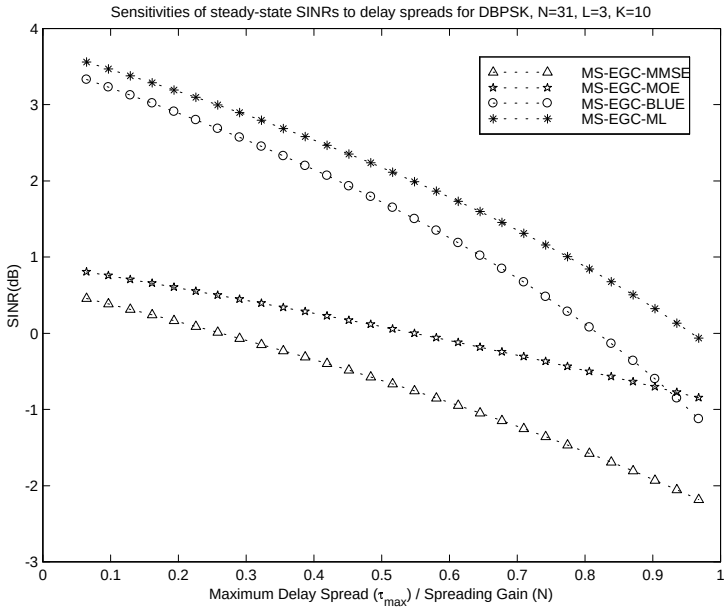

Figure 3.7: Steady state output SINRs of the adaptive full-rank EGC filter banks vs. the maximum allowable delay spread for DBPSK modulated signal over a Rayleigh fading channel with $L = 3$ and $f_d T_s = 5 \times 10^{-3}$. τ_{max} ranges from 2 to N chips times.

The BER performance for both of BPSK/DBPSK modulated systems are also given in Fig. 3.8 and Fig. 3.9, respectively. A Gold Code of length $N = 31$ is adopted for the simulations. For BPSK the performance of these filter banks are very close to each others, though the SINRs of the MRC MMSE/ML FBs outperform the other two in random code simulations. As implied by the results of the output SINRs for DBPSK, the EGC-ML-FB obviously outperforms the other filter banks, and the EGC-MMSE-FB is not suggested for non-coherent adaptive detection for DS-CDMA systems.

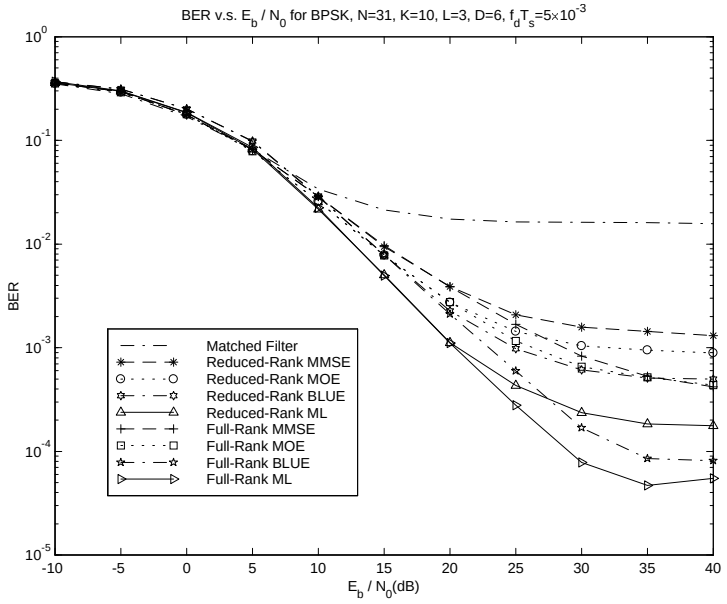

Figure 3.8: BER of the adaptive reduced-rank MRC filter banks for BPSK modulated signal over a Rayleigh fading channel with $L = 3$ and $f_dT_s = 5 \times 10^{-3}$. $\tau_{max} = 10$ chips. $D = 6$ for all reduced-rank filter banks.

3.8 Conclusion

A common framework for the multistage implementations of the reduced-rank MMSE, MOE, ML and BLUE filter banks has been developed in this chapter. Based on this common framework, the performance of a family of the MRC as well as the differential EGC schemes are examined in the context of coherent and non-coherent detection of DS-CDMA in multi-path fading channels. Simulation results show that the output SINRs of the reduced-rank filter banks can attain the full-rank performance with the number of stages $D = 6$. The output SINRs of the pre-combining filters can achieve the same levels of the performance of the MRC filter banks with much lower ranks, thus, faster convergence. Although the output SINRs of the

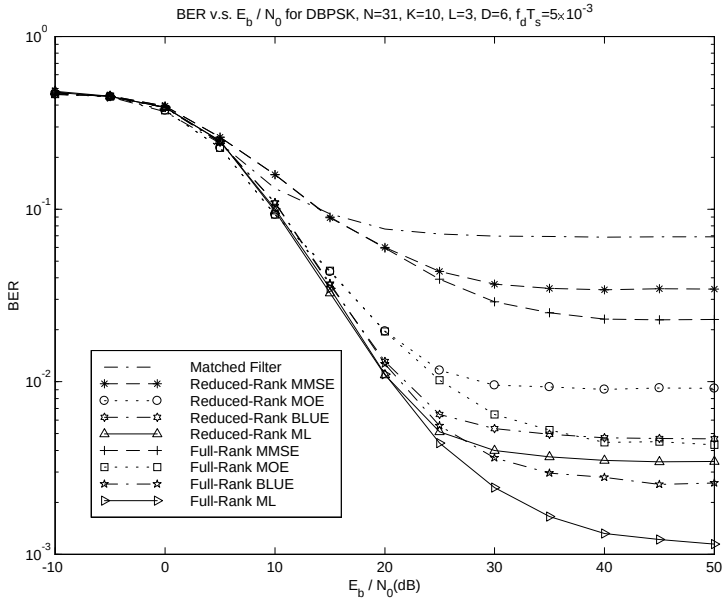

Figure 3.9: BER of the adaptive reduced-rank EGC filter banks for DBPSK modulated signal over a Rayleigh fading channel with $L = 3$ and $f_dT_s = 5 \times 10^{-3}$. $\tau_{max} = 10$ chips. $D = 6$ for all reduced-rank filter banks.

multistage MRC MMSE/ML FBs are the highest among the MRC filter banks, the bias effects of the MMSE/MOE FBs as channel estimators dominate the performance for non-coherent EGC schemes and thus cause significant performance degradation. Therefore the proposed EGC-ML-FB with unbiased BLUE channel estimator exhibits superior performance over the EGC MMSE/MOE FBs proposed in [21] without introducing any extra implementation efforts.

Chapter 4

Performance Analysis for Multistage MMSE-Based Receivers

The performance of the multistage MMSE-based filter banks are studied in this chapter. Under the common framework for multistage implementations, the output SINRs of the multistage MRC MMSE/MOE/BLUE/ML filter banks are characterized for multipath Rayleigh fading channels. A generic bit error rate (BER) formula is also provided for reduced-rank coherent and non-coherent differential detections using these filter banks. Consistent with the results of output SINRs, BERs using different filter banks are equal in flat fading channels for each class of detection schemes.

The output SINRs are shown monotonically increasing with the number of stages, and are upper bounded by a number equal the resolvable paths of the desired user's channel. The condition for asymptotically achieving the upper bound is provided as a testing threshold, D_{int}, for the existence of a BER floor of coherent detection. The

influence due to the channel mismatch of differential detection is also analyzed to form another controlling factor for the BER floor of non-coherent multiuser detection. Based on these analysis, a deterministic rule for choosing the number of stages is suggested: For systems having capacity to suppressed interference asymptotically, as low a number as to pass the threshold D_{int} is suggested. For highly loaded systems or channels with rich scattering such that the threshold is equal to the spreading gain, a stage of 6 is observed to nearly achieve the full-rank performance over a wide range of operating conditions.

4.1 Analysis of Steady-State Output SINRs

The steady-state output SINRs will be derived for the reduced-rank MRC filter banks in this section. The essence of reduced-rank filtering is to project the received signal vector onto a lower dimensional subspace, thus reducing the number of filter coefficients to be estimated. For the convenience of presentation, the reduced-rank MMSE-based filter banks are listed below using the transformation matrix $\mathbf{T}_{LD}$ given by (A.5).

$$\omega_{mmse} = \mathbf{R}_T^{-1}\mathbf{S}_T\mathbf{A}_1 \tag{4.1}$$

$$\omega_{moe} = \mathbf{R}_T^{-1}\mathbf{S}_T(\mathbf{S}_T^H\mathbf{R}_T^{-1}\mathbf{S}_T)^{-1}\mathbf{S}_T^H\mathbf{S}_T\mathbf{A}_1 \tag{4.2}$$

$$\omega_{blue} = \mathbf{C}_T^{-1}\mathbf{S}_T(\mathbf{S}_T^H\mathbf{C}_T^{-1}\mathbf{S}_T)^{-1} \tag{4.3}$$

$$\omega_{ml} = \mathbf{C}_T^{-1}\mathbf{S}_T\mathbf{A}_1, \tag{4.4}$$

where $\mathbf{R}_T \equiv \mathbf{T}_{LD}\mathbf{R}\mathbf{T}_{LD}^H$, $\mathbf{C}_T \equiv \mathbf{T}_{LD}\mathbf{C}\mathbf{T}_{LD}^H$ and $\mathbf{S}_T \equiv \mathbf{T}_{LD}\mathbf{S}_{1+}$ with $\mathbf{R}^{N\times N} \equiv E(\mathbf{y}\mathbf{y}^H)$ and $\mathbf{C}^{N\times N} \equiv E(\mathbf{I}_1\mathbf{I}_1^H)$.

It is shown in Chapter 3 that the above four filter banks share a common framework for multistage implementations modulo distinctive output scaling matrices. The common structure is shown in Fig. 4.1. The generic form for their soft outputs can be written as

$$\mathbf{z} \equiv \omega^H \mathbf{T}_{LD}\mathbf{y} = \mathbf{M}[\mathbf{d}_1 - \boldsymbol{\Upsilon}_{\mathbf{y}_1\mathbf{d}_1}^H \mathbf{R}_{\mathbf{y}_1}^{-1}\mathbf{y}_1], \tag{4.5}$$

where $\mathbf{d}_1^{L\times 1} \equiv \mathbf{H}_1^H\mathbf{y}$, $\mathbf{y}_1^{(D-1)L\times 1} \equiv \mathbf{B}_1\mathbf{y}$, $\mathbf{R}_{\mathbf{y}_1} \equiv E(\mathbf{y}_1\mathbf{y}_1^H)$, being the auto-correlation matrix of $\mathbf{y_1}$ and $\boldsymbol{\Upsilon}_{\mathbf{y}_1\mathbf{d}_1} \equiv E(\mathbf{y}_1\mathbf{d}_1^H)$, being the cross-correlation matrix of $\mathbf{y}_1$ and $\mathbf{d}_1$. For scaling matrices, $\mathbf{M} \equiv \mathbf{A}_1\mathbf{U}_1^H\mathbf{E}_1^{-1}$ for the MMSE filter bank, and is denoted as $\mathbf{M}_{mmse}$. Other scaling matrices are: $\mathbf{M}_{moe} \equiv \mathbf{A}_1\mathbf{U}_1^H$, $\mathbf{M}_{blue} \equiv \mathbf{A}_1^{-1}\mathbf{U}_1^{-1}$ and $\mathbf{M}_{ml} \equiv \mathbf{A}_1\mathbf{U}_1^H\mathbf{F}_1^{-1}$, where

$$\begin{aligned}
\mathbf{E}_1 &\equiv E[(\mathbf{d}_1 - \boldsymbol{\Upsilon}_{\mathbf{y}_1\mathbf{d}_1}^H \mathbf{R}_{\mathbf{y}_1}^{-1}\mathbf{y}_1)(\mathbf{d}_1 - \boldsymbol{\Upsilon}_{\mathbf{y}_1\mathbf{d}_1}^H \mathbf{R}_{\mathbf{y}_1}^{-1}\mathbf{y}_1)^H] \\
&= (\mathbf{R}_{\mathbf{d}_1} - \boldsymbol{\Upsilon}_{\mathbf{y}_1\mathbf{d}_1}^H \mathbf{R}_{\mathbf{y}_1}^{-1}\boldsymbol{\Upsilon}_{\mathbf{y}_1\mathbf{d}_1}) \qquad (4.6) \\
\mathbf{F}_1 &\equiv \mathbf{E}_1 - \mathbf{U}_1\mathbf{A}_1^2\mathbf{U}_1^H, \qquad (4.7)
\end{aligned}$$

with $\mathbf{R}_{\mathbf{d}_1} \equiv E(\mathbf{d}_1\mathbf{d}_1^H)$, being the auto-correlation matrix of $\mathbf{d_1}$. Obviously $\mathbf{E}_1$ is the error correlation matrix of the MMSE filtering with the filter $\omega_1 = \mathbf{R}^{-1}\boldsymbol{\Upsilon}_{\mathbf{y}_1\mathbf{d}_1}$.

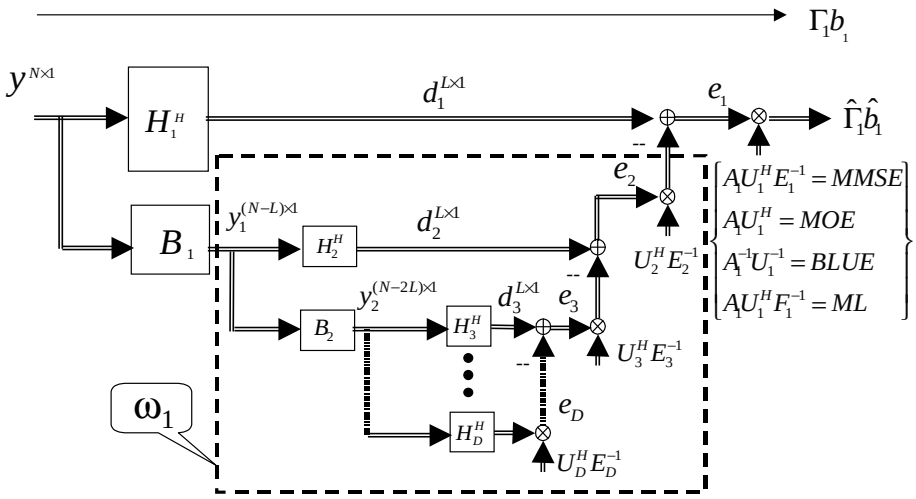

Figure 4.1: The common structure for the D-stage MMSE/MOE/BLUE/ML-FBs in multi-path fading channels. The output scaling matrix is $\mathbf{A}_1\mathbf{U}_1^H\mathbf{E}_1^{-1}$ for MS-MMSE-FB, $\mathbf{A}_1\mathbf{U}_1^H$ for MS-MOE-FB, $\mathbf{A}_1^{-1}\mathbf{U}_1^{-1}$ for MS-BLUE-FB and $\mathbf{A}_1\mathbf{U}_1^H\mathbf{F}_1^{-1}$ for MS-ML-FB.

For steady-state analysis, the auto-correlation matrix $\mathbf{R}$ of the received signal $\mathbf{y}$ of DS-CDMA in multipath Rayleigh fading channels is given by

$$\mathbf{R} = \sum_{k=1}^{K} \mathbf{S}_{k+}\mathbf{A}_k^2\mathbf{S}_{k+}^H + \mathbf{S}_{k-}\mathbf{A}_k^2\mathbf{S}_{k-}^H + N_0\mathbf{I}, \tag{4.8}$$

where $\mathbf{A}_k = \mathrm{diag}([A_{k1}, \ldots, A_{kL_k}])$, $\mathbf{S}_{k+} = [\mathbf{s}_{k1}^+, \ldots, \mathbf{s}_{kL_k}^+]$, $\mathbf{S}_{k-} = [\mathbf{s}_{k1}^-, \ldots, \mathbf{s}_{kL_k}^-]$. Substituting $\mathbf{R}$ back into Proposition 1 yields the reduced-rank transformation matrix, $\mathbf{T}_{LD}$. For the convenience of notation, $\mathbf{T}_{LD}$ is rewritten in the form of

$$\mathbf{T}^H \equiv [\mathbf{H}_1|\ \mathbf{H}_{1\perp}]\,, \quad \mathbf{H}_{1\perp}^{N\times(D-1)L} = [\mathbf{H}_2|\ \ldots\ |\ \mathbf{H}_D]\,. \tag{4.9}$$

where the subscription LD for indicating the rank of matrix is dropped. In the sequel, all operations are conducted with this more general reduce-rank transformed matrix $\mathbf{T}$. To indicate the total applying stages and to avoid the confusion with $\mathbf{E}_D$, which is the output auto-correlation matrix of the matched filter $\mathbf{H}_D$ in Fig 4.1, we use $\mathbf{S}_D$ and $\mathbf{F}_D$ to denote $\mathbf{E}_1$ and $\mathbf{F}_1$, respectively, for the D-stage implementations of filter banks, which are

$$\mathbf{S}_D = \mathbf{H}_1^H\mathbf{R}\mathbf{H}_1 - \mathbf{H}_1^H\mathbf{R}\mathbf{H}_{1\perp}(\mathbf{H}_{1\perp}^H\mathbf{R}\mathbf{H}_{1\perp})^{-1}\mathbf{H}_{1\perp}^H\mathbf{R}\mathbf{H}_1 \tag{4.10}$$

$$\mathbf{F}_D = \mathbf{S}_D - \mathbf{U}_1\mathbf{A}_1^2\mathbf{U}_1^H. \tag{4.11}$$

by replacing $\mathbf{B}_1^H$ with $\mathbf{H}_{1\perp}$ and $\mathbf{E}_1$ with $\mathbf{S}_D$ in (4.6) and (4.7).

4.1.1 Output SINRs of the MMSE-based filter banks

Based on the common multistage structure, we will derive SINRs of the MMSE-based filter banks for coherent multiuser detection of short-code DS-CDMA. A multi-path Rayleigh fading channel is assumed for each user. We start by looking for filter banks that can maximize SINR. This will be investigated in two perspectives: the instantaneous SINR v.s. the output SINR defined herein.

Conditioned on channel parameters, the filter bank which maximizes the instantaneous SINR is given by [9]

$$\arg\min_{\omega} \frac{E^2(\omega^H \mathbf{y}|\Gamma_1 b_1)}{Var(\omega^H \mathbf{y}|\Gamma_1 b_1)} = \arg\min_{\omega} \frac{\omega^H \mathbf{S}_{1+}\mathbf{A}_1\Gamma_1\Gamma_1^H\mathbf{A}\mathbf{S}_{1+}^H\omega}{\omega^H\mathbf{C}\omega}. \tag{4.12}$$

Let $\mathbf{x}_1 = \omega\mathbf{C}^{\frac{1}{2}}$ and $\mathbf{x}_2 = \mathbf{C}^{\frac{-1}{2}}\mathbf{S}_{1+}\mathbf{A}_1\Gamma_1$. By the Cauchy inequality

$$\frac{\omega^H \mathbf{S}_{1+}\mathbf{A}_1\Gamma_1\Gamma_1^H\mathbf{A}\mathbf{S}_{1+}^H\omega}{\omega^H\mathbf{C}\omega} = \frac{\|\mathbf{x}_1^H\mathbf{x}_2\|^2}{\|\mathbf{x}_1\|^2} \leq \frac{\|\mathbf{x}_1\|^2\|\mathbf{x}_2\|^2}{\|\mathbf{x}_1\|^2}. \tag{4.13}$$

Equality holds if $\mathbf{x}_1 = \kappa \cdot \mathbf{x}_2$. From above, the filter bank which maximizs the instantaneous SINR is actually the ML filter bank $\omega_{ml} = \mathbf{C}^{-1}\mathbf{S}_{1+}\mathbf{A}_1\Gamma_1$. The corresponding SINR is equal to $\Gamma_1^H\mathbf{A}_1\mathbf{S}_{1+}^H\mathbf{C}^{-1}\mathbf{S}_{1+}\mathbf{A}_1\Gamma_1$, conditioning on the current fading coefficient vector. Taking the expectation with respect to Γ_1 of a Rayleigh fading channel yields the average SINR:

$$E(\Gamma_1^H\mathbf{A}_1\mathbf{S}_{1+}^H\mathbf{C}^{-1}\mathbf{S}_{1+}\mathbf{A}_1\Gamma_1) = tr(\mathbf{A}_1\mathbf{S}_{1+}^H\mathbf{C}^{-1}\mathbf{S}_{1+}\mathbf{A}_1). \tag{4.14}$$

The instantaneous SINRs of the MMSE, MOE and BLUE receivers can also be evaluated by substituting corresponding filters, ω, into (4.12). However, to obtain the closed-form formulae for average SINRs would be much more complicated and does not lead to direct intuitions for assessing their performance. On the other hand, we can assume a MRC filter bank of the form $\omega\Gamma_1$, where ω is not a function of the

fading coefficient vector Γ_1, and define an output SINR to be the ratio of mean squared to variance as given by

$$SINR \equiv \frac{E(\Gamma_1^H \omega^H \mathbf{y} \mid b_1 = 1)^2}{Var(\Gamma_1^H \omega^H \mathbf{y} \mid b_1 = 1)}. \tag{4.15}$$

Evaluations of this SINR is much more easier. Moreover, as will be shown in the next section, it has direct connection to BER performance. Throughout this paper, this SINR measure is referred to as output SINR and will be used more often for the performance evaluations of the MMSE/MOE/BLUE filter banks in contrast to (4.14), which is solely used for the ML filter bank and is referred to as average SINR.

The first question regarding the output SINR is what filter will maximize this SINR. To answer this question, we need to work out the expectations involved in (4.15). Ignoring the effect of ISI, the auto-correlation matrix of $\mathbf{y}$ conditioned on $\Gamma_1 b_1$ follows

$$E(\mathbf{y}\mathbf{y}^H | \Gamma_1 b_1) = \mathbf{R} - \mathbf{S}_{1+}\mathbf{A}_1^2\mathbf{S}_{1+}^H + \mathbf{S}_{1+}\mathbf{A}_1\Gamma_1\Gamma_1^H\mathbf{A}_1\mathbf{S}_{1+}^H. \tag{4.16}$$

The variance of MRC filter's output becomes

$$\begin{aligned} & Var(\Gamma_1^H \omega^H \mathbf{y} \mid b_1 = 1) \\ & = E(\Gamma_1^H \omega^H \mathbf{S}_{1+}\mathbf{A}_1\Gamma_1\Gamma_1\mathbf{A}_1\mathbf{S}_{1+}^H\omega\Gamma_1) + \Gamma_1^H\omega^H(\mathbf{R} - \mathbf{S}_{1+}\mathbf{A}_1^2\mathbf{S}_{1+}^H)\omega\Gamma_1 \\ & - E(\Gamma_1^H \omega^H \mathbf{y} \mid b_1 = 1)^2. \end{aligned} \tag{4.17}$$

To deal with the fourth moment term, we need the following lemma [19]. If $\mathbf{x} \sim \mathcal{N}(\mathbf{0}, \mathbf{C_x})$, then for $\mathbf{A}$ and $\mathbf{B}$ Hermitian matrices

$$E(\mathbf{x}^H\mathbf{A}\mathbf{x}\mathbf{x}^H\mathbf{B}\mathbf{x}) \;=\; tr(\mathbf{A}\mathbf{C_x})tr(\mathbf{B}\mathbf{C_x}) + tr(\mathbf{A}\mathbf{C_x}\mathbf{B}\mathbf{C_x}). \tag{4.18}$$

Consider filter banks which satisfy the constraint[1]: $\omega^H\mathbf{S}_{1+}\mathbf{A}_1$ is Hermitian. For Rayleigh fading channels, where $\mathbf{C_x} = \mathbf{I}$, $E(\Gamma_1^H\omega^H\mathbf{y} \;|b_1 = 1) = tr(\omega^H\mathbf{S}_{1+}\mathbf{A}_1)$ and $Var(\Gamma_1^H\omega^H\mathbf{y} \;|b_1 = 1) = tr(\omega^H\mathbf{R}\omega)$, the filter bank that maximizes the output SINR becomes

$$\arg\min_{\omega} \frac{E(\Gamma_1^H\omega^H\mathbf{y} \;|b_1 = 1)^2}{Var(\Gamma_1^H\omega^H\mathbf{y} \;|b_1 = 1)} = \arg\min_{\omega} \frac{tr^2(\omega^H\mathbf{S}_{1+}\mathbf{A}_1)}{tr(\omega^H\mathbf{R}\omega)}. \tag{4.19}$$

Taking the derivative with respect to ω and setting to zero yields

$$2tr(\omega^H\mathbf{S}_{1+}\mathbf{A}_1)[tr(\omega^H\mathbf{R}\omega)\mathbf{A}_1\mathbf{S}_{1+}^H - tr(\omega^H\mathbf{S}_{1+}\mathbf{A}_1)\omega^H\mathbf{R}] = \mathbf{0}. \tag{4.20}$$

The solution is exactly the MMSE filter bank $\omega_{mmse} = \mathbf{R}^{-1}\mathbf{S}_{1+}\mathbf{A}_1$, and the corresponding output SINR is equal to $tr(\mathbf{A}_1\mathbf{S}_{1+}^H\mathbf{R}^{-1}\mathbf{S}_{1+}\mathbf{A}_1)$.

Now, there are two maximizing filter banks from two different perspectives. A series of subsequent questions will be in what forms the reduced-rank MMSE, MOE, BLUE and ML filter banks present their output SINRs, by how much the output

[1]For all the filter banks considered within the scope of this paper satisfy this constraint. Under this constraint, it is more straightforward to derive the maximizing filter. However, the MMSE filter can still be proved maximizing the output SINR without imposing this constraint.

SINR of the MMSE receiver differs from the others. In the sequel, we shall characterize the output SINRs of all these receivers and explore some important properties of them.

Conditioned on the channel coefficient Γ_1, the decision statistic of a multistage multiuser receivers considered in this paper is obtained from the MRC of the filter's soft outputs as $\psi(m) \equiv \Gamma_1^H(m)\mathbf{z}(m)$. Ignoring the desired user's self inter symbol interference (ISI), the steady-state output SINR for each multistage receiver in multipath Rayleigh fading channels is given by the following proposition.

Proposition 2 *The steady-state output SINRs of the D-stage MRC MMSE/MOE/ BLUE/ML multiuser receivers, (rank=DL), are given by.*

$$
\begin{aligned}
SINR_{mmse} &= tr(\mathbf{A}_1\mathbf{U}_1^H\mathbf{S}_D^{-1}\mathbf{U}_1\mathbf{A}_1) && (4.21)\\
SINR_{moe} &= \frac{tr^2(\mathbf{A}_1\mathbf{U}_1^H\mathbf{U}_1\mathbf{A}_1)}{tr(\mathbf{A}_1\mathbf{U}_1^H\mathbf{S}_D\mathbf{U}_1\mathbf{A}_1)} && (4.22)\\
SINR_{blue} &= \frac{L^2}{tr((\mathbf{U}_1\mathbf{A}_1)^{-1}\mathbf{S}_D(\mathbf{U}_1\mathbf{A}_1)^{-H})} && (4.23)\\
SINR_{ml} &= \frac{tr^2[\mathbf{A}_1\mathbf{U}_1^H\mathbf{F}_D^{-1}\mathbf{U}_1\mathbf{A}_1]}{tr[\mathbf{A}_1\mathbf{U}_1^H\mathbf{F}_D^{-1}\mathbf{U}_1\mathbf{A}_1 + (\mathbf{A}_1\mathbf{U}_1^H\mathbf{F}_D^{-1}\mathbf{U}_1\mathbf{A}_1)^2]}, && (4.24)
\end{aligned}
$$

where $\mathbf{F}_D = \mathbf{S}_D - \mathbf{U}_1\mathbf{A}_1^2\mathbf{U}_1^H$, *[cf. (4.11)].*

Proof: The proof is given in Appendix B.1. ■

Remarks :

From (B.1) $\sim$ (B.4) and (B.7) $\sim$ (B.10), the conditional covariance matrices of the filter banks can be readily obtained in these forms

$$\begin{aligned} Var(\psi_{mmse}|\Gamma_1 b_1) &= \Gamma_1^H(\mathbf{M}_S - \mathbf{M}_S^2)\Gamma_1 && (4.25)\\ Var(\psi_{moe}|\Gamma_1 b_1) &= \Gamma_1^H(\mathbf{A}_1\mathbf{U}_1^H\mathbf{S}_D\mathbf{U}_1\mathbf{A}_1 - (\mathbf{A}_1\mathbf{U}_1^H\mathbf{U}_1\mathbf{A}_1)^2)\Gamma_1 && (4.26)\\ Var(\psi_{blue}|\Gamma_1 b_1) &= \Gamma_1^H(\mathbf{M}_S^{-1} - \mathbf{I})\Gamma_1 && (4.27)\\ Var(\psi_{ml}|\Gamma_1 b_1) &= \Gamma_1^H(\mathbf{M}_F)\Gamma_1, && (4.28) \end{aligned}$$

where $M_S = \mathbf{A}_1\mathbf{U}_1^H\mathbf{S}_D^{-1}\mathbf{U}_1\mathbf{A}_1$ and $M_F = \mathbf{A}_1\mathbf{U}_1^H\mathbf{F}_D^{-1}\mathbf{U}_1\mathbf{A}_1$. Employing the positive definiteness of a covariance function, we obtain the following properties:

1. From (4.27), we have $\Lambda \leq \mathbf{I}$. $\mathbf{Q}\Lambda\mathbf{Q}^H \equiv \mathbf{A}_1\mathbf{U}_1^H\mathbf{S}_D^{-1}\mathbf{U}_1\mathbf{A}_1$.

2. From (4.25), $\Lambda - (\Lambda)^2 \geq \mathbf{0}$, therefore

$$\mathbf{0} \leq \Lambda \leq \mathbf{I}. \qquad (4.29)$$

3. Concluding from 1 and 2 yields

$$0 \leq SINR_{mmse} = tr(\mathbf{A}_1\mathbf{U}_1^H\mathbf{S}_D^{-1}\mathbf{U}_1\mathbf{A}_1) = tr(\Lambda) \leq L. \qquad (4.30)$$

Since the MMSE filter bank maximizes the output SINR defined in (4.15), L constitutes the upper bound for the output SINRs of the MRC MMSE-based filter banks.

4. From (4.28), it directly shows $\mathbf{A}_1\mathbf{U}_1^H\mathbf{F}_D^{-1}\mathbf{U}_1\mathbf{A}_1 > \mathbf{0}$, where $\mathbf{Q}\Lambda_F\mathbf{Q}^H \equiv \mathbf{A}_1\mathbf{U}_1^H\mathbf{F}_D^{-1}\mathbf{U}_1\mathbf{A}_1$.

Moreover, (4.14) shows that the average SINR of the full-rank ML receiver is simply equal to $E(\omega_{ml}^H\mathbf{y}|b_1 = 1)$. Thus, by (B.4), the average SINR of the reduced-rank ML receiver, in the sense of (4.12), is equal to

$$SINR_{ml}^{avg} = tr(\mathbf{A}_1\mathbf{U}_1^H\mathbf{F}_D^{-1}\mathbf{U}_1\mathbf{A}_1). \tag{4.31}$$

It has been shown in (4.20) that the full-rank MMSE FB maximizes the output SINR defined by (4.15). Given by the analytical results in proposition 2, we are able to characterize the performance differences between the output SINRs of the multistage MMSE-based filter banks for all possible stages. A necessary condition is given for the equality of the output SINRs of these filter banks.

Proposition 3 *Inequalities for the steady-state output SINRs of D-stage MRC MMSE/MOE/BLUE/ML multiuser receivers.*

1. *The performance bound for the output SINR of the MOE receiver.*

$$L \geq SINR_{mmse}^D \geq SINR_{moe}^D. \tag{4.32}$$

If $\mathbf{S}_D = \kappa\mathbf{I}$ *and* $\kappa \geq \frac{1}{L}tr(\mathbf{U}_1\mathbf{A}_1^2\mathbf{U}_1^H)$*, then* $SINR_{mmse} = SINR_{moe}$.

2. *The performance bound for the output SINR of the BLUE receiver.*

$$L \geq SINR_{mmse}^D \geq \ SINR_{blue}^D. \tag{4.33}$$

If $\mathbf{A}_1\mathbf{U}_1^H\mathbf{S}_D^{-1}\mathbf{U}_1\mathbf{A}_1 = \kappa\mathbf{I},\ 0 \leq \kappa \leq 1$*, then* $SINR_{mmse} = SINR_{blue}$.

3. *The performance bound for the output SINR of the ML filter bank.*

$$L \geq SINR_{mmse}^D \geq \ SINR_{ml}^D. \tag{4.34}$$

$SINR_{mmse} = SINR_{ml}$ *if and only if* $\Lambda_F = \kappa\mathbf{I},\ \kappa > 0$*, i.e.* $\mathbf{A}_1\mathbf{U}_1^H\mathbf{S}_D^{-1}\mathbf{U}_1\mathbf{A}_1 = \frac{\kappa}{\kappa+1}\mathbf{I}$.

4. *If* $\mathbf{A}_1\mathbf{U}_1^H\mathbf{U}_1\mathbf{A}_1 = \kappa_1\mathbf{I},\ \kappa_1 \geq 0$*, (i.e.* $\frac{1}{\sqrt{\kappa_1}}\mathbf{U}_1\mathbf{A}_1$ *is a unitary matrix), and* $\mathbf{S}_D = \kappa_2\mathbf{I}$*,* $\kappa_2 \geq \kappa_1$*, then*

$$L \geq SINR_{mmse}^D = SINR_{moe}^D = SINR_{blue}^D = SINR_{ml}^D. \tag{4.35}$$

Proof: The proof is given in Appendix B.2. ■

Judging from the form of $\mathbf{S}_D$, (4.10), it is very difficult to have it a diagonal matrix. Moreover, $\mathbf{U}_1 = \mathbf{H}_1^H\mathbf{S}_{1+}$ is a by product of applying the Gram-Schmidt process to the effective steering matrix $\mathbf{S}_{1+}$. $\mathbf{S}_{1+}$ is a function of the spreading

sequence and the path delays of the desired user. Having $\mathbf{U}_1\mathbf{A}_1 = \sqrt{\kappa_1}\mathbf{I}$ means the columns of $\mathbf{S}_{1+}$ are orthogonal to each others. So, in general the equality is unlikely to happened in practice. However, Corollary 1 gives a situation where the equality holds naturally.

Corollary 1 *For the multistage MRC MMSE/MOE/BLUE/ML receivers of DS-CDMA in flat Rayleigh fading channels*

$$SINR^D_{mmse} = SINR^D_{moe} = SINR^D_{blue} = SINR^D_{ml}. \tag{4.36}$$

Proof: In flat fading channels, $\mathbf{A}_1, \mathbf{U}_1$ and $\mathbf{S}_D$ are scalars ($L = 1$). By (4.30), $\mathbf{A}_1\mathbf{U}_1^H\mathbf{S}_D^{-1}\mathbf{U}_1\mathbf{A}_1 \leq 1$. Thus $\mathbf{S}_D = \kappa_2 \geq \mathbf{A}_1\mathbf{U}_1^H\mathbf{U}_1\mathbf{A}_1 = \kappa_1$. According to Proposition 3, the equality holds for any spreading sequence $\mathbf{S}_{1+}$ of the desired user. ■

As will be shown later in Section 4.4, this corollary gives another justification for the fact that BER performance are the same for the multistage MMSE/MOE/BLUE/ML receivers in flat fading channels.

From Proposition 2, it is clear that the output SINRs are all related to the kernels of $SINR_{mmse}$ and $SINR^{avg}_{ml}$. Which are $K_{mmse} \equiv \mathbf{A}_1\mathbf{U}_1^H\mathbf{S}_D^{-1}\mathbf{U}_1\mathbf{A}_1$ and $K_{ml} \equiv \mathbf{A}_1\mathbf{U}_1^H\mathbf{F}_D^{-1}\mathbf{U}_1\mathbf{A}_1$, respectively. In Section 4.2 they will also be shown playing important roles in BER performances of the MMSE-based filter banks. In the next section, the structure of the kernels will be discussed in details. Before leaving this section, it is necessary to show that the eigenvalues of this kernels are monotonically increasing with respect to the desired user's power.

Proposition 4 *Ignoring the self-ISI of the desired user, the eigenvalues of* $\mathbf{A}_1\mathbf{U}_1^H\mathbf{S}_D^{-1}\mathbf{U}_1\mathbf{A}_1$ *and* $\mathbf{A}_1\mathbf{U}_1^H\mathbf{F}_D^{-1}\mathbf{U}_1\mathbf{A}_1$ *are both monotonically increasing with respect to* $\mathbf{A}_1$.

Proof: It has been shown in Chapter 3 that

$$\mathbf{S}_D = \mathbf{U}_1\mathbf{A}_1^2\mathbf{U}_1^H + E[(\mathbf{H}_1^H\mathbf{I}_1 - \omega_1^H\mathbf{H}_{1\perp}^H\mathbf{I}_1)(\mathbf{H}_1^H\mathbf{I}_1 - \omega_1^H\mathbf{H}_{1\perp}^H\mathbf{I}_1)^H]. \tag{4.37}$$

Ignoring self-ISI in (3.13), $\mathbf{I}_1$ is no longer a function of $\mathbf{A}_1$. By (4.11), $\mathbf{F}_D$ is independent of $\mathbf{A}_1$. For a short period of time the transmission environment is considered stationary, thus the proportions among the powers on each transmission path do not changed with time, temporarily. Increasing the desired user's power by a factor of κ leaves $\mathbf{A}_1^+ = \kappa\mathbf{A}_1,\ \kappa > 1$, which results in $\mathbf{A}_1^+\mathbf{U}_1^H\mathbf{F}_D^{-1}\mathbf{U}_1\mathbf{A}_1^+ = \kappa^2\mathbf{Q}\Lambda_F\mathbf{Q}^H \equiv \mathbf{Q}\Lambda_F^+\mathbf{Q}^H$. Since $\kappa > 1$, $\Lambda_F^+ > \Lambda_F$. By (B.23), $\Lambda^+ > \Lambda$. This completes the proof. ■

4.1.2 The structures of output SINRs

The analytical results and performance limits for output SINRs have been provided in the previous section. Proposition 3 shows that all output SINRs are upper bounded by the number of resolvable paths of the desired user. For multistage implementations, an important property would be wether SINRs increase with applying stages. If yes, how do they get improved. This problem can be investigated from two perspectives as it has been done for SINRs. For ML filter bank, its average SINR is available and equal to the trace of K_{ml}. Therefore, the answer lies in the structure

of K_{ml}. For other three filter banks, still we are able to study their output SINRs. Looking at the output SINR of the MOE filter bank, if $\mathbf{A}_1\mathbf{U}_1^H\mathbf{S}_D\mathbf{U}_1\mathbf{A}_1$ of (4.22) is rewritten into $\mathbf{M}_I(\mathbf{U}_1\mathbf{A}_1)^{-1}\mathbf{S}_D(\mathbf{A}_1\mathbf{U}_1^H)^{-1}\mathbf{M}_I$, where $\mathbf{M}_I \equiv \mathbf{A}_1\mathbf{U}_1^H\mathbf{U}_1\mathbf{A}_1$, then according to Proposition 2, the output SINRs of the MMSE/MOE/BLUE filter banks are only functions of $\mathbf{A}_1\mathbf{U}_1^H\mathbf{S}_D^{-1}\mathbf{U}_1\mathbf{A}_1 \equiv \mathbf{Q}\Lambda\mathbf{Q}^H$. Their updating properties are all related to the structure of K_{mmse}. Therefore the problem boils down to characterizing the properties of Λ and Λ_F with respect to stages. To approach this problem, we need to explore the structure of $\mathbf{A}_1\mathbf{U}_1^H\mathbf{S}_D^{-1}\mathbf{U}_1\mathbf{A}_1$.

Given that $\mathbf{A}_1$ and $\mathbf{S}_{1+}$ are fixed, $\mathbf{U}_1$ is a constant matrix. The convergence of output SINRs solely depends on the evolving structure of $\mathbf{S}_D^{-1}$. It has been shown in [8] for the MSWF that $E(d_i d_j^*) = 0$, for $|j-i| > 1$ and $1 \le i, j \le D$. This property also holds for the MMSE-based filter banks covered in this paper, since $E(\mathbf{d}_i\mathbf{d}_j^H) = \mathbf{H}_i^H\mathbf{R}\mathbf{H}_j = E(\mathbf{H}_i^H\mathbf{y}\mathbf{y}^H\mathbf{B}_i^H)\mathbf{B}_{i+1}^H\cdots\mathbf{B}_{j-1}^H\mathbf{H}_j = \boldsymbol{\Upsilon}_{\mathbf{y}_i\mathbf{d}_i}^H\mathbf{H}_j = \mathbf{0}$, for $|i-j| > 1$ and $1 \le i, j \le D$. In addition, $\mathbf{H}_i^H\mathbf{R}\mathbf{H}_{i+1} = E(\mathbf{H}_i^H\mathbf{y}\mathbf{y}^H\mathbf{B}_i^H)\mathbf{H}_{i+1} = \boldsymbol{\Upsilon}_{\mathbf{y}_i\mathbf{d}_i}^H\mathbf{H}_{i+1} = \mathbf{U}_{i+1}^H$, thus $\mathbf{T}\mathbf{R}\mathbf{T}^H$ is a block tri-diagonal matrix of the form

$$\mathbf{T}\mathbf{R}\mathbf{T}^H = [\mathbf{H}_1|\mathbf{H}_{1\perp}]^H\mathbf{R}[\mathbf{H}_1|\mathbf{H}_{1\perp}] = \begin{bmatrix} \mathbf{R}_{d_1} & \mathbf{U}_2^H & \mathbf{0} & \cdots & \mathbf{0} \\ \mathbf{U}_2 & \mathbf{R}_{d_2} & \mathbf{U}_3^H & \ddots & \vdots \\ \mathbf{0} & \mathbf{U}_3 & \ddots & \ddots & \mathbf{0} \\ \vdots & \ddots & \ddots & \mathbf{R}_{d_{D-1}} & \mathbf{U}_D \\ \mathbf{0} & \cdots & \mathbf{0} & \mathbf{U}_D & \mathbf{R}_{d_D} \end{bmatrix}. \quad (4.38)$$

Let $\mathbf{H}_{i\perp}$ denote $[\mathbf{H}_{i+1}, \cdots, \mathbf{H}_D]$, for $i = 1, \cdots, D-1$. Applying the block tri-diagonal property to (4.10) and recursively employing the matrix inversion lemma [14] for every resultant matrix $(\mathbf{H}_{i\perp}^H \mathbf{R} \mathbf{H}_{i\perp})^{-1}$ yields

$$\mathbf{S}_D^{-1} = [\mathbf{R}_{d_1} - \mathbf{U}_2^H [\mathbf{R}_{d_2} - \mathbf{U}_3^H [\cdots \mathbf{U}_{D-1}^H [\mathbf{R}_{d_{D-1}} - \mathbf{U}_D^H \mathbf{R}_{d_D}^{-1} \mathbf{U}_D]^{-1} \mathbf{U}_{D-1}]^{-1} \cdots]^{-1} \mathbf{U}_3]^{-1} \mathbf{U}_2]^{-1}. \tag{4.39}$$

Recall the structure of the MSWF. Pruning a filter bank at stage i, $i < D$, the removed part from stage $i+1$ to stage D forms a reduced-rank MMSE filter bank ω_i which minimizes $\|\mathbf{d}_i - \omega_i^H \mathbf{y}_i\|^2$. The corresponding error correlation matrix $\mathbf{E}_i = E[(\mathbf{d}_i - \omega_i^H \mathbf{y}_i)(\mathbf{d}_i - \omega_i^H \mathbf{y}_i)^H]$ is equal to $(\mathbf{R}_{\mathbf{d}_i} - \mathbf{\Upsilon}_{\mathbf{y}_i \mathbf{d}_i}^H \mathbf{R}_{\mathbf{y}_i}^{-1} \mathbf{\Upsilon}_{\mathbf{y}_i \mathbf{d}_i})$, with $\mathbf{E}_D = \mathbf{R}_{\mathbf{d}_D}$ for the last stage and $SINR_{MMSE} = tr(\mathbf{A}_1 \mathbf{U}_1^H \mathbf{E}_1^{-1} \mathbf{U}_1 \mathbf{A}_1)$, [*cf.* (4.21), where $\mathbf{E}_1$ is denoted as $\mathbf{S}_D$ to indicate the total stages]. Therefore the output SINR of ω_i, denoted as $SINR_{mmse}^i$, is equal to $tr(\mathbf{U}_i^H \mathbf{E}_i^{-1} \mathbf{U}_i)$, $2 \le i \le D-1$. [2] And, similar to the structure of (4.39) for $\mathbf{S}_D$, $\mathbf{E}_i = [\mathbf{R}_{d_i} - \mathbf{U}_{i+1}^H [\cdots [\mathbf{R}_{d_{D-1}} - \mathbf{U}_D^H \mathbf{R}_{d_D}^{-1} \mathbf{U}_D] \cdots] \mathbf{U}_{i+1}]$. Therefore, $\mathbf{E}_i$ possesses a recursive structure of the form

$$\mathbf{E}_i = [\mathbf{R}_{d_i} - \mathbf{U}_{i+1}^H \mathbf{E}_{i+1}^{-1} \mathbf{U}_{i+1}], \ i = 1, \cdots, D-1, \tag{4.40}$$

with $\mathbf{E}_D = \mathbf{R}_{d_D}$. This structure can be more clearly seen for flat Rayleigh fading channels.

[2] For the convenience of analysis, we have made $\mathbf{A}_1$ explicit in expressing the the cross-correlation $E(\mathbf{y}\mathbf{d}_0^H) = \mathbf{H}_1 \mathbf{U}_1 \mathbf{A}_1$ of the first stage, where $\mathbf{d_0} \equiv \Gamma_1 b_1$. For stage 2 to stage D, $E(\mathbf{y}_{i-1}\mathbf{d}_{i-1}^H) = \mathbf{H}_i \mathbf{U}_i$, $i \in \{2, \cdots, D\}$.

Let α_i denote $\|\mathbf{U}_i\|^2$ and β_i denote $\mathbf{R}_{d_i}$ for scalar cases. The output SINR of the matched-filter $\mathbf{H}_i$, denoted as $SINR^i_{mf}$, at each stage i can been shown equal to $\frac{\alpha_i}{\beta_i}$. The output SINR of the MMSE filter ω_i constructed with stage i to stage D is equal to

$$SINR^i_{mmse} = \frac{\alpha_i}{\beta_i - SINR^{i+1}_{mmse}}, \tag{4.41}$$

where, for the last stage, $SINR^D_{mmse}$ is simply equal to $SINR^D_{mf} = \frac{\alpha_D}{\beta_D}$. An interesting property shown by this formula is that the MMSE filter differs from the matched-filter by subtracting $SINR^{i+1}_{mmse}$ from the denominator of $SINR^i_{mf}$. As a result, the output SINR of the multistage MMSE receiver over a flat Rayleigh fading channel can be expressed as a continued-fraction of the form

$$SINR_{mmse} = \frac{\alpha_1}{\beta_1 - \cfrac{\alpha_2}{\beta_2 - \cfrac{\alpha_3}{\ddots \cfrac{}{\beta_D}}}} = \frac{\alpha_1}{\mathbf{S}_D}, \tag{4.42}$$

where $\alpha_1 = \mathbf{A}_1\mathbf{U}_1^H\mathbf{U}_1\mathbf{A}_1$. α_1 and $\mathbf{S}_D$ are both scalars in this case. Other multistage MOE/BLUE/ML filter banks also possess the same property, since their output SINRs are equal in flat Rayleigh fading channels.

For scalar cases, it is clear from (4.42) that the output SINR gets increased by adding every extra stage. For multipath fading channels, we need to show that the eigenvalues of Λ increase with the number of stages. For the convenience of analysis, redefine $\mathbf{A}_1\mathbf{U}_1^H\mathbf{S}_D^{-1}\mathbf{U}_1\mathbf{A}_1 \equiv \mathbf{Q}_{1:D}\Lambda_{1:D}\mathbf{Q}_{1:D}^H$ and $\mathbf{A}_1\mathbf{U}_1^H\mathbf{S}_{D-1}^{-1}\mathbf{U}_1\mathbf{A}_1 \equiv$

$\mathbf{Q}_{1:(D-1)}\Lambda_{1:(D-1)}\mathbf{Q}_{1:(D-1)}^H$ to be the kernels, K_{mmse}, of the D-stage and (D-1)-stage MMSE filter banks, respectively. Their properties are given the Theorem 1.

Theorem 1 *The eigenvalues of the output error correlation matrix of the multistage MMSE-FB is monotonically increasing with the number of stages. i.e.*

$\Lambda_{1:D} > \Lambda_{1:(D-1)},\ 2 \leq D \leq N.$

Proof: The proof is given in Appendix B.3. ■

The output SINR of the reduced-rank MMSE filter bank is simply equal to the trace of K_{mmse}, so $SINR_{mmse}$ increases with the number of stages. For the output SINRs of the MOE and BLUE filter banks, their numerators are all constants and the denominators are functions of K_{mmse}^{-1}. For the BLUE filter bank, the denominator is $trace(K_{mmse}^{-1})$, so $SINR_{blue}$ increases with the number of stages. For the MOE filter bank, $\mathbf{A}_1\mathbf{U}_1^H\mathbf{S}_D\mathbf{U}_1\mathbf{A}_1 = \mathbf{M}_I^2 K_{mmse}^{-1}\mathbf{M}_I^2$, where $\mathbf{M}_I \equiv \mathbf{A}_1\mathbf{U}_1^H\mathbf{U}_1\mathbf{A}_1$. Similar to the proof of Theorem 1, we can easily obtain the eigenvalues of $\mathbf{A}_1\mathbf{U}_1^H\mathbf{S}_D\mathbf{U}_1\mathbf{A}_1$ decrease as the eigenvalues of K_{mmse}^{-1} decrease. Therefore $SINR_{moe}$ increases.

For ML filter banks, we are more interested in the $SINR_{ml}^{avg} = trace(K_{ml})$. Redefine $\mathbf{A}_1\mathbf{U}_1^H\mathbf{F}_D^{-1}\mathbf{U}_1\mathbf{A}_1 \equiv \mathbf{Q}_{1:D}\Lambda_{F_{1:D}}\mathbf{Q}_{1:D}^H$ and $\mathbf{A}_1\mathbf{U}_1^H\mathbf{F}_{D-1}^{-1}\mathbf{U}_1\mathbf{A}_1 \equiv \mathbf{Q}_{1:(D-1)}\Lambda_{F_{1:(D-1)}}$ $\mathbf{Q}_{1:(D-1)}^H$ to be the kernels, K_{ml}, of the D-stage and (D-1)-stage ML filter banks, respectively.

Theorem 2 *The eigenvalues of the output error correlation matrix of the multistage ML-FB is monotonically increasing with the number of stages. i.e.*

$\Lambda_{F_{1:D}} > \Lambda_{F_{1:(D-1)}},\ 2 \leq D \leq N.$

Proof: By Matrix Inversion Lemma, (B.24) can be rewritten as

$$\begin{aligned} \Lambda &= (\Lambda_F^{-1} + \mathbf{I})^{-1} = \mathbf{I} - (\mathbf{I} + \Lambda_F)^{-1} \\ \mathbf{I} &= (\mathbf{I} + \Lambda_F)(\mathbf{I} - \Lambda). \end{aligned} \tag{4.43}$$

This shows that each pair of λ_i and $\lambda_{f_i},\ i = 1 \cdots L$, forms a parabolic function shown in Fig. 4.2, with the asymptotic lines at $\lambda_i = 1$ and $\lambda_{f_i} = -1$, respectively. Due to the physical constraints: $0 \leq \lambda \leq 1$ and $\lambda_{f_i} \geq 0$ given in Remarks 2 and 4, only the upper branch is valid. λ_{f_i} is monotonically increasing with λ_i. The relationship between the increments $\triangle\lambda$ and $\triangle\lambda_f$ is given by their Laurent series expansion

$$\triangle\lambda_f = \frac{\triangle\lambda}{(1-\lambda)(1-\lambda-\triangle\lambda)},\ \triangle\lambda < 1 - \lambda. \tag{4.44}$$

As given in Theorem 1, $\triangle\lambda$ increase with the number of stages, so does the $\triangle\lambda_f$. ■

Since $SINR_{ml}^{avg} = trace(\Lambda_F)$, Theorem 1 and 2 guarantee that SINRs of the multistage MMSE/MOE/BLUE/ML filter banks increase with the number of stages.

4.2 BER Analysis

We have seen from previous analysis for some properties of the output SINR of the multistage MRC filter banks when channel information is available. In absence of channel status, especially in fast fading environments, EGC schemes are preferred for

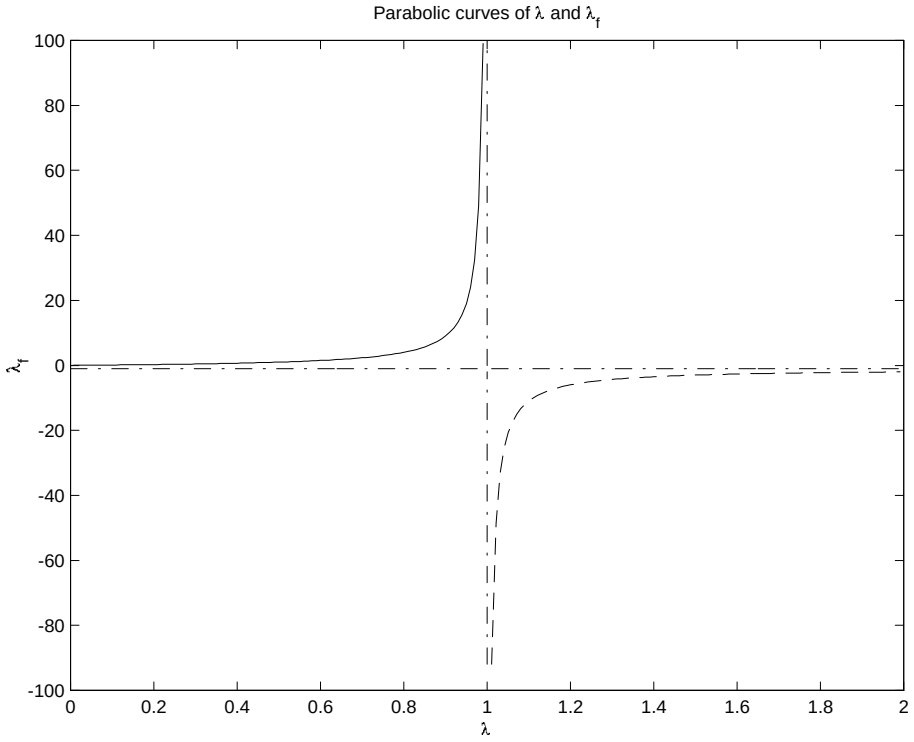

Figure 4.2: Parabolic curves of the eigenvalues λ_i and $\lambda_{f_i},\ i = 1 \cdots L$.

non-coherent detection. Due to the common structure for the MMSE/MOE/BLUE/ML filter banks, a variety of EGC schemes can be formed out of two temporally adjacent outputs chosen from one or two filter banks without causing any extra complexity for implementations. For EGC using two adjacent outputs of the same filter bank is referred to as homogenous EGC, for EGC employing two distinct filter banks is referred to as heterogenous EGC. To investigate the relationship between the rank of filtering and its BER, in the sequel, BERs for all of the MRC and homogenous EGC schemes will be characterized along with some heterogenous EGC schemes of special interest.

The analysis is motivated by the BER analysis for homogenous EGC MMSE/MOE multiuser receivers presented in [21]. Its approach can be easily extended to incorporated BER analysis for both of the MRC and EGC schemes. It is briefly introduced as follows. Define matrix

$$\mathbf{J} = \frac{1}{2}\begin{bmatrix} \mathbf{0} & \mathbf{I} \\ \mathbf{I} & \mathbf{0} \end{bmatrix} \tag{4.45}$$

and

$$\mathbf{x} = \begin{bmatrix} \mathbf{g}^H & \mathbf{z}(m)^H \end{bmatrix}^H \tag{4.46}$$

where $\mathbf{g}$ is a combining vector with the same dimension of $\mathbf{z}(m)$. $\mathbf{g} = \Gamma_1(m)$ for the case of MRC filter banks and $\mathbf{g} = \mathbf{z}(m-1)$ for the case of EGC filter banks. Notice that $\mathbf{z}(m-1)$ could come from the same filter or not, in general. Decision statistic φ can be expressed as

$$\varphi = Re[\mathbf{g}^H \mathbf{z}(m)] = \mathbf{x}^H \mathbf{J} \mathbf{x} \tag{4.47}$$

In the presence of the Gaussian random noise, decision statistic φ is a Gaussian quadratic form. Its moment generating function (MGF), defined as $M(s)$, is given by

$$M(s) = E[e^{-s\varphi}] = [det(\mathbf{I} + s\mathbf{J}\Phi)]^{-1} \tag{4.48}$$

where $\Phi = E(\mathbf{x}\mathbf{x}^H)$. By assigning $b_1(m) = 1$ for the case of BPSK modulation, or $b_1(m) = b_1(m-1)$ for the case of DBPSK modulation, the BER is given by [21]

$$Pr(\mathbf{z}^H\mathbf{J}\mathbf{z} < 0) = -\sum_{RHP} Res\left\{\frac{M(s)}{s}\right\} \tag{4.49}$$

Based on this formula, BER analysis for MRC and EGC schemes can be conducted under the same framework. We start with the analysis for MRC filter banks and then move into the more complicated derivations for EGC filter banks. Finally a generic BER formula is proposed for these two classes of combinings.

4.2.1 BER Analysis for Maximal Ratio Combining

With (4.49), it suffices to show the MGF, $M(s)$, for each filter bank. Since $\mathbf{z}(m) = \omega^H\mathbf{T}\mathbf{y}(m)$ and $\mathbf{x}^H = [\Gamma_1(m)^H \;\; \mathbf{z}^H(m)]$, we have

$$\Phi = E(\mathbf{x}\mathbf{x}^H) = \left[\begin{array}{c|c} \mathbf{I} & \mathbf{A}_1\mathbf{S}_{1+}^H\mathbf{T}^H\omega \\ \hline \omega^H\mathbf{T}\mathbf{S}_{1+}\mathbf{A}_1 & \omega^H\mathbf{T}\mathbf{R}\mathbf{T}^H\omega \end{array}\right]. \tag{4.50}$$

Substituting Φ back into (4.48) yields

$$det[\mathbf{I} + s\mathbf{J}\Phi] = det\left[\begin{array}{c|c} \mathbf{I} + \frac{s}{2}\omega^H\mathbf{T}\mathbf{S}_{1+}\mathbf{A}_1 & \frac{s}{2}\omega^H\mathbf{T}\mathbf{R}\mathbf{T}^H\omega \\ \hline \frac{s}{2}\mathbf{I} & \mathbf{I} + \frac{s}{2}\mathbf{A}_1\mathbf{S}_{1+}^H\mathbf{T}^H\omega \end{array}\right]. \tag{4.51}$$

This expression can be further simplified with the following lemma (see [14]).

$$det\begin{bmatrix} \mathbf{A}_{11} & \mathbf{B}_{12} \\ \mathbf{B}_{21} & \mathbf{A}_{22} \end{bmatrix} = det(\mathbf{A}_{11})det(\mathbf{A}_{22} - \mathbf{B}_{21}\mathbf{A}_{11}^{-1}\mathbf{B}_{12}). \tag{4.52}$$

Which yields

$$\begin{aligned} det[\mathbf{I} + s\mathbf{J}\Phi] &= det(\mathbf{I} + \frac{s}{2}\omega^H\mathbf{T}\mathbf{S}_{1+}\mathbf{A}_1) \times \\ & \quad det[\mathbf{I} + \frac{s}{2}\mathbf{A}_1\mathbf{S}_{1+}^H\mathbf{T}^H\omega - \frac{s^2}{4}(\mathbf{I} + \frac{s}{2}\omega^H\mathbf{T}\mathbf{S}_{1+}\mathbf{A}_1)^{-1}\omega^H\mathbf{T}\mathbf{R}\mathbf{T}^H\omega]. \end{aligned} \tag{4.53}$$

As stated before, $\omega^H\mathbf{T}\mathbf{S}_{1+}\mathbf{A}_1$ is Hermitian. A signal correlation matrix $\mathbf{E}_S$ and an output correlation matrix $\mathbf{E}_O$ can be defined for these kinds of filter banks ω as follows

$$\mathbf{E}_S \equiv \omega^H\mathbf{T}\mathbf{R}_S\mathbf{T}^H\omega = (\omega^H\mathbf{T}\mathbf{S}_{1+}\mathbf{A}_1)^2 \tag{4.54}$$

$$\mathbf{E}_O \equiv \omega^H\mathbf{T}\mathbf{R}\mathbf{T}^H\omega, \tag{4.55}$$

where $\mathbf{R}_S \equiv \mathbf{S}_{1+}\mathbf{A}_1^2\mathbf{S}_{1+}^H$. Let $\mathbf{A} = \mathbf{I} + \frac{s}{2}\mathbf{E}_S^{\frac{1}{2}}$, (4.53) can be rewritten as

$$det[\mathbf{I} + s\mathbf{J}\Phi] = det(\mathbf{A}^2)det[\mathbf{I} - \frac{s^2}{4}(\mathbf{A}^{-1}\mathbf{E}_O\mathbf{A}^{-1})]. \tag{4.56}$$

For MS-MMSE/BLUE/ML-FBs, it can be shown that $\mathbf{E}_O^{\frac{1}{2}}\mathbf{A} = \mathbf{A}\mathbf{E}_O^{\frac{1}{2}}$. Therefore, (4.56) can be simplified to

$$\begin{aligned} det[\mathbf{I} + s\mathbf{J}\Phi] &= det(\mathbf{A} - \frac{s}{2}\mathbf{E}_O^{\frac{1}{2}})det(\mathbf{A} + \frac{s}{2}\mathbf{E}_O^{\frac{1}{2}}) \\ &= det[\mathbf{I} - \frac{s}{2}(\mathbf{E}_O^{\frac{1}{2}} - \mathbf{E}_S^{\frac{1}{2}})]det[\mathbf{I} + \frac{s}{2}(\mathbf{E}_O^{\frac{1}{2}} + \mathbf{E}_S^{\frac{1}{2}})]. \end{aligned} \tag{4.57}$$

This equation allows us to separate the the right-half-plane (RHP) poles and the left-half-plane (LHP) poles of $M(s)$ directly. The first determinant on the right-hand side decides the RHP poles and the second determines the LHP poles. Although we don't have direct evidence to show that (4.57) is generally true for MOE filter bank, however it does hold in flat fading channels, and works perfectly in more general multipath fading channels by simulation verifications. So, we take (4.57) as a general formula for $M(s)^{-1}$ of MRC.

Our major goal is to investigate the relationship between BERs and the number of applying stages. By (4.57), the analysis is simplified to examining the structures of $\omega^H\mathbf{T}\mathbf{S}_{1+}\mathbf{A}_1$ and $\omega\mathbf{T}\mathbf{R}\mathbf{T}^H\omega$ for each type of reduced-rank filter banks. Following the procedure given in Chapter 3 for the derivations of these reduced-rank filter banks, the expressions of $\mathbf{E}_O$ and $\mathbf{E}_S$ for the corresponding filter banks can also be obtained. The detail derivations are provided in Appendix B.4. The results of $M(s)^{-1}$ for each filter bank are listed in Table 4.1. It is clear from Table 4.1 and (4.11) that all $M(s)$ terms are functions of $\mathbf{A}_1\mathbf{U}_1^H\mathbf{S}_D^{-1}\mathbf{U}_1\mathbf{A}_1$, explicitly or implicitly, whose trace is the output SINR of the MMSE filter bank. It is given by (4.29)

Filter	$M(s)^{-1}$
MMSE	$det[\mathbf{I} - \frac{s}{2}(\mathbf{E}_S^{\frac{1}{4}} - \mathbf{E}_S^{\frac{1}{2}})]det[\mathbf{I} + \frac{s}{2}(\mathbf{E}_S^{\frac{1}{4}} + \mathbf{E}_S^{\frac{1}{2}})]$; $\mathbf{E}_S = (\mathbf{A}_1\mathbf{U}_1^H\mathbf{S}_D^{-1}\mathbf{U}_1\mathbf{A}_1)^2$
MOE	$det[\mathbf{I} - \frac{s}{2}((\mathbf{A}_1\mathbf{U}_1^H\mathbf{S}_D\mathbf{U}_1\mathbf{A}_1)^{\frac{1}{2}} - \mathbf{E}_S^{\frac{1}{2}})]det[\mathbf{I} + \frac{s}{2}((\mathbf{A}_1\mathbf{U}_1^H\mathbf{S}_D\mathbf{U}_1\mathbf{A}_1)^{\frac{1}{2}} + \mathbf{E}_S^{\frac{1}{2}})]$; $\mathbf{E}_S = (\mathbf{A}_1\mathbf{U}_1^H\mathbf{U}_1\mathbf{A}_1)^2$
BLUE	$det[\mathbf{I} - \frac{s}{2}((\mathbf{A}_1\mathbf{U}_1^H\mathbf{S}_D^{-1}\mathbf{U}_1\mathbf{A}_1)^{\frac{-1}{2}} - \mathbf{I})]det[\mathbf{I} + \frac{s}{2}((\mathbf{A}_1\mathbf{U}_1^H\mathbf{S}_D^{-1}\mathbf{U}_1\mathbf{A}_1)^{\frac{-1}{2}} + \mathbf{I})]$; $\mathbf{E_S} = \mathbf{I}$
ML	$det[\mathbf{I} - \frac{s}{2}((\mathbf{E}_S^{\frac{1}{2}} + \mathbf{E}_S)^{\frac{1}{2}} - \mathbf{E}_S^{\frac{1}{2}})]det[\mathbf{I} + \frac{s}{2}((\mathbf{E}_S^{\frac{1}{2}} + \mathbf{E}_S)^{\frac{1}{2}} + \mathbf{E}_S^{\frac{1}{2}})]$; $\mathbf{E}_S = (\mathbf{A}_1\mathbf{U}_1^H\mathbf{F}_D^{-1}\mathbf{U}_1\mathbf{A}_1)^2$

Table 4.1: $M(s)^{-1}$ for maximal ratio combining filter banks.

that $\mathbf{A}_1\mathbf{U}_1^H\mathbf{S}_D^{-1}\mathbf{U}_1\mathbf{A}_1$ is upper bounded by the identity matrix. Its convergence with respect to the number of stages is characterized by (4.39). As the number of stages increases, $\mathbf{A}_1\mathbf{U}_1^H\mathbf{S}_D^{-1}\mathbf{U}_1\mathbf{A}_1$ also increases monotonically towards $\mathbf{I}$. This implies that the RHP poles for each MGF in Table 4.1 will move closer and closer to the origin point. Intuitively, the residue of $\frac{M(s)}{s}$ will become smaller and smaller, and thus bringing down the BER. More detail analysis will be given in Section 4.4 for cross comparisons of BER between MRC and EGC schemes.

4.2.2 BER Analysis for Differential Equal Gain Combining

There are two classes of multistage differential EGC schemes will be analyzed in this section. One is the homogeneous EGC, where a filter's output is multiplied by the conjugate transpose of its preceding one. The decision statistic is equal to $\varphi = Re(z(m-1)^H z(m))$. The other is the heterogeneous EGC, where a filter's output is combined with the preceding output of a filter other than itself. The corresponding

decision statistic is equal to $\varphi = Re(z_1(m-1)^H z_2(m))$. Similar to the $M(s)^{-1}$ of MRC schemes, the $M(s)^{-1}$ for the homogeneous EGC MMSE/MOE/BLUE-FBs is shown in Appendix B.5 and can be expressed in the form of

$$det[\mathbf{I} + s\mathbf{J}\Phi] = det[\mathbf{I} - \frac{s}{2}(\mathbf{E}_O - \rho\mathbf{E}_S)]det[\mathbf{I} + \frac{s}{2}(\mathbf{E}_O + \rho\mathbf{E}_S)], \tag{4.58}$$

where $\mathbf{E}_S \equiv \omega^H \mathbf{T}\mathbf{R}_S\mathbf{T}^H\omega$ and $\mathbf{E}_O \equiv \omega^H\mathbf{T}\mathbf{R}\mathbf{T}^H\omega$. Comparing with (4.57), the formula for MRC schemes, $\mathbf{E}_S^{\frac{1}{2}}$ and $\mathbf{E}_O^{\frac{1}{2}}$ have been raised by the power of 2 for EGC schemes. Furthermore, the auto-correlation value ρ, [*cf.* (2.27)], of two adjacent channel states also appears in the expression accounting for the energy lose of non-exact channel combining. Intuitively, this difference can be interpreted as that there are two filters' outputs contributing to the decision statistic of EGC, while there is only one output involved in the decision statistic of MRC. Therefore, only the squared roots of $\mathbf{E}_O$ and $\mathbf{E}_S$ have appeared in the $M(s)$ of MRC. Since, perfect channel information is assumed given for MRC schemes, so $\rho = 1$ and shows no influence on the final expression of $M(s)$. The details of $M(s)^{-1}$ for each kind of homogeneous EGC filter bank are listed in Table 4.2. Again, $M(s)$ are all explicit functions of $\mathbf{A}_1\mathbf{U}_1^H\mathbf{S}_D^{-1}\mathbf{U}_1\mathbf{A}_1$. The discussions for the convergence of BERs of MRC schemes with respect to $\mathbf{A}_1\mathbf{U}_1^H\mathbf{S}_D^{-1}\mathbf{U}_1\mathbf{A}_1$ also apply for this type of EGC schemes.

For heterogeneous EGC, there are two combining schemes are of special interest: the BLUE-MMSE and the BLUE-ML combinings, because the BLUE filter is a minimum variance unbiased (MVU) estimator for $\Gamma_1 b_1$ in the presence of Gaussian

Filter	$M(s)^{-1}$
MMSE	$det[\mathbf{I}-\frac{s}{2}(\mathbf{E}_S^{\frac{1}{2}}-\rho\mathbf{E}_S)]det[\mathbf{I}+\frac{s}{2}(\mathbf{E}_S^{\frac{1}{2}}+\rho\mathbf{E}_S)]$; $\mathbf{E}_S=(\mathbf{A}_1\mathbf{U}_1^H\mathbf{S}_D^{-1}\mathbf{U}_1\mathbf{A}_1)^2$
MOE	$det[\mathbf{I}-\frac{s}{2}(\mathbf{A}_1\mathbf{U}_1^H\mathbf{S}_D\mathbf{U}_1\mathbf{A}_1-\rho\mathbf{E_S})]det[\mathbf{I}+\frac{s}{2}(\mathbf{A}_1\mathbf{U}_1^H\mathbf{S}_D\mathbf{U}_1\mathbf{A}_1+\rho\mathbf{E_S})]$; $\mathbf{E}_S=(\mathbf{A}_1\mathbf{U}_1^H\mathbf{U}_1\mathbf{A}_1)^2$
BLUE	$det[\mathbf{I}-\frac{s}{2}((\mathbf{A}_1\mathbf{U}_1^H\mathbf{S}_D^{-1}\mathbf{U}_1\mathbf{A}_1)^{-1}-\rho\mathbf{I})]det[\mathbf{I}+\frac{s}{2}((\mathbf{A}_1\mathbf{U}_1^H\mathbf{S}_D^{-1}\mathbf{U}_1\mathbf{A}_1)^{-1}+\rho\mathbf{I})]$; $\mathbf{E}_S=\mathbf{I}$

Table 4.2: $M(s)^{-1}$ for differential equal gain combining filter banks.

noise and the MMSE and ML filter banks maximize output SINRs in the senses of (4.14) and (4.12), respectively. It is shown in Appendix B.6 that the $M(s)^{-1}$ for these two combinings is merely a generalization of (4.58) with $\mathbf{E}_S=\mathbf{E}_{S_1}^{\frac{1}{2}}\mathbf{E}_{S_2}^{\frac{1}{2}}$ and $\mathbf{E}_O=\mathbf{E}_{O_1}^{\frac{1}{2}}\mathbf{E}_{O_2}^{\frac{1}{2}}$. Thus,

$$det[\mathbf{I}+s\mathbf{J}\Phi]=det[\mathbf{I}-\frac{s}{2}(\mathbf{E}_{O_1}^{\frac{1}{2}}\mathbf{E}_{O_2}^{\frac{1}{2}}-\rho\mathbf{E}_{S_1}^{\frac{1}{2}}\mathbf{E}_{S_2}^{\frac{1}{2}})]det[\mathbf{I}+\frac{s}{2}(\mathbf{E}_{O_1}^{\frac{1}{2}}\mathbf{E}_{O_2}^{\frac{1}{2}}+\rho\mathbf{E}_{S_1}^{\frac{1}{2}}\mathbf{E}_{S_2}^{\frac{1}{2}})], \quad (4.59)$$

where $\mathbf{E}_{O_i}=\omega_i^H\mathbf{T}\mathbf{R}\mathbf{T}^H\omega_i$, $\mathbf{E}_{S_i}^{\frac{1}{2}}=\omega_i^H\mathbf{T}\mathbf{S}_{1+}\mathbf{A}_1,\ i=1,2$, and $\mathbf{E}_O=(\mathbf{E}_{O_1}\mathbf{E}_{O_2})^{\frac{1}{2}}$. The inverses of their MGFs are given by

$$M(s)_{blue-mmse}^{-1} = det[\mathbf{I}-\frac{s}{2}(\mathbf{I}-\rho\Lambda)]det[\mathbf{I}+\frac{s}{2}(\mathbf{I}+\rho\Lambda)] \quad (4.60)$$

$$M(s)_{blue-ml}^{-1} = det[\mathbf{I}-\frac{s}{2}(\mathbf{I}+\Lambda_F-\rho\Lambda_F)]det[\mathbf{I}+\frac{s}{2}(\mathbf{I}+\Lambda_F+\rho\Lambda_F)], \quad (4.61)$$

where $\mathbf{A}_1\mathbf{U}_1^H\mathbf{S}_D^{-1}\mathbf{U}_1\mathbf{A}_1=\mathbf{Q}\Lambda\mathbf{Q}^H$ and $\mathbf{A}_1\mathbf{U}_1^H\mathbf{F}_D^{-1}\mathbf{U}_1\mathbf{A}_1=\mathbf{Q}\Lambda_F\mathbf{Q}^H$.

Compared with the results of MRC and homogeneous EGC schemes, it is immediately clear that (4.57) and (4.58) are only special cases of (4.59) of the general

heterogeneous EGC schemes. For MRC, there is only on filter's output involved in each decision statistic. So only $\mathbf{E}_O^{\frac{1}{2}}$ and $\mathbf{E}_S^{\frac{1}{2}}$ are present in (4.57). For homogeneous EGC, two outputs of the same filter contribute to each decision statistic, hence, $\mathbf{E}_O$ and $\mathbf{E}_S$ are present in (4.58).

Although the applicability of this formula (4.59) to all possible heterogeneous EGC schemes are not fully verified, since the simplification procedure seems to vary case by case. As far as our concern goes, this formula provides a good generic BER expression for the two classes of combinings scheme of interest. In the sequel, the analysis of BER is cross-verified with simulations.

4.3 Numerical Results

The analytic results of various MRC and EGC detectors are demonstrated herein and verified with their simulated results for a DS-CDMA system in multipath Rayleigh fading channels. Each user's signal in the system is considered propagating through a 3-path fading channel (i.e. $L = 3$) with the normalized Doppler shift $f_d T_s = 5 \times 10^{-3}$ for each path. There are 10 users in the system. Signature sequences are randomly chosen from a set of Gold codes of length N=31 for all users in the system. For simplicity, all users are assumed to have the same power, and the power is equally distributed among the paths of a user. To confine the strength of ISI which is ignored in the above analysis, the path delay τ_{kl} for each user is randomly generated with uniform distribution over $[0, 5T_c)$ under the constraint that the delay spread

$|\max_l\{\tau_{kl}\} - \min_l\{\tau_{kl}\}| < \tau_{max} = 5T_c$. Finally, BPSK and DBPSK signalings are empolyed, respectively, for the demonstrations of BER performance for coherent MRC and non-coherent EGC schemes.

Fig. 4.3 presents the convergence of the output SINRs with respect to the number of stages (D) for the multistage MRC MMSE/MOE/BLUE/ML-FBs at $E_b/N_0 = 20dB$. The applying stages ranges from 1 to 11. Filters' ranks $= D \times L$, with $D = 11$ corresponding to full-rank implementations. The upper diagram shows the output SINRs in the sense of (4.15). The analytic results are drawn using the formulae from (4.21) to (4.24), respectively. The lower one shows the convergence of the average SINR (4.31) of the MRC ML-FB. Both SINRs measures converge rapidly to the full-rank performance.

Fig. 4.4 shows the BER performance of the MRC MMSE/MOE/BLUE/ML-FBs. The BERs of the reduced-rank schemes with $D = 6$, (*i.e.* rank $= 6 \times L$) and the BERs of the full-rank schemes are simulated and compared with the analytic results listed in Table 4.1. Obviously, the ML receiver outperforms the other three, since ML-FB maximizes the conditional SINR (4.12). The analytic results are very close to the simulated results because only the desired user's ISI is ignored in the BER analysis for MRC schemes.

Fig. 4.5 shows the BER performance for the reduced-rank and the full-rank schemes using the EGC MMSE-MMSE and MOE-MOE combining methods proposed in [21] and the BLUE-ML combining proposed herein. The analytic results

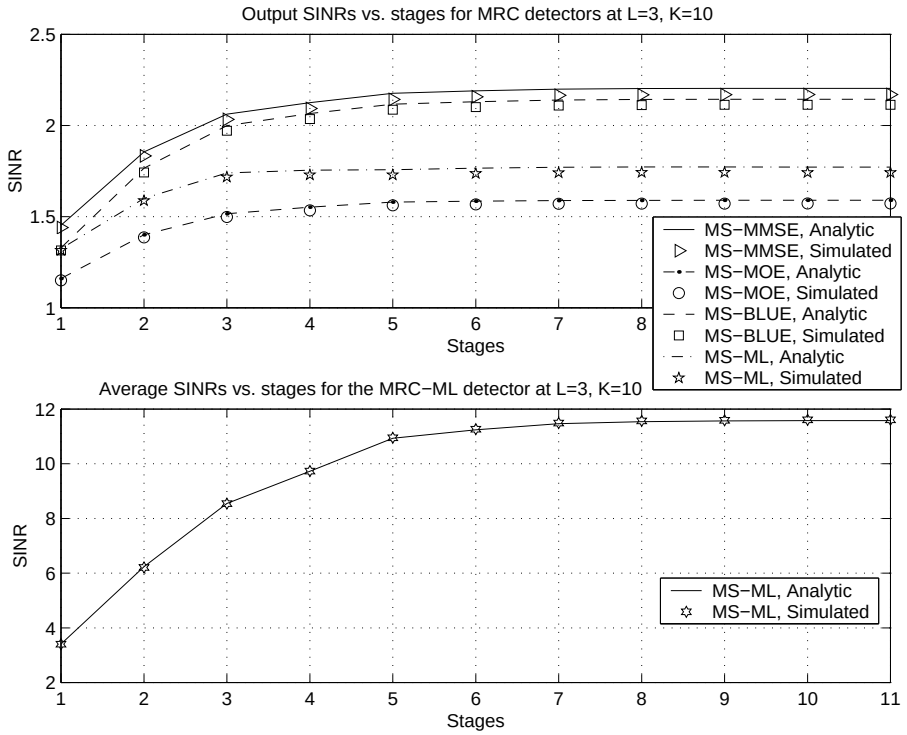

Figure 4.3: Convergence of the steady-state output SINRs with respect to the number of stages. Filters' ranks $= D \times L$. $D = 11$ corresponds to the full-rank implementation, $(N = 31)$. The upper plot is the output SINRs of (4.15), and the lower plot is the average SINR (4.31) of the MRC ML-FB.

are obtained from (B.50) and the formulae listed in Table 4.2. Obviously, the BLUE-ML combining presents the best performance over the other two schemes because BLUE-FB is the ML channel estimator of $\Gamma_1 b_1$ for the linear Gaussian Model and the ML-FB is the corresponding ML symbol detector in the same model. The analytic results are also close but a little bit smaller than the simulated results because all users' ISIs are ignored in the BER analysis for differential EGC schemes.

Fig. 4.6 shows the performance degradation using EGC schemes with the BLUE-FB served as the channel estimator in comparison with MRC schemes where perfect

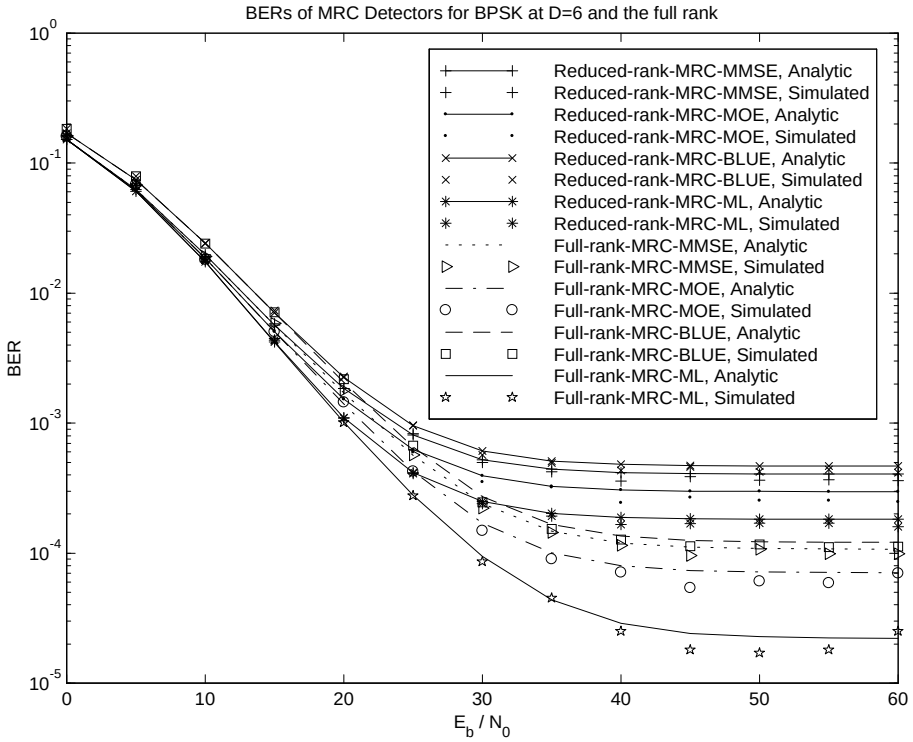

Figure 4.4: BERs of the MRC filter banks. There are 10 user in the system and N=31. The number of path for each user is equal to 3, ($L = 3$). The reduced-rank receivers are implemented with the number of stages $D = 6$, *i.e.* rank=18.

channel information is given for combinings. Reduced-rank implementations with $D = 6$ are used in this simulation. Performance of two maximizing filter banks in different senses, *i.e.* MMSE and ML, are shown together with the BLUE-BLUE combining where the filter itself also serves as a symbol detector. Cross-compared with the BER performance of EGC schemes shown in Fig. 4.5, we know that BLUE-ML comparing presents the best performance without introducing extra complexities for implementations.

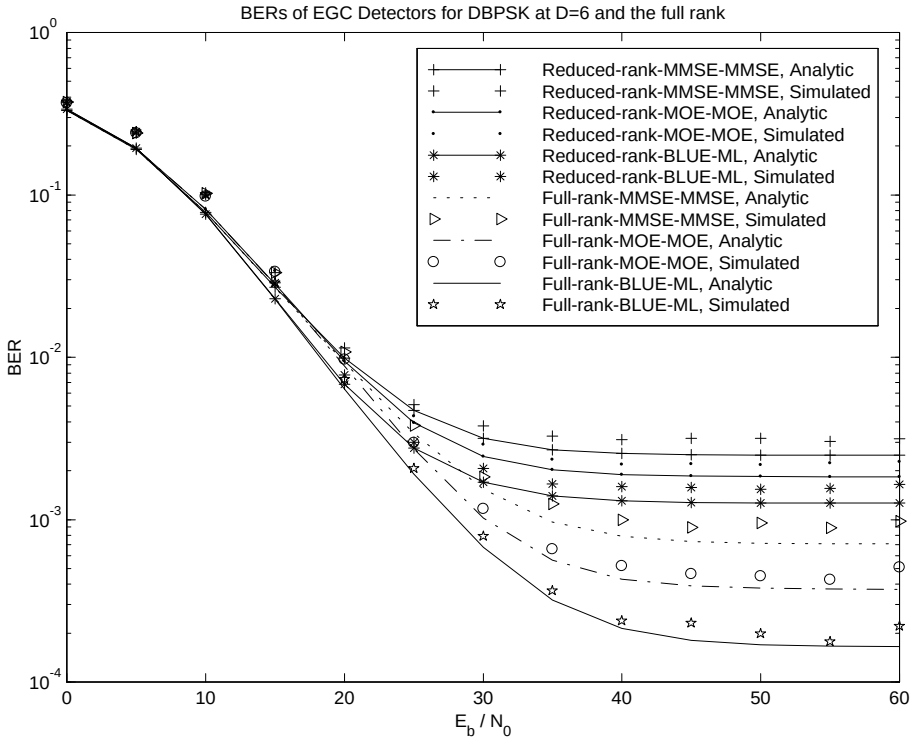

Figure 4.5: BER comparisons for the EGC MMSE-MMSE, MOE-MOE and the BLUE-ML filter banks. There are 10 user in the system and N=31. The number of path for each user is equal to 3, ($L = 3$). The reduced-rank receivers are implemented with the number of stages $D = 6$, *i.e.* rank=18.

We noted that under this system loading, (K=10, L=3), filters are not able to fully suppress MAI and ISI. The eigenvalues of Λ saturate in the high SNR regime such that both of the MRC and EGC schemes suffer from BER floors. The reason can be roughly seen from the BER formulae of the MRC-MMSE-FB and EGC-MMSE-FB in flat fading channels. Which are $BER_{MRC} = 0.5(1 - \lambda^{\frac{1}{2}})$ and $BER_{EGC} = 0.5(1-\rho\lambda)$, respectively from Table 4.1 and 4.2. Moreover, the auto-correlation value ρ in Table 4.2 will also constitutes performance bounds for EGC schemes in addition to the saturation of Λ. So it is needed to clarify those effects on BER performance.

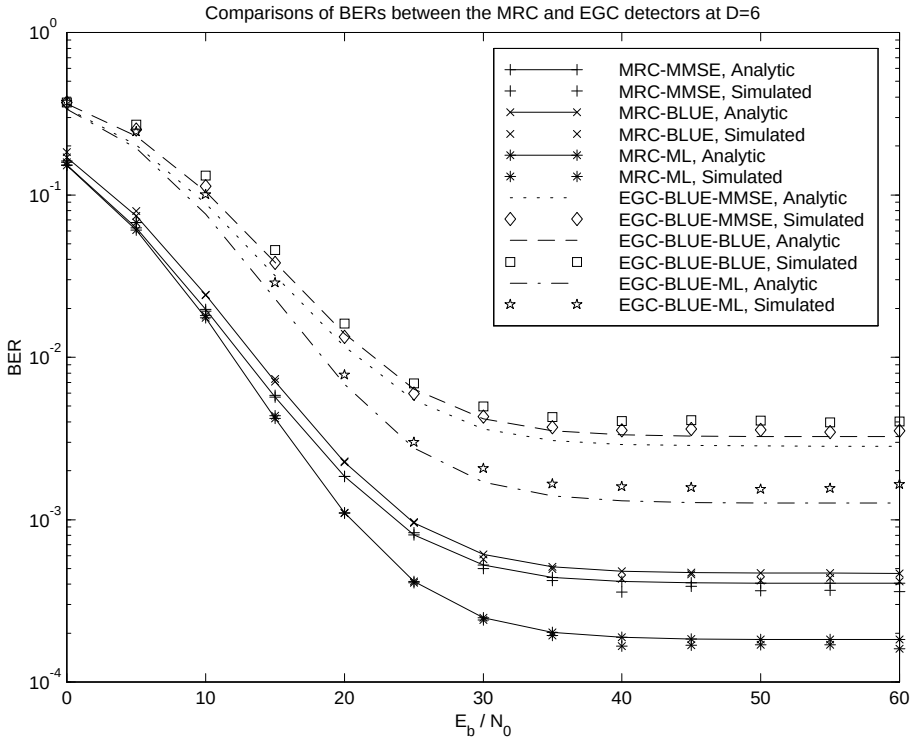

Figure 4.6: Performance comparisons for BERs of the EGC BLUE-ML and BLUE-MMSE detectors with those of the MRC ML and MMSE detectoes. There are 10 users in the system and N=31. The number of paths for each user is equal to 3, ($L = 3$). The number of applying stages for reduced-rank implementations is $D = 6$.

Due to the structure analysis for K_{mmse} and K_{ml} as well as the analytic results of BERs given in Section 4.2, a closer look into the mechanism for interference cancellation becomes possible. More detail discussions for the relationship between filters' ranks and performance bounds will be given in the next section.

4.4 Performance Bounds

As have been shown in the preceding section, both of the EGC and MRC receivers could suffer from performance bounds. The reasons can be linked to the saturation of Λ. To understand performance limitations, first we would like to check the achievability for the upper bound of Λ. This is given in the following proposition.

Proposition 5 *The upper bound* $\mathbf{I}$ *of* Λ *can be achieved if and only if the residual interference* $\mathbf{H}_1^H\mathbf{I}$ *due to MAI, ISI and noise could be fully suppressed by filter* ω_1*.*

Proof: Refer to the expression for $\mathbf{S}_D$ in (4.10).

($\Longrightarrow$) If $\mathbf{A}_1\mathbf{U}_1^H\mathbf{S}_D^{-1}\mathbf{U}_1\mathbf{A}_1 = \Lambda = \mathbf{I}$, then $\mathbf{S}_D = \mathbf{U}_1\mathbf{A}_1^2\mathbf{U}_1^H$. Again from (4.37)

$$\mathbf{S}_D = \mathbf{U}_1\mathbf{A}_1^2\mathbf{U}_1^H + E[(\mathbf{H}_1^H\mathbf{I}_1 - \omega_1^H\mathbf{H}_{1\perp}^H\mathbf{I}_1)(\mathbf{H}_1^H\mathbf{I}_1 - \omega_1^H\mathbf{H}_{1\perp}^H\mathbf{I}_1)^H].$$

Comparing the above two equations for $\mathbf{S}_D$, we immediately have

$$E[(\mathbf{H}_1^H\mathbf{I}_1 - \omega_1^H\mathbf{H}_{1\perp}^H\mathbf{I}_1)(\mathbf{H}_1^H\mathbf{I}_1 - \omega_1^H\mathbf{H}_{1\perp}^H\mathbf{I}_1)^H] = \mathbf{0}. \tag{4.62}$$

($\Longleftarrow$) Conversely, let $E[(\mathbf{H}_1^H\mathbf{I}_1 - \omega_1^H\mathbf{H}_{1\perp}^H\mathbf{I}_1)(\mathbf{H}_1^H\mathbf{I}_1 - \omega_1^H\mathbf{H}_{1\perp}^H\mathbf{I}_1)^H] = \mathbf{0}$, then $\mathbf{S}_D = \mathbf{U}_1\mathbf{A}_1^2\mathbf{U}_1^H$. Therefore, $\mathbf{A}_1\mathbf{U}_1^H\mathbf{S}_D^{-1}\mathbf{U}_1\mathbf{A}_1 = \mathbf{I} = \Lambda$. ■

This proposition tells that having $\Lambda = \mathbf{I}$ is almost impossible, in theory. So, we look for other possibilities like will be: what can we do to suppress interference as much as possible, what are the rules for choosing the ranks of filters and how are

they related to performance limits. We proceed the analysis for MRC and EGC schemes, respectively.

4.4.1 Performance limitations of MRC schemes

To fully remove a random noise seems impractical. But in the high SNR regime, where the noise covariance $N_0 \sim 0$, having $\Lambda \sim \mathbf{I}$ depends on whether a filter can remove MAI and ISI efficiently. For linear receivers, intuitively it is related to the available degrees of freedom, D_{free}, for suppressing interferences. Recall the structure of multistage filtering in Fig. 4.1. The first stage is actually a matched filter for extracting the desired user's information. So, from the second stage down to the Dth stage are available for suppress interferences. Hence, we can define a quantity $:D_{free} = (D-1) \times L$ for assessing the capability for interference suppression. On the other hand, the capability also depends on the dimension that interferences could span. Therefore, a measure for evaluating the dimension of interferences, D_{int}, can be defined to be the rank of the auto-correlation matrix of MAI plus ISI [*cf.* (3.13)], *i.e.*

$$\begin{aligned} D_{int} &= \text{rank}(E[(\mathbf{I}_1 - \mathbf{n})(\mathbf{I}_1 - \mathbf{n})^H]) \\ &= \text{rank}\left(\mathbf{S}_{1-}\mathbf{A}_1^2\mathbf{S}_{1-}^H + \sum_{k=2}^{K} \mathbf{S}_{k+}\mathbf{A}_k^2\mathbf{S}_{k+}^H + \mathbf{S}_{k-}\mathbf{A}_k^2\mathbf{S}_{k-}^H\right). \end{aligned} \tag{4.63}$$

Note that the Gaussian noise is excluded in this definition. Proposition 6 provides a condition for fully suppressing interferences in the high SNR regime.

Proposition 6 *As $N_0 \sim 0$, MAI and ISI can be fully suppressed if $D_{free} \geq D_{int}$.*

Proof: Define $\mathbf{C}_I \equiv E[(\mathbf{I}_1 - \mathbf{n})(\mathbf{I}_1 - \mathbf{n})^H]$, then $\mathbf{C} = E[\mathbf{I}_1\mathbf{I}_1^H] = \mathbf{C}_I + N_0\mathbf{I}$. Eq. (4.37) can be manipulated into

$$\begin{aligned}
\mathbf{S}_D &= \mathbf{U}_1\mathbf{A}_1^2\mathbf{U}_1^H + E[(\mathbf{H}_1^H\mathbf{I}_1 - \omega_1^H\mathbf{H}_{1\perp}^H\mathbf{I}_1)(\mathbf{H}_1^H\mathbf{I}_1 - \omega_1^H\mathbf{H}_{1\perp}^H\mathbf{I}_1)^H] \\
&= \mathbf{U}_1\mathbf{A}_1^2\mathbf{U}_1^H + (\mathbf{H}_1^H - \omega_1^H\mathbf{H}_{1\perp}^H)\mathbf{C}_I(\mathbf{H}_1 - \mathbf{H}_{1\perp}\omega_1) + N_0(\omega_1^H\omega_1 + \mathbf{I}) \\
&\simeq \mathbf{U}_1\mathbf{A}_1^2\mathbf{U}_1^H + (\mathbf{H}_1^H - \omega_1^H\mathbf{H}_{1\perp}^H)\mathbf{C}_I(\mathbf{H}_1 - \mathbf{H}_{1\perp}\omega_1), \quad \text{as } N_0 \sim 0. \qquad (4.64)
\end{aligned}$$

Let $\mathbf{C}_I = \mathbf{Q}_I\Sigma\mathbf{Q}_I^H,\ \Sigma = diag(\sigma_1, \cdots, \sigma_{D_{int}}),\ 0 \leq D_{int} \leq N$, be the singular value decomposition of $\mathbf{C}_I$. Thus,

$$(\mathbf{H}_1^H - \omega_1^H\mathbf{H}_{1\perp}^H)\mathbf{C}_I(\mathbf{H}_1 - \mathbf{H}_{1\perp}\omega_1) = (\mathbf{H}_1^H - \omega_1^H\mathbf{H}_{1\perp}^H)\mathbf{Q}_I\Sigma^{\frac{1}{2}}\Sigma^{\frac{1}{2}}\mathbf{Q}_I^H(\mathbf{H}_1 - \mathbf{H}_{1\perp}\omega_1).$$

To fully suppress interferences, we need $\mathbf{H}_1^H\mathbf{Q}_I\Sigma^{\frac{1}{2}} - \omega_1^H\mathbf{H}_{1\perp}^H\mathbf{Q}_I\Sigma^{\frac{1}{2}} = \mathbf{0}$. For a D-stage implementation, $\mathbf{H}_{1\perp}^H$ is of dimension $N \times (D-1)L$ and $\omega_1 : (D-1)L \times L$, $D_{free} = (D-1)L$. Therefore, $\mathbf{H}_1^H\mathbf{Q}_I\Sigma^{\frac{1}{2}} : L \times D_{int}$ and $\mathbf{H}_{1\perp}^H\mathbf{Q}_I\Sigma^{\frac{1}{2}} : D_{free} \times D_{int}$. To each column of ω_1, there are D_{int} equations for D_{free} variables. It takes $D_{free} \geq D_{int}$ to have solutions for $\mathbf{H}_1^H\mathbf{Q}_I\Sigma^{\frac{1}{2}} = \omega_1^H\mathbf{H}_{1\perp}^H\mathbf{Q}_I\Sigma^{\frac{1}{2}}$. This completes the proof. ■

Therefor, by proposition 5 and 6, $\Lambda \sim \mathbf{I}$ asymptotically as $D_{free} \geq D_{int}$. Fig. 4.7 reveals this property. In this simulation study, we set $E_b/N_0 = 60dB$ such that the noise power is negligible. Since L=2 for each user, $D_{free} = 2(D-1)$ and is a function of the number of applying stages, D. The lower plot shows the effective

dimension of interference, D_{int}, with respect to the number of users in the system. Cross-referencing to the upper plot, we can see that BERs jump up extremely fast whenever the condition $D_{free} - D_{int} \geq 0$ is violated. Fig. 4.8 elaborates this point with simulations employing various numbers (L) of resolvable transmission paths for users. Concluding from this two figures, as long as a reduced-rank filter can sustain the requirement of $D_{free} \geq D_{int}$, interference can be suppressed effectively regardless of filters' ranks in the high SNR regime.

In scenarios where the strength of Gaussian noise is comparable to that of MAI and ISI, or whenever a system is highly loaded such that $D_{free} < D_{int}$, Λ will go saturated with the number of stages very quick. The SINR curve, which is the curve of $trace(\Lambda)$, in Fig. 4.3 reflects this phenomena. Not only does the saturation of Λ degrade BER performance, but also constitutes a performance bound of BER floor as shown in Fig. 4.4. Fig. 4.9 illustrates this performance bound in more details with simulations at $K = 10$, $L = 2$ and $D_{int} = 28$. As we can see, as long as $D_{free} \geq D_{int}$, the cases of D=15 and the full-rank one, BER floors can be avoided for MRC schemes and performance is very close to the single user bound. However, the same reasoning doesn't apply to the EGC schemes. They still suffer from BER floors even though there no longer exists BER floors for MRC schemes after $D \geq 15$. To see this, we need to analyze the BER formulae for EGC schemes in the next section.

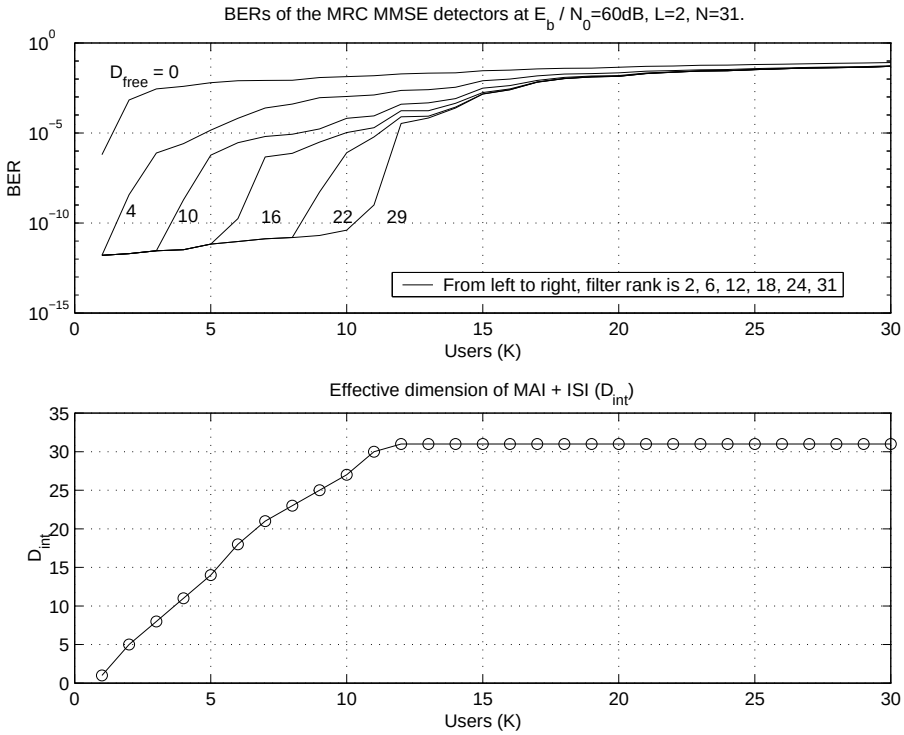

Figure 4.7: BERs of the reduced-rank EGC BLUE-ML filter banks. From the top to bottom, each curve corresponds to a implementation with the number of stages ranging from 1 to 11, where 11 relates to the full-rank implementation.

As a conclusion, to fully take the advantage of reduced-rank filtering, a rule of thumb for choosing the number of stages is that: If the system is not fully load, *i.e.* $D_{int} \leq (N-1) \times L$, then chose D as low as to just pass the requirement for $(D-1) \times L \geq D_{int}$. Otherwise, set $D = 6$ where Λ usually has saturated by observations. The same number of 6 was also observed in [12] according to the result of large-system analysis.

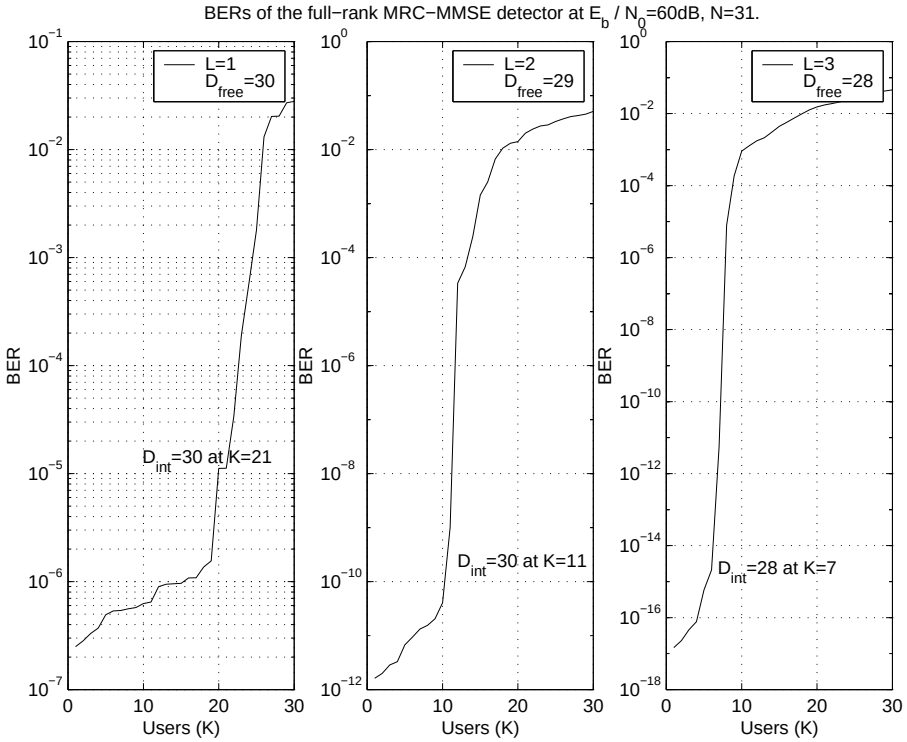

Figure 4.8: BERs of the reduced-rank EGC BLUE-ML filter banks. From the top to bottom, each curve corresponds to a implementation with the number of stages ranging from 1 to 11, where 11 relates to the full-rank implementation.

4.4.2 Performance limitations of EGC schemes

To fully understand the performance of EGC schemes in high SNR regimes, we use EGC-MMSE combing as an example to discuss the BER formula in detail. Similar phenomena will happen to other EGC schemes, since they all share the same multistage structure. First, we do some simplifications similar to what have been done for deriving BER formulae.

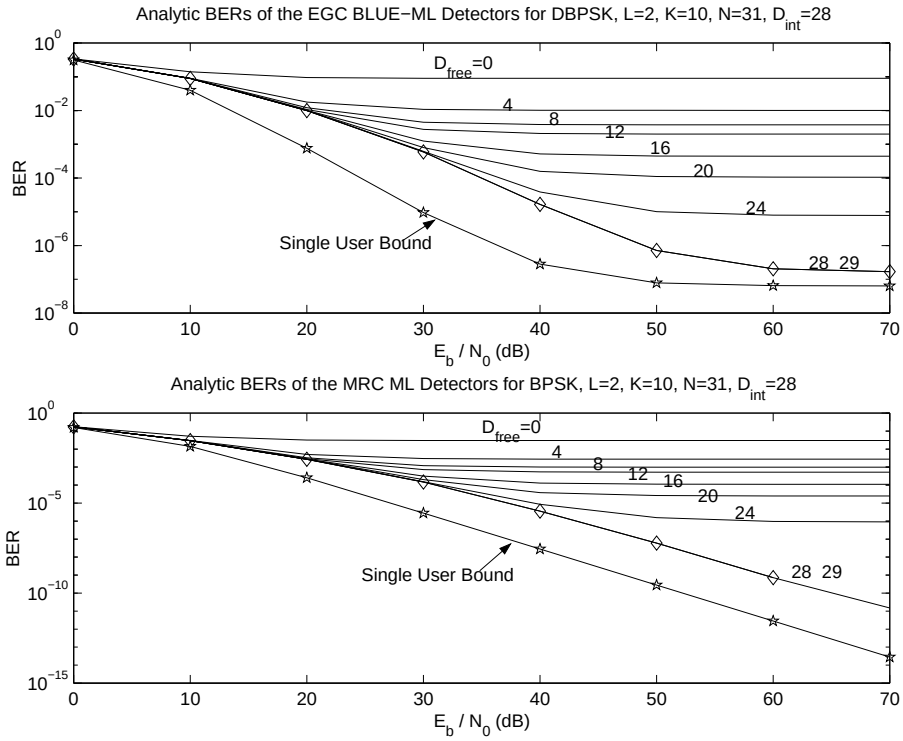

Figure 4.9: BERs of the reduced-rank EGC BLUE-ML filter banks. From the top to bottom, each curve corresponds to a implementation with the number of stages ranging from 1 to 11, where 11 relates to the full-rank implementation.

Ignoring ISI from all users, the second term on the right hand side of (4.8), the auto-correlation matrix R becomes

$$\tilde{\mathbf{R}} = \mathbf{S}_{1+}\mathbf{A}_1^2\mathbf{S}_{1+}^H + \sum_{k=2}^{K} \mathbf{S}_{k+}\mathbf{A}_k^2\mathbf{S}_{k+}^H + N_0\mathbf{I} \equiv \mathbf{R}_S + \mathbf{R}_I, \tag{4.65}$$

where $\mathbf{R}_S = \mathbf{S}_{1+}\mathbf{A}_1^2\mathbf{S}_{1+}^H$ and $\mathbf{R}_I = \sum_{k=2}^{K} \mathbf{S}_{k+}\mathbf{A}_k^2\mathbf{S}_{k+}^H + N_0\mathbf{I}$. Define the interference covariance matrix $\mathbf{N}_I$ with respect to the desired user as $\mathbf{N}_I = \omega^H\mathbf{T}\mathbf{R}_I\mathbf{T}^H\omega$. Thus,

$\mathbf{E}_O = \omega^H \mathbf{T}\mathbf{R}\mathbf{T}^H\omega \simeq \omega^H \mathbf{T}(\mathbf{R}_I + \mathbf{R}_S)\mathbf{T}^H\omega = \mathbf{E}_S + \mathbf{N}_I$. Equation (4.58) can be rewritten as

$$det[\mathbf{I} + s\mathbf{J}\Phi] = det[\mathbf{I} - \frac{s}{2}((1-\rho)\mathbf{E}_S + \mathbf{N}_I)]det[\mathbf{I} + \frac{s}{2}((1+\rho)\mathbf{E}_S + \mathbf{N}_I)]. \quad (4.66)$$

Since $\mathbf{E}_S$ and $\mathbf{E}_O$ for each filter bank have already been given in Appendix C, $\mathbf{N}_I$ can be obtained by subtracting $\mathbf{E}_S$ from $\mathbf{E}_O$. Now casting the analysis to the EGC-MMSE-FB, we have $\mathbf{E}_S = \mathbf{Q}\Lambda^2\mathbf{Q}^H$ and $\mathbf{E}_O = \mathbf{E}_S^{\frac{1}{2}}$, where $\mathbf{A}_1\mathbf{U}_1^H\mathbf{S}_D^{-1}\mathbf{U}_1\mathbf{A}_1 = \mathbf{Q}\Lambda\mathbf{Q}^H$ and $\Lambda = \text{diag}(\lambda_1, \cdots, \lambda_L)$. Thus, $\mathbf{N}_I = \mathbf{Q}(\Lambda - \Lambda^2)\mathbf{Q}^H$. Substituting these terms back into (4.66) yields

$$det[\mathbf{I} + s\mathbf{J}\Phi] = det[\mathbf{I} - \frac{s}{2}(\Lambda - \rho\Lambda^2)]det[\mathbf{I} + \frac{s}{2}(\Lambda + \rho\Lambda^2)]. \quad (4.67)$$

From (4.29), it is clear that the first determinant on the right hand side decides the RHP poles, since $\rho < 1$. To calculate the residue with respect to RHP poles, $s = \frac{2}{\lambda_i(1-\rho\lambda_i)},\ i = 1 \ldots L$, is substituted back into the second determinant of (4.67). For simplicity, we consider the case where the eigenvalues are all distinct. Inserting (4.67) back into (4.49) and calculating the residual yields

$$\begin{aligned} BER_{EG-MMSE} &= \sum_{i=1}^{L} \left\{ \frac{\lambda_i(1-\rho\lambda_i)}{\lambda_i(1-\rho\lambda_i) + \lambda_i(1+\rho\lambda_i)} \cdot \right. \\ &\left. \prod_{j=1, j\neq i}^{L} \left[\frac{\lambda_i(1-\rho\lambda_i)}{\lambda_i(1-\rho\lambda_i) + \lambda_j(1+\rho\lambda_j)} \cdot \frac{\lambda_i(1-\rho\lambda_i)}{\lambda_i(1-\rho\lambda_i) - \lambda_j(1-\rho\lambda_j)} \right] \right\}. \end{aligned} \quad (4.68)$$

Since multipath only improves performance and do not make receivers physically different. To highlight key effects, we consider the case for flat fading channels. Thus, $0 \leq E_S = \lambda^2 \leq 1$, and $0 \leq N_I = \lambda - \lambda^2 \leq \frac{1}{4}$. The upper bound of N_I can be easily obtained by taking its derivative with respect to λ and setting to zero. Also, by (B.23),

$$\Lambda_F = (\Lambda^{-1} - \mathbf{I})^{-1} = \Lambda + \Lambda^2 + \Lambda^2 \cdots.$$

Thus,

$$0 \leq \frac{E_S}{N_I} = \frac{\lambda}{1-\lambda} = \lambda_f = \lambda + \lambda^2 + \cdots \leq \infty.$$

Assuming $D_{free} \geq D_{int}$, in the high SNR regime $\lambda \sim 1$. So $\frac{E_S}{N_I} = \lambda_f \sim \infty$. In this case, the BER of the EGC-MMSE receiver can be manipulated into the form of

$$\begin{aligned} BER_{EG-MMSE} &= \frac{\lambda(1-\rho\lambda)}{2\lambda} = \frac{(1-\rho)\lambda^2 + \lambda - \lambda^2}{2(\lambda^2 + \lambda - \lambda^2)} = \frac{(1-\rho)E_S + N_I}{2(E_S + N_I)} \\ &= \frac{(1-\rho)}{2(1 + N_I/E_S)} + \frac{N_I/E_S}{2(1 + N_I/E_S)} \\ &\simeq \frac{(1-\rho)}{2} + \frac{N_I/E_S}{2} \quad \text{as} \quad \frac{N_I}{E_S} \ll 1. \end{aligned} \tag{4.69}$$

This shows that the BER is controlled by two factors, the first term is due to the channel mismatch between two adjacent symbol interval and the second is related to E_S/N_I. So, even if $N_I/E_S \sim 0$ when $D_{free} \geq D_{int}$ at high SNR, a differential EGC scheme still suffers from a BER floor due to the auto-correlation value of a fading process. The same phenomena applies to other EGC schemes. Actually, by similar procedure, BERs for all EGC schemes, heterogeneous or not, can be easily

shown equivalent over a flat Rayleigh fading channel. We also note that (4.69) has the same form of BER formula to the DBPSK demodulation of non-spread systems. The difference is that E_S/N_I is replaced by E_b/N_0 for DBPSK demodulation. Where E_b and N_0 are the signal and the noise variances, respectively. Here E_S and N_I are the corresponding filtered signal and filtered interference variances.

The remaining question is how much does the performance of EGC schemes deviates from that of MRC schemes. For comparison, we consider the MRC-MMSE detector in flat Rayleigh fading channels.

From Table 4.1, the $M^{-1}(s)$ for MRC-MMSE can be shown equal to

$$det[\mathbf{I} + sJ\Phi] = det[\mathbf{I} - \frac{s}{2}(\mathbf{\Lambda^{\frac{1}{2}}} - \mathbf{\Lambda})]det[\mathbf{I} + \frac{s}{2}(\mathbf{\Lambda^{\frac{1}{2}}} + \mathbf{\Lambda})]. \tag{4.70}$$

Casting it into a flat fading channel, the resultants BER is given by

$$BER_{MRC} = \frac{1 - \lambda^{\frac{1}{2}}}{2}. \tag{4.71}$$

Similarly, the BERs of all MRC schemes are the same in flat fading channels. For comparison, the BER for all EGC schemes in flat fading channels is shown below

$$BER_{EGC} = \frac{1 - \rho\lambda}{2}. \tag{4.72}$$

As a result, the BER for MRC schemes is only a function of the eigenvalue λ. When $D_{free} \geq D_{int}$, the eigenvalue λ keeps approaching its upper bound, one, as E_b/N_0 increases higher and higher, so BER_{MRC} can keep dropping down without hitting a BER floor. Fig. 4.10 illustrates this point by presenting the BERs of EGC BLUE-MMSE and BLUE-ML schemes versus the BERs of MRC-MMSE and MRC-ML schemes. In this simulation, system parameters are set to: $K = 10$, $N = 31$, $D_{int} = 18$ and $f_d T_s = 5 \times 10^{-3}$. For full-rank schemes, $D_{free} - D_{int} = 12$ and $\rho = J_0(2\pi f_d T_s) = 0.99975$. BERs of EGC schemes hit a bound at $0.5 \times (1 - \rho) = 1.25 \times 10^{-4}$. On the other hand, for reduced-rank schemes, $D_{free} - D_{int} = -7$. λ saturates at a value $\lambda_{sat} \simeq 0.9998$ due to residual interferences. This SNR saturation causes a BER floor at $0.5 \times (1 - \lambda_{sat}^{\frac{1}{2}}) \simeq 5 \times 10^{-5}$ for MRC schemes and a BER floor at $0.5 \times (1 - \rho\lambda_{sat}) \simeq 2.25 \times 10^{-4}$ for EGC schemes. This explains why BERs of MRC and EGC schemes behave like two horizontal lines travelling at a fixed distance in the high SNR regime. Similar arguments can also explain the same phenomena for multipath fading channels demonstrated in Fig. 4.6, where $D_{free} = 15$ and $D_{int} = 31$.

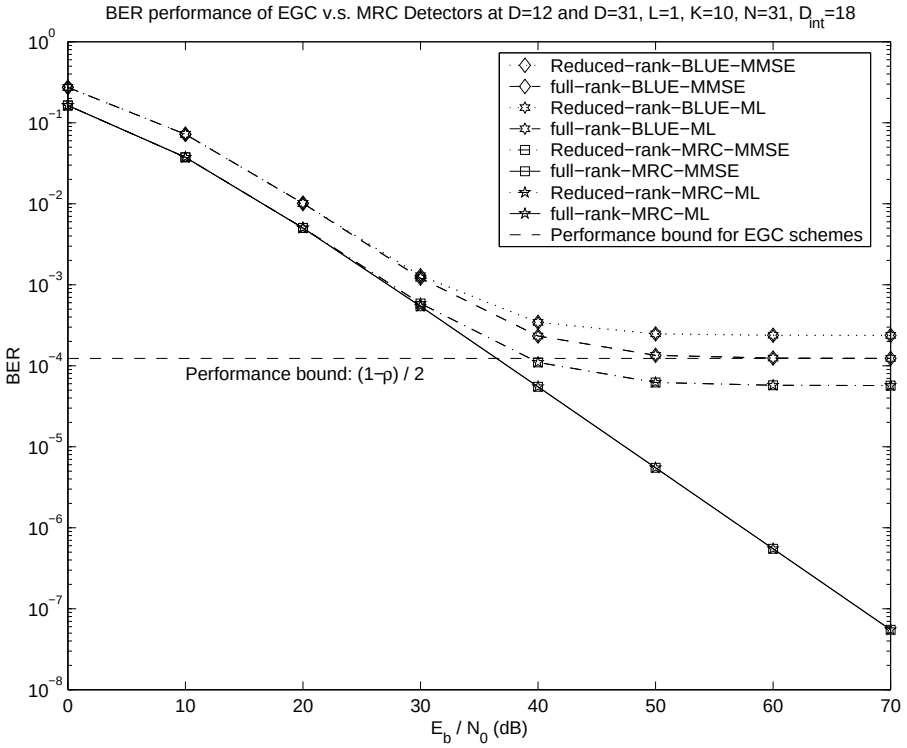

Figure 4.10: Performance comparisons of BERs for the EGC BLUE-ML and BLUE-MMSE detectors v.s the MRC ML and MMSE detectors. Two cases of implementations with $D = 6$ and the full-rank ones are shown in this figure. The simulation environment is a flat Rayleigh fading channel with $f_d T_s = 5 \times 10^{-3}$. All users have equal power.

Chapter 5

Blind Detection using the EM Algorithm

In Chapters 3 and 4, a group of multistage blind detection methods were introduced for symbol detection based on differential EGC to combat phase uncertainties in multipath fading channels. Due to noncoherent differential combining, detectors' performance is limited by the Doppler frequency of a fading channel (or, in other words, channel mismatch between two time-adjacent symbols), even if the degree of freedom of the system, D_{free}, is larger than the dimension of MAI, D_{int}. One natural way to overcome the limitation arising from channel mismatch is to perform joint channel estimation and symbol detection. Moreover, for multiuser detection (MUD) in direct-sequence code-division multiple access (DS-CDMA) systems, it is desirable to achieve near single user system performance without resorting to schemes of exponential complexity. An effective approach is to use iterative soft interference cancellation, *e.g.* [27]. To this end and for fading channels in particular, the channel parameter estimation as well as the soft output evaluation for all users should be performed jointly and refined at each iteration. By considering these two

facts, joint channel estimation and symbol detection emerges as a promising and practical approach for blind MUD for DS-CDMA.

One approach to joint channel estimation and symbol detection is based on the expectation maximization (EM) algorithm [6]. Similar to many blind estimation schemes, *e.g.* [24], the blind implementation of the EM algorithm suffers from the channel phase ambiguity, even if it is possible to obtain good estimation of the channel gain. The inherent phase ambiguity problem is usually handled by differential encoding in the single user system. However, in the context of suppressing multiple access interference (MAI) for DS-CDMA systems, the phase ambiguity reduction has to be addressed explicitly.

In this chapter, a low-complexity sliding-window scheme is proposed for channel tracking based on the EM algorithm and a noncoherent maximum *a posteriori* probability (MAP) multi-user detector. By exploiting the property of discrete random phase ambiguity of channel estimates, the proposed scheme can track the channel phase even if the channel is in a deep fading situation. In conjunction with iterative soft interference cancellation, the proposed detector can achieve near single user system performance of a polynomial complexity with respect to the number of users.

5.1 System Model for Dispersive Multipath Fading Channels

The system model in Chapter 2 is extended and re-formulated in this section so that we can handle the more realistic dispersive channel, where a significant amount of symbol delay may occur and address joint channel estimation and MUD of DS-CDMA under the framework of the EM algorithm.

Let us begin with the discrete-time signal model introduced in (5.1). The received signal vector $\mathbf{y}$ obtained by collecting N consecutive samples of the matched filter output is given by [21]

$$\mathbf{y}(m) = \sum_{k=1}^{K} \sum_{l=1}^{L_k} A_{kl}\gamma_{kl}(m) \cdot [\mathbf{s}_{kl}^{+} b_k(m - m_{kl}) + \mathbf{s}_{kl}^{-} b_k(m - m_{kl} - 1)] + \mathbf{n}(m), \quad (5.1)$$

where $m_{kl} = \lfloor \frac{\tau_{kl}}{T_s} \rfloor$ is no longer confined to $\{0, 1\}$. This means the symbol delay along each transmission path could be longer than one symbol interval. Let us define $h_{kl}(m) \equiv A_{kl} \times \gamma_{kl}(m)$ and $\mathbf{g}_{kl}(m_{kl}) \equiv \mathbf{s}_{kl}^{+} b_k(m - m_{kl}) + \mathbf{s}_{kl}^{-} b_k(m - m_{kl} - 1)$. The received signal can be expressed in matrix form by

$$\mathbf{y}(m) = \sum_{k=1}^{K} \sum_{l=1}^{L_k} \mathbf{g}_{kl}(m_{kl}) h_{kl}(m) + \mathbf{n}(m) = \sum_{k=1}^{K} \mathbf{G}_k(\xi_k^m)\mathbf{h}_k(m) + \mathbf{n}(m), \quad (5.2)$$

where $\mathbf{h}_k(m) \equiv [h_{k0}, \cdots, \ h_{k(L_k-1)}]^T$ and $\mathbf{G}_k(\xi_k^m) = [\mathbf{g}_{k0}, \cdots, \mathbf{g}_{k(L_k-1)}]$, and where time indices m and m_{kl} are omitted for convenience. Let the spreading sequence c_k

and the time delay τ_k be fixed, the system matrix $\mathbf{G}_k(\xi_k^m)$ is a function of the symbol state $\xi_k^m \equiv [b_k(m), \cdots, b_k(m-L_k^p)]$, where $L_k^p \equiv \lceil \frac{\max(\tau_{kl})}{T_s} \rceil$ is the largest symbol delay for the kth user. The overall received signal can be expressed using a multiple input multiple output (MIMO) channel model of the form

$$\begin{aligned} \mathbf{y}(m) &= \left[\mathbf{G}_0(\xi_0^m) \cdots \mathbf{G}_{K-1}(\xi_{K-1}^m) \right] \begin{bmatrix} \mathbf{h}_0(m) \\ \vdots \\ \mathbf{h}_{K-1}(m) \end{bmatrix} + \mathbf{n}(m) \\ &\equiv \mathbf{G}(m)\mathbf{h}(m) + \mathbf{n}(m). \end{aligned} \tag{5.3}$$

5.2 Channel Estimation Using the EM Algorithm

The complexity for simultaneously estimating the channels of all users is prohibitively high. Its complexity is $\mathbf{O}(|\mathcal{B}|^{K(L_p+1)})$, where $L_p \equiv max_k\{L_k^p, \}$ is the largest symbol delay among all users. Furthermore, a large number of samples of the received signal has to be collected to maintain the quality of the estimate. That is detrimental to tracking a fast fading channel. To control the complexity and reduce the number of samples required for estimation, channels of each user will be estimated separately. When dealing with the kth user's signal, all interfering users' signals are collected as

a colored Gaussian distributed interference signal $\mathbf{I}_k$. The received signal (5.3) can be rewritten as

$$\begin{aligned}\mathbf{y}(m) &= \mathbf{G}_k(\xi_k^m)\mathbf{h}_k(m) + \sum_{i=0,i\neq k}^{K-1} \mathbf{G}_i(\xi_i^m)\mathbf{h}_i(m) + \mathbf{n}(m) \\ &\equiv \mathbf{G}_k(\xi_k^m)\mathbf{h}_k(m) + \mathbf{I}_k(m) + \mathbf{n}(m). \end{aligned} \tag{5.4}$$

The covariance matrix of $\mathbf{I}_k(m) + \mathbf{n}(m)$ can be calculated as

$$\mathbf{C}_k(m) = E[(\mathbf{I}_k(m) + \mathbf{n}(m))(\mathbf{I}_k(m) + \mathbf{n}(m))^H]. \tag{5.5}$$

Now, we view the symbol stream b_k as the missing data and express the parameter set up to time m for user k by $\Theta_k(m) = [\theta_k(0), \cdots, \theta_k(m)]$, where $\theta_k(m) = \{\mathbf{h}_k(m), \mathbf{C}_k(m)\}$. The complete data for the EM algorithm is $\{\mathbf{y}(0), \cdots, \mathbf{y}(m), b_k(0), \cdots, b_k(m)\}$. Under this setting, the Kullback-Leibler (K-L) measure for the kth user at the ℓth iteration can be written as

$$\begin{aligned}\mathbf{Q}(\Theta_k, \Theta_k^{\ell-1}) &= \sum_{m=0}^{M-1} \sum_{\xi_k^m} \log \Big\{ \frac{1}{(2\pi)^N det(\mathbf{C}_k)} \exp -[\mathbf{y}(m) - \mathbf{G}_k(\xi_k^m)\mathbf{h}_k(m)]^H \cdot \\ &\quad \mathbf{C}_k^{-1}(m)[\mathbf{y}(m) - \mathbf{G}_k(\xi_k^m)\mathbf{h}_k(m)] \Big\} P_k(\mathcal{Y}, \xi_k^m | \Theta_k^{\ell-1}), \end{aligned} \tag{5.6}$$

where $\mathcal{Y} \equiv \{\mathbf{y}(0) \cdots \mathbf{y}(M-1)\}$, $P_k(\mathcal{Y}, \xi_k^m | \Theta_k) \propto P_k(\xi_k^m | \mathcal{Y}, \Theta_k)$ and $\Theta_k \equiv \Theta_k(M)$ for simplicity. Then, the EM algorithm can be written as

E-step: Compute $\mathbf{Q}(\Theta_k, \Theta_k^{\ell-1})$;

M-step: $\Theta_k^{\ell} = arg\max_{\Theta_k} \mathbf{Q}(\Theta_k, \Theta_k^{\ell-1})$.

Given state $\Theta_k^{\ell-1}$ to evaluate the K-L measure, new state Θ_k^{ℓ} is obtained by maximizing the K-L measure with respect to Θ_k. By iterating the above procedure, the algorithm is guaranteed to converge to a locally optimal steady-state Θ_k [6]. However, the direct implementation for the optimization of $\Theta_k(M)$ is extremely complicated and non-causal. To comprise between the complexity of the algorithm and the fidelity of the parameter estimates for a fading channel, two schemes are proposed. One is a sliding window scheme, where Θ_k is treated as a deterministic unknown over the current window. The other is a recursive optimization scheme based on the recursive EM proposed in [34]. The applicability of these algorithms relies on the fading speed and the acceptable complexity. The sliding window scheme is introduced next, which is followed by the recursive EM algorithm.

5.2.1 The Sliding Window EM Algorithm

The sliding-window EM algorithm [30] is used here to approximate time-varying channel parameters. The smoothing lags are denoted by L_s and L_p. The window slides forward by L symbols each time, and the index set at the mth window is $W(m) = \{n : \quad mL - L_p, \cdots, mL + L + L_s - 1\}, \quad m = 0, \cdots, \infty$. The $L_s + L_p + L$

consecutive samples of $\mathbf{y}$ inside the mth window gives the concatenated received signal

$$\mathcal{Y}(m) \;=\; \Big[\; \mathbf{y}(mL - L_p) \cdots \mathbf{y}(mL + L + L_s - 1) \;\Big]. \tag{5.7}$$

Let channel parameters $\mathbf{h}_k(m)$ and $\mathbf{C}_k(m)$ be deterministic unknown constants over the mth window and $\Theta_k = \theta_k(m)$. The K-L measure with respect to the mth window is given by

$$\begin{aligned}\mathbf{Q}(\theta_k, \theta_k^{\ell-1}) \;=\; & \sum_{n \in W(m)} \sum_{\xi_k^n} \log \Bigg\{ \frac{1}{(2\pi)^N det(\mathbf{C}_k)} \exp -[\mathbf{y}(n) - \mathbf{G}_k(\xi_k^n)\mathbf{h}_k]^H \cdot \\ & \mathbf{C}_k^{-1}[\mathbf{y}(n) - \mathbf{G}_k(\xi_k^n)\mathbf{h}_k] \Big\} P_k(\mathcal{Y}(m), \xi_k^n | \theta_k^{\ell-1}).\end{aligned} \tag{5.8}$$

It is assumed that matrix $\mathbf{G}_k(\xi_k^n)$ is of full column rank and $\mathbf{C}_k(m)$ is constant within this window. The optimal channel estimate is given by

$$\begin{aligned}\mathbf{h}_k^{\ell}(m) \;=\; & \Bigg[\sum_{n \in W(m)} \sum_{\xi_k^n} [\mathbf{G}_k^H (\mathbf{C}_k(m))^{-1} \mathbf{G}_k] P_k(\mathcal{Y}, \xi_k^n | \theta_k^{\ell-1}) \Bigg]^{-1} \cdot \\ & \sum_{n \in W(m)} \sum_{\xi_k^n} [\mathbf{G}_k^H (\mathbf{C}_k(m))^{-1} \mathbf{y}] P_k(\mathcal{Y}, \xi_k^n | \theta_k^{\ell-1}).\end{aligned} \tag{5.9}$$

Alternatively, the estimate of the covariance matrix, given by $\mathbf{h}_k^{\ell}(m)$, is equal to

$$\begin{aligned}\mathbf{C}_k^{l}(m) = & \Bigg[\sum_{\xi_k^n} P_k(\mathcal{Y}, \xi_k^n | \theta_k^{\ell-1}) \Bigg]^{-1} \cdot \\ & \sum_{n \in W(m)} \sum_{\xi_k^n} \Big\{ [\mathbf{y} - \mathbf{G}_k \mathbf{h}_k^{\ell}][\mathbf{y} - \mathbf{G}_k \mathbf{h}_k^{\ell}]^H \Big\} P_k(\mathcal{Y}, \xi_k^n | \theta_k^{\ell-1}).\end{aligned} \tag{5.10}$$

For simplicity, the symbol state ξ_k^n as the variable of the system matrix $\mathbf{G}_k(\xi_k^n)$ is dropped as shown above. It is clear that $\mathbf{G}_k = \mathbf{G}_k(\xi_k^n)$. To avoid the singularity of $\mathbf{C}_k^l$, $\mathbf{C}_k(m)$ is held constant during the iteration and is updated window by window at the end of the iteration process with the following formula:

$$\mathbf{C}_k(m+1) = \lambda \mathbf{C}_k(m) + (1-\lambda)\mathbf{C}_k(m). \tag{5.11}$$

The new update of $\theta_k(m)$ at the ℓth iteration becomes $\theta_k^\ell(m) = \{\mathbf{h}_k^\ell(m), \mathbf{C}_k(m)\}$. The probability $P_k(\mathcal{Y}, \xi_k^n|\theta_k)$ can be evaluated using the BCJR algorithm [1] by passing the message from the current window to the next one [30].

5.2.2 The Recursive EM Algorithm

To track a time-varying channel, a recursive estimation scheme is developed here based on the above sliding-window EM algorithm. Channel estimation is performed window by window, where channel parameters in a window are treated as deterministic unknowns and characterized via a dynamic evolution model. The essence of the recursive estimation scheme lies in the use of a dynamic model to describe the evolution of estimation parameters. For fading channels, a widely used model is the autoregressive moving average (ARMA) filter [5]. Here, the dynamics of fading channel parameters are modeled by an AR filter as

$$\boldsymbol{h}_k(m) = \mathbf{F}_k \boldsymbol{h}_k(m-1), \tag{5.12}$$

where $\boldsymbol{h}_k(m) = [\mathbf{h}_k^T(m), \cdots, \mathbf{h}_k^T(m - N_h + 1)]^T$, and where N_h is the order of the model and $\mathbf{F}_k$ is an $(N_h \cdot L_k) \times (N_h \cdot L_k)$ matrix. Then, the received signal with respect to user k can be rewritten as

$$\begin{aligned} \mathbf{y}(m) &= [\mathbf{G}_k(\xi_k^m), \mathbf{0}_{N\times(N_h-1)L_k}]\boldsymbol{h}_k(m) + \mathbf{I}_k(m) + \mathbf{n}(m) \\ &\equiv \mathbf{G}'_k(\xi_k^m)\boldsymbol{h}_k(m) + \mathbf{I}_k(m) + \mathbf{n}(m). \end{aligned} \tag{5.13}$$

Let $\boldsymbol{h}^{\ell}_{k:(m|m-1)}$ denote $\boldsymbol{h}^{\ell}_k(m)$ at the ℓth iteration obtained from $\boldsymbol{h}^{\ell}_k(m-1)$ using dynamic model (5.12). The corresponding Θ^{ℓ}_k is expressed by $\Theta^{\ell}_{k:(m|m-1)} = \{\Theta_k(m-1)^{\ell}, \mathbf{h}^{\ell}_{k:(m|m-1)}\}$. The covariance matrix $\mathbf{C}_k$ is assumed to be constant during the current window. Then, the K-L measure up to time m at the ℓth iteration can be rewritten as

$$\begin{aligned} \mathbf{Q}(\Theta_k(m), \Theta^{\ell-1}_{k:(m|m-1)}) &= \sum_{i=0}^{m}\sum_{\xi_k^i} \log\left\{\frac{1}{(2\pi)^N det(\mathbf{C}_k)}\exp -[\mathbf{y}(i) - \mathbf{G}'_k(\xi_k^i)\boldsymbol{h}_k(i)]^H\cdot \right. \\ &\quad \left. \mathbf{C}_k^{-1}[\mathbf{y}(i) - \mathbf{G}'_k(\xi_k^i)\boldsymbol{h}_k(i)]\right\} P_k(\mathcal{Y}, \xi_k^i|\Theta^{\ell-1}_{k:(m|m-1)}) \\ &= \mathbf{Q}(\Theta_k(m-1), \Theta_k^{\ell-1}(m-1)) + \\ &\quad \sum_{\xi_k^m} \log\left\{\frac{1}{(2\pi)^N det(\mathbf{C}_k)}\exp -[\mathbf{y}(m) - \mathbf{G}'_k(\xi_k^i)\boldsymbol{h}_k(m)]^H\cdot \right. \\ &\quad \left. \mathbf{C}_k^{-1}[\mathbf{y}(m) - \mathbf{G}'_k(\xi_k^i)\boldsymbol{h}_k(m)]\right\} P_k(\mathcal{Y}, \xi_k^m|\Theta^{\ell-1}_{k:(m|m-1)}). \end{aligned} \tag{5.14}$$

Now, let us approximate $\mathbf{Q}(\Theta_k(m-1), \Theta_k^{\ell-1}(m-1))$ by $\mathbf{Q}(\Theta_k(m-1), \Theta^{\ell-1}_{k:(m-1|m-2)})$ and define $\tilde{\mathbf{G}}_k(m) \equiv \mathbf{C}_k^{-1}\sum_{\xi_k^m}\mathbf{G}'_k(\xi_k^m)P_k(\mathcal{Y}\xi_k^m|\Theta^{\ell-1}_{k:(m|m-1)})$,

$\tilde{\mathbf{C}}_k^{-1}(m) \equiv \sum_{\xi_k^m} (\mathbf{G}_k'(\xi_k^m))^H \mathbf{C}_k^{-1} \mathbf{G}_k'(\xi_k^m) P_k(\mathcal{Y}, \xi_k^m | \Theta_{k:(m|m-1)}^{\ell-1})$ and

$\tilde{\boldsymbol{h}}_k(m) \equiv \tilde{\mathbf{C}}_k \tilde{\mathbf{G}}_k^H(m) \mathbf{y}(m)$. Eq. (5.14) can be reformulated as

$$\begin{aligned} \mathbf{Q}(\Theta_k(m), \Theta_{k:(m|m-1)}^{\ell-1}) \;\simeq\; & \mathbf{Q}(\Theta_k(m-1), \Theta_{k:(m-1|m-2)}^{\ell-1}) \\ & -[\tilde{\boldsymbol{h}}_k(m) - \boldsymbol{h}_k(m)]^H \tilde{\mathbf{C}}_k^{-1}(m) [\tilde{\boldsymbol{h}}_k(m) - \boldsymbol{h}_k(m)] \\ & -\mathbf{y}^H(m) \mathbf{C}_k^{-1} \mathbf{y}(m) + \mathbf{y}^H(m) \tilde{\mathbf{G}}_k(m) \tilde{\mathbf{C}}_k(m) \tilde{\mathbf{G}}_k^H(m) \mathbf{y}(m) \\ & - \log\{(2\pi)^N det(\mathbf{C}_k)\}. \end{aligned} \tag{5.15}$$

Since matrix $\mathbf{C}_k$ is assumed to be constant when evaluating channel coefficients $\boldsymbol{h}_k$, the last three terms of the preceding K-L measure can be dropped. Thus, we have

$$\begin{aligned} \mathbf{Q}(\Theta_k(m), \Theta_{k:(m|m-1)}^{\ell-1}) \;\simeq\; & \mathbf{Q}(\Theta_k(m-1), \Theta_{k:(m-1|m-2)}^{\ell-1}) \\ & -[\tilde{\boldsymbol{h}}_k(m) - \boldsymbol{h}_k(m)]^H \tilde{\mathbf{C}}_k^{-1}(m) [\tilde{\boldsymbol{h}}_k(m) - \boldsymbol{h}_k(m)]. \end{aligned} \tag{5.16}$$

The channel estimate $\boldsymbol{h}_k(m)$ at the ℓth iteration is obtained by maximizing the K-L measure, *i.e.*

$$\boldsymbol{h}_k^{\ell}(m) = arg \max_{\boldsymbol{h}_k(m)} \mathbf{Q}(\Theta_k(m), \Theta_{k:(m|m-1)}^{\ell-1}). \tag{5.17}$$

A recursive second-order approximation to the above optimization was proposed in [34]. According to the recursive updating rule, the channel update is given by

$$\boldsymbol{h}_k^{\ell}(m) \;=\; \boldsymbol{h}_{k:(m|m-1)} - \left(\frac{\partial^2 \mathbf{Q}(\Theta_k(m), \Theta_{k:(m|m-1)}^{\ell-1})}{\partial^2 \boldsymbol{h}_k(m)} \bigg| \boldsymbol{h}_{k:(m|m-1)} \right)^{-1}.$$

$$\left(\frac{\partial \mathbf{Q}(\Theta_k(m), \Theta_{k:(m|m-1)}^{\ell-1})}{\partial \boldsymbol{h}_k(m)} \bigg| \boldsymbol{h}_{k:(m|m-1)} \right). \tag{5.18}$$

An important feature of this recursive updating rule is that it guarantees the monotonic increasing of the likelihood functions. In view of this, we apply this recursive EM algorithm in developing our channel update formula.

By substituting (5.17) in (5.18), we can obtain the first order derivative of the K-L measure as

$$\frac{\partial \mathbf{Q}(\Theta_k(m), \Theta_{k:(m|m-1)}^{\ell-1})}{\partial \boldsymbol{h}_k(m)} \bigg| \boldsymbol{h}_{k:(m|m-1)} = \tilde{\mathbf{C}}_k^{-1}(m)[\tilde{\boldsymbol{h}}_k(m) - \boldsymbol{h}_{k:(m|m-1)}], \tag{5.19}$$

since

$$\frac{\partial \mathbf{Q}(\Theta_k(m-1), \Theta_{k:(m-1|m-2)}^{\ell-1})}{\partial \boldsymbol{h}_k(m)} \bigg| \boldsymbol{h}_{k:(m|m-1)} = 0,$$

the second-order derivative of the K-L measure is given by

$$\frac{\partial^2 \mathbf{Q}(\Theta_k(m), \Theta_{k:(m|m-1)}^{\ell-1})}{\partial^2 \boldsymbol{h}_k(m)} \bigg| \boldsymbol{h}_{k:(m|m-1)} = -\tilde{\mathbf{C}}_k^{-1}(m) + \left(\frac{\partial \boldsymbol{h}_k(m-1)}{\partial \boldsymbol{h}_k(m)} \right)^H \left(\frac{\partial^2 \mathbf{Q}(\Theta_k(m-1), \Theta_{k:(m-1|m-2)}^{\ell-1})}{\partial^2 \boldsymbol{h}_k(m-1)} \bigg| \boldsymbol{h}_{k:(m-1|m-2)} \right) \left(\frac{\partial \boldsymbol{h}_k(m-1)}{\partial \boldsymbol{h}_k(m)} \right). \tag{5.20}$$

Let $\mathbf{P}_{m|m}^{-1} = -\frac{\partial^2 \mathbf{Q}(\Theta_k(m), \Theta_{k:(m|m-1)}^{\ell-1})}{\partial^2 \boldsymbol{h}_k(m)}\Big| \boldsymbol{h}_{k:(m|m-1)}$ and $\mathbf{P}_{m|m-1}^{-1} \equiv \mathbf{F}_k^{-H} \mathbf{P}_{m-1|m-1}^{-1} \mathbf{F}_k^{-1}$. Then, from (5.12), (5.20) can be expressed as $\mathbf{P}_{m|m}^{-1} = \mathbf{P}_{m|m-1}^{-1} + \tilde{\mathbf{C}}_k^{-1}(m)$. By using the Matrix Inversion Lemma [14], we have

$$\mathbf{P}_{m|m} = \mathbf{P}_{m|m-1} - \mathbf{P}_{m|m-1}(\tilde{\mathbf{C}}_k + \mathbf{P}_{m|m-1})^{-1}\mathbf{P}_{m|m-1}, \tag{5.21}$$

where, by definition,

$$\mathbf{P}_{m|m-1} = \mathbf{F}_k \mathbf{P}_{m-1|m-1} \mathbf{F}_k^H. \tag{5.22}$$

The channel update is obtained according to the recursive update rule [34]:

$$\begin{aligned} \boldsymbol{h}_k^{\ell}(m) &= \boldsymbol{h}_{k:(m|m-1)} - \left(\frac{\partial^2 \mathbf{Q}(\Theta_k(m), \Theta_{k:(m|m-1)}^{\ell-1})}{\partial^2 \boldsymbol{h}_k(m)}\Big| \boldsymbol{h}_{k:(m|m-1)} \right)^{-1} \cdot \\ &\quad \left(\frac{\partial \mathbf{Q}(\Theta_k(m), \Theta_{k:(m|m-1)}^{\ell-1})}{\partial \boldsymbol{h}_k(m)}\Big| \boldsymbol{h}_{k:(m|m-1)} \right) \\ &= \mathbf{F}_k \boldsymbol{h}_k(m-1) + \mathbf{P}_{m|m-1}(\tilde{\mathbf{C}}_k + \mathbf{P}_{m|m-1})^{-1}[\tilde{\boldsymbol{h}}_k(m) - \mathbf{F}_k \boldsymbol{h}_k(m-1)]. \end{aligned} \tag{5.23}$$

This leads to a Kalman-like filter, even though there is no statistical channel model involved in the derivation. We can define the Kalman gain $\mathbf{K}_k(m) \equiv \mathbf{P}_{m|m-1}(\tilde{\mathbf{C}}_k + \mathbf{P}_{m|m-1})^{-1}$.

Let us examine the physical meaning of $\tilde{\boldsymbol{h}}_k(m)$, which can be rewritten as

$$\tilde{\boldsymbol{h}}_k(m) = \tilde{\mathbf{C}}_k \tilde{\mathbf{G}}_k^H(m) \mathbf{y}(m)$$

$$= \left[\sum_{\xi_k^m}(\mathbf{G}_k'(\xi_k^m))^H\mathbf{C}_k^{-1}\mathbf{G}_k'(\xi_k^m)P_k(\mathcal{Y},\xi_k^m|\Theta_{k:(m|m-1)}^{\ell-1})\right]^{-1}\cdot$$
$$\left[\sum_{\xi_k^m}(\mathbf{G}_k'(\xi_k^m))^H\mathbf{C}_k^{-1}\mathbf{y}(m)P_k(\mathcal{Y},\xi_k^m|\Theta_{k:(m|m-1)}^{\ell-1})\right]. \quad (5.24)$$

Comparing the above result with (5.9), we see that $\tilde{\boldsymbol{h}}_k(m)$ is actually the ML channel estimate of $\boldsymbol{h}_k(m)$ using the EM algorithm with the window size equal to one. Thus, the update formula tracks the channel by adding an increment to the estimate of the previous time instance. The increment is decided by the Kalman gain as well as the difference between the ML estimate and the predicted values using the channel evolution function.

5.3 Noncoherent MUD and Channel Estimation

The EM algorithm can only guarantee the convergence to a local optimum. If the initial values for EM iterations fall within a neighborhood of the true channel parameters, the EM algorithm can track channel parameters well. However, when the channel gain attenuates to a very small value, the local optimal points are very close to each other, (*e.g.* the same channel gain with an in-phase state and an 180-degree out-of-phase state for the BPSK signal). Then, the EM algorithm becomes vulnerable to channel noise, and may be locked to a false state when channel regains its strength. The best estimate given by the EM algorithm is

$\mathbf{h}_k = [h_{k0}e^{j\phi_{k0}}, \cdots, h_{k(L_k-1)}e^{j\phi_{k(L_k-1)}}]^T$, where h_{kl} is the true channel parameter and ϕ_{kl} is the phase shift, all corresponding to the ith path of user k.

The phase error $\phi_{k(L_k-1)}$ is not uniformly distributed over $[-\pi, \pi)$. It depends on the modulation scheme. When MPSK is employed, it takes values on the discrete set $\Phi \equiv \{\phi^i = \frac{2i\pi}{M} : i = 0, \cdots, M-1\}$, where M is the constellation size of MPSK due to the following reason. Let us consider the flat fading case. For MPSK modulation, a transmitted symbol $b_k(n) = e^{j\frac{2m\pi}{M}}$ multiplied by a phasor $e^{j\phi_k} = 1$, gives the same log likelihood value in (5.6) with $b_k(n) = 1$ and the phasor $e^{j\phi_k} = e^{j\frac{2m\pi}{M}}$. If the $P_k(b_k(n) = 1|\mathcal{Y}, \theta_k) > P_k(b_k(n) = e^{j\frac{2m\pi}{M}}|\mathcal{Y}, \theta_k)$ due to the concurrence of a deep fading channel and strong channel noise, then the EM algorithm tends to give the channel estimate $h_k e^{j\phi_k}$, where $e^{j\phi_k} = e^{j\frac{2m\pi}{M}}$, rather than $e^{j\phi_k} = 1$. To combat the phase ambiguity and obtain a posterior probability without a priori phase information, we turn to noncoherent detection.

Our scheme is based on the noncoherent BCJR algorithm [4], which was originally proposed to deal with uniformly distributed phase errors over $[-\pi, \pi)$ for the AWGN channel. An iterative scheme is developed for noncoherent detection over multipath DS-CDMA channels in the following subsections.

5.3.1 Noncoherent Detection over Flat Fading Channels

The noncoherent BCJR algorithm [4] is extended to flat-fading CDMA channels with a discrete phase error ϕ_k over the set $\Phi \equiv \{\phi^i = \frac{2i\pi}{M} : i = 0, \cdots, M-1\}$

in this subsection. An extension of the scheme to perform noncoherent detection over multipath channels will be given in the next subsection under the framework of iterative interference cancellation.

Define the extended symbol state $\zeta_k^n \equiv \{b_k(n-1), \cdots, b_k(n-q_k)\} = \{\mu_k^n, S_k^{n-p_k+1}\}$, where $\mu_k^n \equiv \{b_k(n-1), \cdots, b_k(n-p_k+1)\}$, with $p_k - 1$ being the length of the channel phase memory, $S_k^{n-p_k+1} \equiv \{b_k(n-p_k), \cdots, b_k(n-p_k-L_k^p+2)\}$, with $L_k^p - 1$ being the length of the symbol state memory, and $q_k = p_k + L_k^p - 2$ is the length of the extended channel memory. Note that the number of path $L_k = 1$ and the largest possible symbol delay $L_k^p = 2$ for flat fading channels. Let $\mathbf{y}_{n-P_k+1}^n$ denote $\{\mathbf{y}(n-P_k+1), \cdots, \mathbf{y}(n)\}$. The probability density function of $\mathbf{y}_{n-P_k+1}^n$ conditioned on the parameter set $\{b_k(n), \zeta_k^n, \theta_k, \phi_k\}$ is given by

$$P(\mathbf{y}_{n-p_k+1}^n | b_k(n), \zeta_k^n, \theta_k, \phi_k) = \frac{1}{(\pi \det(\mathbf{C}))^{p_k}} \cdot \exp\left\{ -\sum_{i=0}^{p_k-1} (\mathbf{y}_{n-i} - \mathbf{G}_k(\xi_k^{n-i}) h_k e^{j\phi_k})^H \mathbf{C}_k^{-1} (\mathbf{y}_{n-i} - \mathbf{G}_k(\xi_k^{n-i}) h_k e^{j\phi_k}) \right\} \quad (5.25)$$

Marginalizing the phase error ϕ_k out of the conditional probability $P(\mathbf{y}_{n-p_k+1}^n | b_k(n), \zeta_k^n, \theta_k, \phi_k)$ with respect to set Φ yields

$$\begin{aligned} \gamma_k(b_k(n), \zeta_k^n | \theta_k) &\equiv \sum_{\phi_k} P(\mathbf{y}_{n-p_k+1}^n | b_k(n), \zeta_k^n, \theta_k, \phi_k) d\phi \\ &= \frac{\exp\{Q_k(b_k(n), \zeta_k^n, \theta_k)\}}{(\pi \det(\mathbf{C}_k))^{p_k}} \cdot \frac{1}{M} \sum_{i=0}^{|\Phi|} \exp\left(2 |F_k(b_k(n), \zeta_k^n, \theta_k)| \cos(\phi_k^i + \omega)\right), \quad (5.26) \end{aligned}$$

where $F_k(b_k(n), \zeta_k^n, \theta_k) \equiv \sum_{i=0}^{p_k-1} \mathbf{y}_{n-i}^H \mathbf{C}_k^{-1} \mathbf{G}_k(\xi_k^{n-i}) h_k$, ω is the phase angle of $F_k(b_k(n), \zeta_k^n, \theta_k)$ and $Q_k(b_k(n), \zeta_k^n, \theta_k) \equiv -\sum_{i=0}^{p_k-1} [\mathbf{y}_{n-i}^H \mathbf{C}_k^{-1} \mathbf{y}_{n-i} + h_k^H \mathbf{G}_k^H(\xi_k^{n-i}) \mathbf{C}_k^{-1} \mathbf{G}_k(\xi_k^{n-i}) h_k]$. For BPSK, $\Phi = \{0, \pi\}$, then γ_k is equal to

$$\begin{aligned} \gamma_k(b_k(n), \zeta_k^n | \theta_k) &= \frac{1}{(\pi \det(\mathbf{C}_k))^{p_k}} \exp\{Q_k(b_k(n), \zeta_k^n, \theta_k)\} \cdot \\ &\quad \cosh\{2\Re[F_k(b_k(n), \zeta_k^n, \theta_k)]\}. \end{aligned} \tag{5.27}$$

The posterior probability of $b_k(n)$ is given by

$$P(b_k(n)|\mathcal{Y}, \theta_k) = \sum_{\zeta_k^n} \alpha_k(b_k(n), \zeta_k^n | \theta_k) \gamma_k(b_k(n), \zeta_k^n | \theta_k) \beta_k(b_k(n), \zeta_k^n | \theta_k). \tag{5.28}$$

The variable $\alpha_k(b_k(n), \zeta_k^n | \theta_k)$ can be obtained using the forward recursion

$$\begin{aligned} \alpha_k(b_k(n), \zeta_k^n | \theta_k) &= \sum_{b_k(n-q_k-1)} \alpha_k(b_k(n-1), \zeta_k^{n-1} | \theta_k) \cdot \\ &\quad \frac{\eta_k(b_k(n), \zeta_k^n, b_k(n-q_k-1) | \theta_k)}{\gamma_k(b_k(n), \zeta_k^n | \theta_k)}, \end{aligned} \tag{5.29}$$

the variable $\beta_k(b_k(n), \zeta_k^n | \theta_k)$ can be updated using the backward recursion

$$\begin{aligned} \beta_k(b_k(n), \zeta_k^n | \theta_k) &= \sum_{b_k(n+1)} \beta_k(b_k(n+1), \zeta_k^{n+1} | \theta_k) \cdot \\ &\quad \frac{\eta_k(b_k(n+1), \zeta_k^{n+1}, b_k(n-q_k) | \theta_k)}{\gamma_k(b_k(n), \zeta_k^n | \theta_k)}, \end{aligned} \tag{5.30}$$

where the parameter set $\{\zeta_k^{n+1}, b_k(n-q_k)\}$ is equal to $\{b_k(n), \zeta_k^n\}$, and

$$\begin{aligned}
& \eta_k(b_k(n), \zeta_k^n, b_k(n-q_k-1)|\theta_k) \\
\equiv\ & \sum_{\phi_k} P(\mathbf{y}_{n-p_k}^n | b_k(n), \zeta_k^n, \theta_k, \phi_k) d\phi \\
=\ & \frac{\exp\{Q_k(b_k(n), \zeta_k^n, b_k(n-q_k-1), \theta_k)\}}{(\pi \det(\mathbf{C}_k))^{p_k+1}} \cdot \\
& \frac{1}{M} \sum_{i=0}^{|\Phi|} \exp\left(2\,|F_k(b_k(n), \zeta_k^n, b_k(n-q_k-1), \theta_k)| \cos(\phi_k^i + \omega)\right), \qquad (5.31)
\end{aligned}$$

where

$$Q_k(b_k(n), \zeta_k^n, b_k(n-q_k-1), \theta_k) \equiv -\sum_{i=0}^{p_k} [\mathbf{y}_{n-i}^H \mathbf{C}_k^{-1} \mathbf{y}_{n-i} + h_k^H \mathbf{G}_k^H(\xi_k^{n-i}) \mathbf{C}_k^{-1} \mathbf{G}_k(\xi_k^{n-i}) h_k]$$

and

$$F_k(b_k(n), \zeta_k^n, b_k(n-q_k-1), \theta_k) \equiv \sum_{i=0}^{p_k} \mathbf{y}_{n-i}^H \mathbf{C}_k^{-1} \mathbf{G}_k(\xi_k^{n-i}) h_k.$$

For BPSK, parameter η_k is given by

$$\begin{aligned}
& \eta_k(b_k(n), \zeta_k^n, b_k(n-q_k-1)|\theta_k) \\
=\ & \frac{1}{(\pi \det(\mathbf{C}_k))^{p_k+1}} \exp\{Q_k(b_k(n), \zeta_k^n, b_k(n-q_k-1), \theta_k)\} \cdot \\
& \cosh\{2\Re[F_k(b_k(n), \zeta_k^n, b_k(n-q_k-1), \theta_k)]\}. \qquad (5.32)
\end{aligned}$$

5.3.2 Channel Adjustment Using Average ML Algorithm

The reliability of the channel estimate using the EM algorithm lies in the accuracy of the posterior probabilities of transmitted symbols. As given by (5.9) for the channel estimate, matrices $[\mathbf{G}_k^H(\mathbf{C}_k(m))^{-1}\mathbf{G}_k]$ and $[\mathbf{G}_k^H(\mathbf{C}_k(m))^{-1}\mathbf{y}]$ associated with each symbol state ξ_k^n are weighted by the posterior probability of the state. If transmitted symbols are known in the training mode, the channel estimator degenerates to the following form:

$$\mathbf{h}_k(m) = \left[\sum_{n\in W(m)} [\mathbf{G}_k^H(\mathbf{C}_k(m))^{-1}\mathbf{G}_k]\right]^{-1} \sum_{n\in W(m)} [\mathbf{G}_k^H(\mathbf{C}_k(m))^{-1}\mathbf{y}]. \tag{5.33}$$

This is exactly the ML channel estimator. Thus, if the posterior probability $P_k(\mathcal{Y}(m), \xi_k^n|\theta_k^{\ell-1}(m))$ in (5.9) obtained by the BCJR algorithm is replaced by the posterior probability obtained by the noncoherent BCJR algorithm, which is immune to phase errors, the estimation scheme is able to track the channel phase more robustly. Motivated by this observation, the channel estimate is modified as

$$\begin{aligned}\tilde{\mathbf{h}}_k(m) &= \left(\sum_{n\in W(m)}\sum_{\xi_k^n}[\mathbf{G}_k^H(\mathbf{C}_k(m))^{-1}\mathbf{G}_k]\mathcal{P}'_k(\mathcal{Y}, \xi_k^n|\theta_k)\right)^{-1} \\ &\quad \cdot \left(\sum_{n\in W(m)}\sum_{\xi_k^n}[\mathbf{G}_k^H(\mathbf{C}_k(m))^{-1}\mathbf{y}]\mathcal{P}'_k(\mathcal{Y}, \xi_k^n|\theta_k)\right).\end{aligned} \tag{5.34}$$

For flat fading channels, the posterior probability, $\mathcal{P}'_k(\mathcal{Y}, \xi_k^n|\theta_k)$, of the symbol state ξ_k^n is given by

$$\mathcal{P}'_k(\mathcal{Y}, \xi_k^n|\theta_k) \propto \sum_{\mu_k^{n-L_k^p+1}} \alpha_k(b_k(n), \zeta_k^n|\theta_k)\gamma_k(b_k(n), \zeta_k^n|\theta_k)\beta_k(b_k(n), \zeta_k^n|\theta_k), \quad (5.35)$$

where $\xi_k^n = \{b_k(n), S_k^n\}$, $\zeta_k^n = \{S_k^n, \mu_k^{n-L_k^p+1}\}$ and $\mu_k^{n-L_k^p+1} = \{b_k(n-L_k^p), \cdots, b_k(n-q_k)\}$.

5.4 Iterative Channel Estimation and MUD

To improve the performance of blind detection for DS-CDMA systems, MAI interference suppression can be employed. To this end, we first need a good channel estimate for each transmission path of each user, which in turn relies on the quality of the posterior probability of the transmitted symbol. A direct extension of the aforementioned noncoherent detection scheme to the multipath fading channel is however complicated. It is still under our current development. However, by exploring the statistical independency among fading coefficients for different paths, the proposed noncoherent detection scheme can be directly applied to symbol detection along each transmission path. Once reliable posterior probabilities of transmitted symbols are available, the phase error coupled with the channel estimate can be compensated using the proposed average ML channel estimation.

5.4.1 Iterative per-path Processing for Multipath Fading Channels

It is assumed that channel coefficients of different transmission paths are uncorrelated. Then, for the lth path of user k, the received signal can be re-written as

$$\begin{aligned}\mathbf{y}(m) &= \mathbf{g}_{kl}(\xi_k^m)h_{kl} + \sum_{j=0,j\neq l}^{L_k-1} \mathbf{g}_{kj}(\xi_k^m)h_{kj} + \sum_{i=0,i\neq k}^{K-1} \mathbf{G}_i(\xi_i^m)\mathbf{h}_i + \mathbf{n}(m) \\ &\equiv \mathbf{g}_{kl}(\xi_k^m)h_{kl} + \mathbf{I}_{kl}(m) + \mathbf{n}(m), \end{aligned} \tag{5.36}$$

where $\mathbf{G}_k = [\mathbf{g}_{k0}, \cdots, \mathbf{g}_{k(L_k-1)}]$ and $\mathbf{g}_{kl}$ is the effective system matrix of the lth path of the kth user. The interference vector $\mathbf{I}_{kl}$ is also complex Gaussian distributed. The associated covariance matrix of $\mathbf{I}_{kl} + \mathbf{n}$ is defined as

$$\mathbf{C}_{kl} = E[(\mathbf{I}_{kl} + \mathbf{n})(\mathbf{I}_{kl} + \mathbf{n})^H]. \tag{5.37}$$

By discarding the diversity gain offered by multipath fading channels, *i.e.* regarding signals from other transmission paths of the same user as interference, the proposed noncoherent detection and channel estimation scheme for flat fading channels can be directly applied for channel estimation path by path. For each path, the noncoherent detector offers a distinct version of the posterior probability $\mathcal{P}'_{kl}(\mathcal{Y}, \xi_k^n|\theta_{kl})$

to the same transmitted symbol of user k. These probabilities can be simply combined to form the posterior probability for user k via

$$\mathcal{P}'_k(\mathcal{Y}, \xi_k^n|\theta_k) = \sum_{l=0}^{L_k-1} \mathcal{P}'_{kl}(\mathcal{Y}, \xi_k^n|\theta_{kl}). \tag{5.38}$$

Finally, to improve the quality of channel estimate using the average ML, the probability $\mathcal{P}'_{kl}(\mathcal{Y}, \xi_k^n|\theta_{kl})$ is substituted back into (5.34) to obtain a new version of $\tilde{\mathbf{h}}_k$.

Once the correct channel phases of all paths are available, the coherent BCJR algorithm [1] can be performed to evaluate the true *a posteriori* probabilities of transmitted symbols by taking into account the diversity gain offered by multipath fading channels. This information is then passed for interference cancellation and symbol detection to be introduced in the next subsection.

5.4.2 Interference Cancellation and Iterative Detection

To perform soft interference cancellation, we should have the soft output of the transmitted symbol. For the BPSK modulation, the soft output of each symbol is given by

$$\tilde{b}_k(n) \equiv \frac{P(b_k(n) = 1|\mathcal{Y}, \theta_k) - P(b_k(n) = -1|\mathcal{Y}, \theta_k)}{P(b_k(n) = 1|\mathcal{Y}, \theta_k) + P(b_k(n) = -1|\mathcal{Y}, \theta_k)}, \tag{5.39}$$

where $P(b_k(n)|\mathcal{Y}, \theta_k)$ is obtained by (5.28). The soft estimate of the interference vector $\mathbf{I}_k$ for user k in (5.4) is obtained by replacing user symbol b_i, $i \neq k$, embedded in $\mathbf{I}_k(m)$ with soft output $\tilde{b}_i$, and by substituting $\tilde{\mathbf{h}}_i$ for $\mathbf{h}_i$. The resulting matrix $\mathbf{G}_i$

is denoted by $\mathbf{G}_i(\tilde{\xi_i^m})$, [cf. (5.4)]. Then, the received signal $\mathbf{y}_k(m)$ for user k after interference cancellation is given by

$$\mathbf{y}_k(m) = \mathbf{y}(m) - \sum_{i=0, i\neq k}^{K-1} \mathbf{G}_i(\tilde{\xi}_i^m)\tilde{\mathbf{h}}_i, \tag{5.40}$$

where $\tilde{\xi}_i^m = \{\tilde{b}_i(m), \cdots, \tilde{b}_i(m - L_i^p + 1)\}$ and $\tilde{\mathbf{h}}_i$ is the set of estimated channel parameters obtained before interference cancellation. By using $\mathbf{y}_k$ for the EM channel estimation, the quality of θ_k can be improved.

Furthermore, to improve the performance of noncoherent symbol detection where the signal is processed path by path, ISI should be cancelled in each iteration using the posterior probabilities of transmitted symbols obtained from the previous iteration. The received signal for the lth path of user k is given by

$$\mathbf{y}_{kl}(m) = \mathbf{y}_k(m) - \sum_{j=0, j\neq l}^{L_k-1} \mathbf{g}_{kj}(\tilde{\xi}_k^m)\tilde{h}_{kj}. \tag{5.41}$$

By iteration, the received signal $\mathbf{y}_{kl}$ will gradually approach the output of a flat fading channel, thus improving the quality of $\tilde{h}_{kj}$. The system diagram and the signal flow chart for the proposed joint channel estimation and noncoherent detection is shown in Fig. 5.1. The whole procedure for channel re-estimation, symbol re-detection and interference cancellation can be repeated until the mean squared error

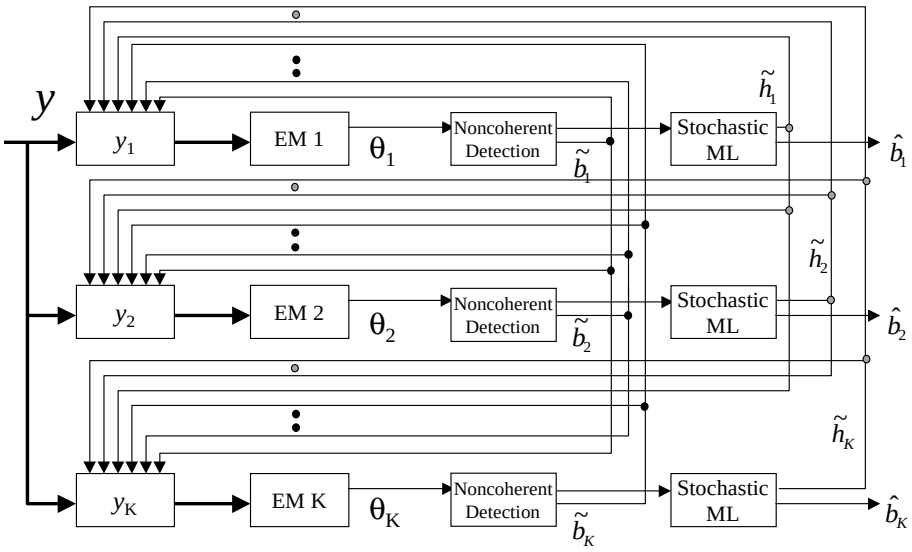

Figure 5.1: The system diagram of the noncoherent EM algorithm for joint channel estimation and multiuser detection.

for channel estimation reaches a steady-state value. When BPSK is employed, the hard decision for user k's symbol is performed at the last stage as

$$\hat{b}_k(n) = \text{sgn}\left[P(b_k(n) = 1|\mathcal{Y}_k, \theta_k) - P(b_k(n) = -1|\mathcal{Y}_k, \theta_k)\right]. \tag{5.42}$$

5.5 Simulation Results

Computer simulations were conducted to demonstrate the performance of the joint channel estimation and symbol detection scheme in fading channels for the DS-CDMA system. Random sequences with length $N = 7$ were adopted as the spreading sequences for the system. The path delays for each user were randomly generated

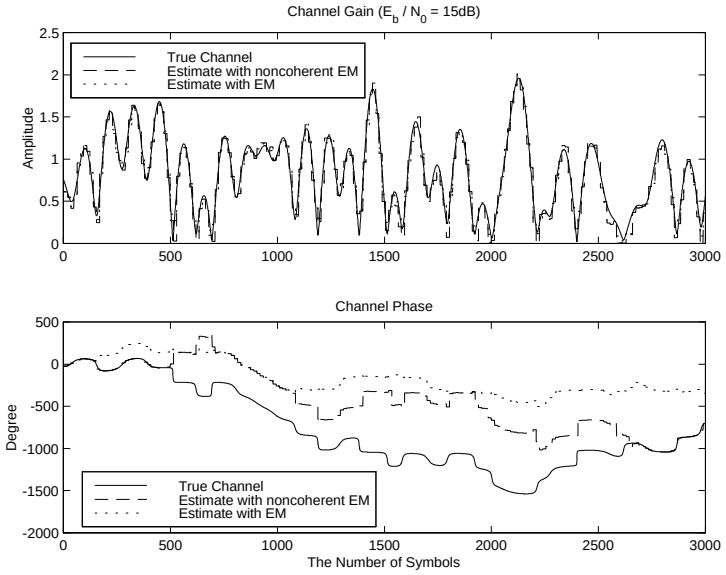

Figure 5.2: The estimated channel amplitudes and phase versus the exact channel coefficients of a flat Rayleigh fading channel with block size = 15, $E_b/N_0 = 15dB$ and $f_dT_s = 5 \times 10^{-3}$.

with uniformly distribution over $[0,\ T_s)$ and assumed to be known. Channel coefficients were generated using Jake's model for the Rayleigh fading channel with the normalized Doppler shift $f_dT_s = 5 \times 10^{-3}$. Two channel conditions were considered in the simulation. One was a flat fading channel with 7 users while the other was a 3-path fading channel with 4 users in the system. All users had the same transmission power. The power of the sampling noise for each chip interval was normalized to one for both of the real part and the imaginary part. Thus, the total noise power was 2. The window size was 15. To initialize the noncoherent BCJR algorithm, the first 3 symbols of each block were assumed given as pilot symbols. Two stages of interference cancellation were applied for each user. First, we examine the channel tracking performance for flat fading channels. The curves of channel amplitudes and

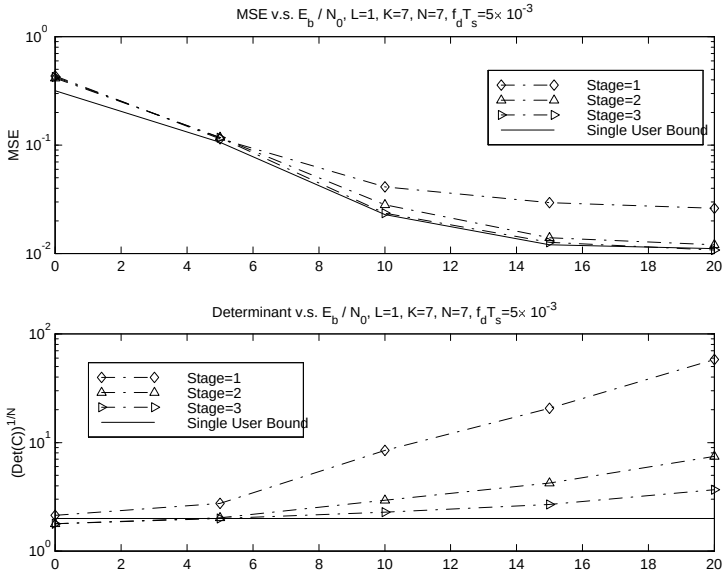

Figure 5.3: The MSE of the channel estimation and the $\sqrt[N]{\det(C_k)}$ value of the residual interference, where C_k is the covariance matrix of MAI plus noise.

phases shown in Fig. 5.2 are results of the EM algorithm and results after phase adjustment with $\frac{E_b}{N_0} = 15dB$. Both schemes give fairly descent estimates of the channel amplitude. however, correct phases can only be provided by the proposed noncoherent EM algorithm. As shown in the figure, the phase estimate given by the EM algorithm may be locked to an out-of-phase degree when the channel is in a deep fading situation. In contrast, the proposed scheme is robust to deep fading. Fig. 5.3 gives the mean square error (MSE) of the channel estimation and the $\sqrt[N]{det(\mathbf{C}_k)}$ value of residual MAI plus noise. The measured $\sqrt[N]{det(\mathbf{C}_k)}$ serves as a performance index for interference cancellation. After two stages of interference cancellation, the value drops from approximately 70 to 3, which is very close to the level of white noise power, indicating that MAI is almost eliminated. The truth is also reflected in

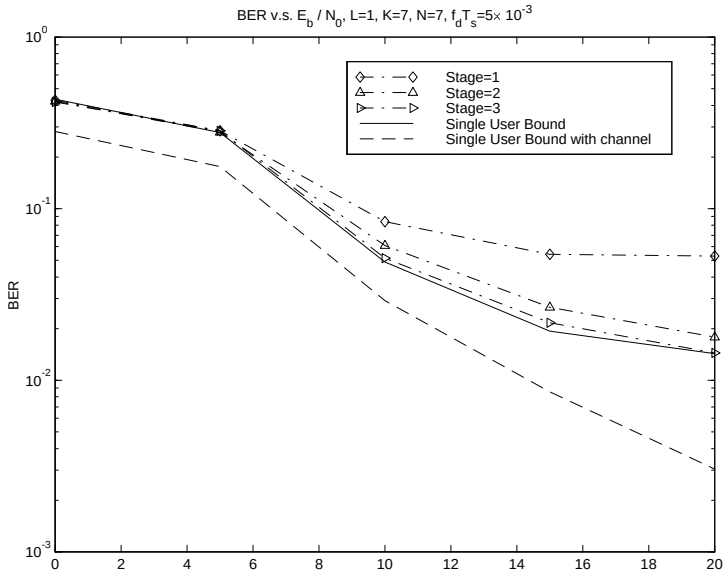

Figure 5.4: The BER performance for a flat Rayleigh fading channel with $K = 7$, $N = 7$ and $f_dT_s = 5 \times 10^{-3}$, where all users have the same power.

the MSE curves. The MSE of the multiple access system reaches the level of a single user system, indicating the effectiveness of the proposed interference cancellation scheme.

Fig. 5.4 shows the BER results for different SNR values. After two iterations, the BER almost attains the single user bound. At high SNR, the performance of detection is dominated by the quality of channel estimation. Since a block-based EM algorithm is used for channel estimation, the channel estimate is constant over the range of the window. Thus, the BER performance is limited by the fading speed (and hence the autocorrelation values of the fading process) and will hit the BER floor at a high SNR value.

Chapter 6

Conclusion and Future Work

6.1 Conclusion

After a brief introduction in Chapter 1 and some background review in Chapter 2, major results of the research were presented in Chapters 3, 4 and 5.

In Chapter 3, a multistage structure was developed for the reduced-rank implementation of the MMSE, MOE, BLUE and ML filter banks. Under this structure, a common framework was proposed for channel estimation and symbol detection in a linear Gaussian model. The performance of a family of the MRC as well as the differential EGC schemes was examined in the context of coherent and non-coherent multiuser detection for DS-CDMA systems in multipath fading channels. For adaptive implementations, it was shown by simulations that the output SINRs of reduced-rank filter banks can attain the full-rank performance with a relatively small number of stages even in a highly loaded system. The output SINRs of pre-combining filters can achieve about the same performance of the MRC filter banks

with a much lower order of filter ranks, thus, demonstrating a faster convergence. Although the output SINR of multistage MRC MMSE-FB is the highest among all MRC filter banks, the bias effect of using the MMSE/MOE FBs as the channel estimator deteriorates the performance for non-coherent EGC schemes, which leads to significant performance degradation of the overall system. Therefore, the proposed adaptive EGC-ML-FB with the unbiased BLUE channel estimator exhibits a superior performance over the EGC MMSE/MOE FBs proposed in [21] with no extra implementation cost.

Based on the framework developed in Chapter 3, the steady-state performance analysis in terms of output SINR and BER was conducted in Chapter 4 for coherent and non-coherent reduced-rank multiuser detectors in multipath Rayleigh fading channels. Analytic results of the output SINRs of multistage MMSE/MOE/BLUE/ML filter banks were characterized at all possible stages. The output SINRs were shown to be monotonically increasing with the number of applying stages and upper bounded by the number of resolvable paths of the transmission channel of the target user. A sufficient condition for the equality of output SINRs was given. As a special case of interest, the output SINRs are equal in flat Rayleigh fading channels. A generic BER formula was also provided for both multistage MRC and EGC filter banks. BERs for each class of combinings were shown to be the same for flat Rayleigh fading channels again, which is consistent with the results for output SINRs.

The analysis for the achievability of output SINRs' upper bound in Chapter 4 provides a good understanding of the BER floor phenomenon. A criterion was given for the existence of BER floors for MRC detectors or not. If $D_{free} \geq D_{int}$, the BER floor phenomenon can be avoided. The EGC case is however more complicated than the MRC case. That is, the BER floors of EGC detectors are also affected by channel mismatch due to differential combining. Even though the condition $D_{free} - D_{int} \geq 0$ is met, the BER floor may still occur in fast fading environments. The floor level depends on the the value of ρ. The lower the ρ value is, the higher the BER floor level.

Generally speaking, for channels with rich scattering and/or of high loading (so that the criterion $D_{free} \geq D_{int}$ is not met), it was verified by simulation results that output SINRs become saturated very fast in only a few stages. A few stages (typcially 6) can achieve the full-rank performance over a wide range of operating conditions. This is consistent with the observations stated in [12] for the random sequence analysis of MSWF. Our above finding also explains well why the approach of reduced-rank filtering with a multistage structure is more appealing than other reduced-rank approaches.

A joint blind channel estimation and MUD algorithm based on the EM algorithm was proposed in Chapter 5. A recursive channel estimator was derived without the knowledge of the transmitted symbol. The noncoherent BCJR algorithm, which was originally proposed for handling the continuous phase in the AWGN channel,

was extended to take care of the discrete phase ambiguity in flat fading DS-CDMA channels. By exploring the discrete random phase ambiguity as a result of the EM algorithm, a phase estimator was proposed in association with the EM algorithm and the noncoherent BCJR detection scheme. The phase estimate was shown to be robust with respect to deep fading, thus making interference cancellation possible. The multi-stage soft interference cancellation scheme not only improves the BER but also reduces the MSE of the estimation scheme. Even though the proposed noncoherent BCJR scheme only works for flat-fading channels in the current development, the proposed scheme can be easily extended to the multipath case when it is in conjunction with iterative cancellation of ISI.

6.2 Future Work

The essence of multistage Wiener filtering is to use successive orthogonal projections to perform residual interference cancellation at each stage. This multistage structure unfolds starting from the matrix of steering vectors $\mathbf{S}_{1+}$, *i.e.* the system matrix $\mathbf{H}$. However, for some applications, we may be interested in the reduced-rank representation of the system matrix (rather than the detection, estimation and filtering processes). So far, there has been no efficient algorithm except for the SVD approach proposed. With the accumulated knowledge obtained in this research, it may be possible to find an efficient method to construct a sequence of subspaces to span the system matrix, which may lead to reduced-rank estimation schemes for

multiple-input multiple-output (MIMO) systems. This is another interesting yet challenging topic to pursue in the future.

Reference List

[1] L. R. Bahl, J. Cocke, F. Jelinek, and J. Raviv, "Optimal decoding of linear codes for minimizing symbol error rate," *IEEE Trans. on Information Theory*, vol. IT-20, pp. 248–287, Mar. 1974.

[2] C. Carlemalm, A. Logothetis, and H. V. Poor, "Channel estimation and demodulation of asynchronous cdma signals in frequency-selection fading channels," in *EUSIPCO*. Tampere, Finland, September 2000.

[3] W. Chen, U. Mitra, and P. Schniter, "On the equivalence of three reduced-rank linear estimators with applications to DS-CDMA," *IEEE Trans. on Information Theory*, vol. 48, no. 9, pp. 2609–2614, Sept. 2002.

[4] G. Colavolpe, G. Ferrari, and Riccardo Raheli, "Noncoherent iterative (Turbo) decoding," *IEEE Trans. on Communications*, vol. 48, no. 9, pp. 1488–1498, Sept. 2000.

[5] Q. Dai and E. Shwedyk, "Detection of bandlimited signals over frequency selective Rayleigh fading channels," *IEEE Trans. on Communications*, vol. 42, no. 2/3/4, pp. 941–950, Feb/Mar/Apr 1994.

[6] A. P. Dempster, N. M. Laird, and D. B. Rubin, "Maximum-likelihood from incomplete data via the EM algorithm," *J. Roy. Statist. Soc.*, vol. 39, pp. 1–17, 1977.

[7] C. N. Georghiades and J. C. Han, "Sequence estimation in the presence of random parameters via the EM algorithm," *IEEE Trans. on Communications*, vol. 47, no. 9, pp. 1297–1302, Sept. 1999.

[8] J. S. Goldstein, I. S. Reed, and L. L. Scharf, "A multistage representation of the wiener filter based on orthogonal projections," *IEEE Trans. on Information Theory*, vol. 44, no. 7, pp. 2943–2959, Nov. 1998.

[9] S. Haykin, *Adaptive Filter Theory*, Prentice Hall, 3rd edition, 1996.

[10] M. L. Honig and J. S. Goldstein, "Adaptive reduced-rank interference suppression based on the multistage wiener filter," *IEEE Trans. on Communications*, vol. 50, no. 6, pp. 986–994, June 2002.

[11] M. L. Honig, U. Madhow, and S. Verdu, "Blind adaptive multiuser detection," *IEEE Trans. on Information Theory*, vol. 41, no. 4, pp. 944–960, July 1995.

[12] M. L. Honig and Weimin Xiao, "Performance of reduced-rank linear interference suppression," *IEEE Trans. on Information Theory*, vol. 47, no. 5, pp. 1928–1946, July 2001.

[13] G. K. Kaleh and R. Vallet, "Joint parameter estimation and symbol detection for linear or nonlinear unknown channels ," *IEEE Trans. on Communications*, vol. 42, no. 7, pp. 2406–2413, July 1994.

[14] Steven. M. Kay, *Fundamentals of statistical signal processing: Estimation theory*, Prentice Hall, 1993.

[15] V. Krishnamurthy and J. B. Moore, "On-line estimation of hidden Markov model parameters based on the Kullback-Leibler information measureF," *IEEE Trans. on Signal Processing*, vol. 41, no. 8, pp. 2557–2573, Aug. 1993.

[16] R. Lupas and S. Verdú, "Linear multiuser detectors for synchronous code-division multiple-access channels," *IEEE Trans. on Information Theory*, vol. 35, pp. 123–136, Jan. 1989.

[17] U. Madhow and M. L. Honig, "MMSE interference suppression for direct-sequence spread-spectrum CDMA," *IEEE Trans. on Communications*, vol. 42, no. 12, pp. 3178–3188, Dec. 1994.

[18] I. D. Marsland, P. T. Mathiopoulos, and S. Kallel, "Noncoherent turbo-equalization for frequency selective Rayleigh fast fading channels," in *Proc. International Symposium on Turbo Codes*. Brest, French, September 1997.

[19] K. S. Miller, *Complex Stochastic Processes*, Addison-Wesley, 1974, available from University Microfilms International, Ann Arbor, Mich.

[20] S. L. Miller, "An adaptive direct-sequence code-division multiple-access receiver for multiuser interference rejection," *IEEE Trans. on Communications*, vol. 43, no. 2, pp. 1556–1565, 1995.

[21] S. L. Miller, M. L. Honig, and L. B. Milstein, "Performance analysis of MMSE receivers for DS-CDMA in frequency-selective fading channels," *IEEE Trans. on Communications*, vol. 48, no. 11, pp. 1919–1929, Nov. 2000.

[22] Y. Song and S. Roy, "Blind adaptive reduced-rank detection for DS-CDMA signals in multipath channels," *IEEE Journal on Selected Areas in Communication*, vol. 17, no. 11, pp. 1960–1970, Nov. 1999.

[23] G. Strang, *Linear Algebra and Its Applications*, Harcourt College Publishers, 3rd edition, 1998.

[24] L. Tong, G. Xu, and T. Kailath, "Blind indetification and equalization based on second-order statistics: A time domain approach," *IEEE Trans. on Information Theory*, vol. 40, no. 2, pp. 340–349, Mar. 1994.

[25] S. Verdú, "Minimum probability of error for asynchronous Gaussian multiple-access channels," *IEEE Trans. on Information Theory*, vol. IT-32, pp. 85–96, Jan. 1986.

[26] X. Wang and H. V. Poor, "Blind adaptive multiuser detection in multipath CDMA channels based on subspace tracking," *IEEE Trans. on Signal Processing*, vol. 46, no. 11, pp. 3030–3044, Nov. 1998.

[27] X. Wang and H. V. Poor, "Iterative (Turbo) soft interference cancellation and decoding for coded CDMA," *IEEE Trans. on Communications*, vol. 47, no. 7, pp. 1046–1061, 1999.

[28] S.-H. Wu, U. Mitra, and C.-C. J. Kuo, "A common framework for blind multi-stage multiuser receivers of DS-CDMA in frequency-selective fading channels," to appear in Globecom 2003.

[29] S.-H. Wu, U. Mitra, and C.-C. J. Kuo, "Multi-stage MMSE/MOE receivers for frequency selective fading channels in DS-CDMA systems," in *Proc. IEEE Globecom*. Taipei, Taiwan, Nov 2002.

[30] S.-H. Wu, U. Mitra, and C.-C. J. Kuo, "Joint channel estimation and multiuser detection for multipath fading channels in DS-CDMA systems," in *Proc. IEEE ICC*. Anchorage, Alaska, May 2003.

[31] S.-H. Wu, U. Mitra, and C.-C. J. Kuo, "Performance analysis of a class of multi-stage DS-CDMA receivers for multipath channels," in *Proc. IEEE Information Theory Workshop (ITW)*. Paris, French, April 2003.

[32] S.-H. Wu, U. Mitra, and C.-C. J. Kuo, "Perfprmance analysis of multistage BLUE/MMSE receivers for DS-CDMA in frequency selective fading channels," in *Proc. IEEE ICC*. Anchorage, Alaska, May 2003.

[33] H. Zamiri-Jafarian and Subbarayan Pasupathy, "Adaptive MLSDE using the EM algorithm," *IEEE Trans. on Communications*, vol. 47, no. 8, pp. 1181–1193, Aug. 1999.

[34] H. Zamiri-Jafarian and Subbarayan Pasupathy, "EM-based recursive estimation of channel parameters," *IEEE Trans. on Communications*, vol. 47, no. 9, pp. 1297–1302, Sept. 1999.

Appendix A

Addendum to Chapter 3

A.1 Proof of Proposition 1

Recall that the matched filter bank of the first stage is given by $E(\mathbf{y}\Gamma_1^H b_1^*) = \mathbf{S}_{1+}\mathbf{A}_1 = \mathbf{H}_1\mathbf{U}_1$. From Fig. 3.1, it shows that $\mathbf{y}_D = \mathbf{B}_D\mathbf{B}_{D-1}\cdots\mathbf{B}_1\mathbf{y}$. Let blocking matrix $\mathbf{B}_i = (\mathbf{I} - \mathbf{H}_i\mathbf{H}_i^H),\ i = 1,\cdots D$, then $\mathbf{y}_D = \prod_{i=D}^{1}(\mathbf{I} - \mathbf{H}_i\mathbf{H}_i^H)\mathbf{y}$ and $\mathbf{d}_D = \mathbf{H}_D^H\prod_{i=D-1}^{1}(\mathbf{I} - \mathbf{H}_i\mathbf{H}_i^H)\mathbf{y}$. The matched filter bank $E(\mathbf{y}_i\mathbf{d}_i^H)$ at each stage i can be factored into $\mathbf{H}_i^{N\times L}\mathbf{U}_i^{L\times L}$ by the Gram-Schmidt process. Now, the proof is achieved by the induction method.

Proof:

1. For stage $i = 2$:

$$\begin{aligned}\boldsymbol{\Upsilon}_{\mathbf{y}_1\mathbf{d}_1} &\equiv E(\mathbf{y}_1\mathbf{d}_1^H) = \mathbf{B}_1\mathbf{R}\mathbf{H}_1 = (\mathbf{I} - \mathbf{H}_1\mathbf{H}_1^H)\mathbf{R}\mathbf{H}_1 = \mathbf{H}_2\mathbf{U}_2,\ \ \mathbf{H}_2^H\mathbf{H}_2 = \mathbf{I}\\ \mathbf{H}_2^H\mathbf{H}_1 &= \mathbf{U}_2^{-H}\mathbf{H}_1^H\mathbf{R}(\mathbf{I} - \mathbf{H}_1\mathbf{H}_1^H)\mathbf{H}_1 = \mathbf{0}. \qquad \text{(A.1)}\end{aligned}$$

So, we have $\mathbf{H}_1^H\mathbf{H}_1 = \mathbf{I}$, $\mathbf{H}_2^H\mathbf{H}_2 = \mathbf{I}$ and $\mathbf{H}_2 \perp \mathbf{H}_1$.

For stage $i = 3$:

$$\begin{aligned}
\boldsymbol{\Upsilon}_{\mathbf{y}_2\mathbf{d}_2} &\equiv E(\mathbf{y}_2\mathbf{d}_2^H) = \mathbf{B}_2\mathbf{R}_{\mathbf{y_1}}\mathbf{H}_2 = (\mathbf{I}-\mathbf{H}_2\mathbf{H}_2^H)(\mathbf{I}-\mathbf{H}_1\mathbf{H}_1^H)\mathbf{R}(\mathbf{I}-\mathbf{H}_1\mathbf{H}_1^H)\mathbf{H}_2 \\
&= (\mathbf{I}-\mathbf{H}_2\mathbf{H}_2^H)(\mathbf{I}-\mathbf{H}_1\mathbf{H}_1^H)\mathbf{R}\mathbf{H}_2 = \mathbf{H}_3\mathbf{U}_3, \quad \mathbf{H}_3^H\mathbf{H}_3 = \mathbf{I} \\
\mathbf{H}_3^H\mathbf{H}_2 &= \mathbf{U}_3^{-H}\mathbf{H}_2^H\mathbf{R}(\mathbf{I}-\mathbf{H}_1\mathbf{H}_1^H)(\mathbf{I}-\mathbf{H}_2\mathbf{H}_2^H)\mathbf{H}_2 = \mathbf{0} \\
\mathbf{H}_3^H\mathbf{H}_1 &= \mathbf{U}_3^{-H}\mathbf{H}_2^H\mathbf{R}(\mathbf{I}-\mathbf{H}_1\mathbf{H}_1^H)(\mathbf{I}-\mathbf{H}_2\mathbf{H}_2^H)\mathbf{H}_1 = \mathbf{0}. \qquad \text{(A.2)}
\end{aligned}$$

Then $\mathbf{H}_i^H\mathbf{H}_i = \mathbf{I},\ i = 1\cdots 3$, $\mathbf{H}_3 \perp \mathbf{H}_2$ and $\mathbf{H}_3 \perp \mathbf{H}_1$.

For $i = D$, assume $\mathbf{H}_i^H\mathbf{H}_i = \mathbf{I},\ i = 1\cdots D-1$, $\mathbf{H}_{D-1} \perp \mathbf{H}_j,\ j = 1,\cdots D-2$,

and

$$\begin{aligned}
\boldsymbol{\Upsilon}_{\mathbf{y}_{D-2}\mathbf{d}_{D-2}} &\equiv E(\mathbf{y}_{D-2}\mathbf{d}_{D-2}^H) = \prod_{j=D-2}^{1}(\mathbf{I}-\mathbf{H}_j\mathbf{H}_j^H)\mathbf{R}\prod_{j=1}^{D-3}(\mathbf{I}-\mathbf{H}_j\mathbf{H}_j^H)\mathbf{H}_{D-2} \\
&= \prod_{j=D-2}^{1}(\mathbf{I}-\mathbf{H}_j\mathbf{H}_j^H)\mathbf{R}\mathbf{H}_{D-2} = \mathbf{H}_{D-1}\mathbf{U}_{D-1}. \qquad \text{(A.3)}
\end{aligned}$$

Then we have:

$$\begin{aligned}
\boldsymbol{\Upsilon}_{\mathbf{y}_{D-1}\mathbf{d}_{D-1}} &\equiv E(\mathbf{y}_{D-1}\mathbf{d}_{D-1}^H) = \mathbf{B}_{D-1}\mathbf{R}_{\mathbf{y}_{D-2}}\mathbf{H}_{D-1} \\
&= \prod_{j=D-1}^{1}(\mathbf{I}-\mathbf{H}_j\mathbf{H}_j^H)\mathbf{R}\prod_{j=1}^{D-2}(\mathbf{I}-\mathbf{H}_j\mathbf{H}_j^H)\mathbf{H}_{D-1} \\
&= \prod_{j=D-1}^{1}(\mathbf{I}-\mathbf{H}_j\mathbf{H}_j^H)\mathbf{R}\mathbf{H}_{D-1} = \mathbf{H}_D\mathbf{U}_D, \quad \mathbf{H}_D^H\mathbf{H}_D = \mathbf{I} \\
\mathbf{H}_D^H\mathbf{H}_l &= \mathbf{U}_D^{-H}\mathbf{H}_{D-1}^H\mathbf{R}\prod_{j=1}^{D-1}(\mathbf{I}-\mathbf{H}_j\mathbf{H}_j^H)\mathbf{H}_l = \mathbf{0},\ l = 1\cdots D-1. \qquad \text{(A.4)}
\end{aligned}$$

Then, $\mathbf{H}_i^H \mathbf{H}_i = \mathbf{I}, \;\; i = 1 \cdots D$, $\mathbf{H}_D \perp \mathbf{H}_j, \; j = 1, \cdots D-1$.

By induction, we have $\mathbf{H}_i^H \mathbf{H}_i = \mathbf{I}$ and $\mathbf{H}_i \perp \mathbf{H}_j, \; i \neq j$.

2. From Fig. 3.1, it shows the received signal $\mathbf{y}$ is multiplied by $\mathbf{H}_1$ & $\mathbf{B}_i, \; i = 1, \cdots D$, to form the filter bank. Then the subspace spanned by D stages implementation is given by

$$\mathcal{T}_{LD} \quad \text{span} \quad \mathbf{T}_{LD}^H \equiv \left[\mathbf{H}_1 | \; \mathbf{B}_1 \mathbf{H}_2 | \; \ldots \; | \prod_{i=1}^{D-1} \mathbf{B}_i \mathbf{H}_D \right] \tag{A.5}$$

Since $\mathcal{H}_D \perp \mathcal{H}_j, \; j = 1, \cdots D-1$, then

$$\prod_{i=1}^{j-1} \mathbf{B}_i \mathbf{H}_j \;\; = \;\; \prod_{i=1}^{j-1} (\mathbf{I} - \mathbf{H}_i \mathbf{H}_i^H) \mathbf{H}_j = \mathbf{H}_j, \; j = 1, \cdots D. \tag{A.6}$$

$$\Longrightarrow \quad \mathcal{T}_{LD} \;\; \text{span} \;\; \mathbf{T}_{LD}^H \;\; = \;\; [\mathbf{H}_1 | \; \mathbf{H}_2 | \; \ldots \; | \; \mathbf{H}_D] \tag{A.7}$$

■

Appendix B

Addendum to Chapter 4

B.1 Proof of Proposition 2

From (4.5), (4.10) and (4.11), the expectation of the decision statistic for each reduced-rank filter bank conditioned on $\Gamma_1 b_1$ is given in the following equations, respectively.

$$E(\psi_{mmse}|\Gamma_1 b_1) = \Gamma_1^H \mathbf{A}_1 \mathbf{U}_1^H \mathbf{S}_D^{-1} \mathbf{U}_1 \mathbf{A}_1 \Gamma_1 b_1 \quad \text{(B.1)}$$

$$E(\psi_{moe}|\Gamma_1 b_1) = \Gamma_1^H \mathbf{A}_1 \mathbf{U}_1^H \mathbf{U}_1 \mathbf{A}_1 \Gamma_1 b_1 \quad \text{(B.2)}$$

$$E(\psi_{blue}|\Gamma_1 b_1) = \Gamma_1^H \Gamma_1 b_1 \quad \text{(B.3)}$$

$$E(\psi_{ml}|\Gamma_1 b_1) = \Gamma_1^H \mathbf{A}_1 \mathbf{U}_1^H \mathbf{F}_D^{-1} \mathbf{U}_1 \mathbf{A}_1 \Gamma_1 b_1. \quad \text{(B.4)}$$

This follows from the fact that $E(\mathbf{d}_1|\Gamma_1 b_1) = E(\mathbf{H}_1^H \mathbf{y}|\Gamma_1 b_1) = \mathbf{H}_1^H \mathbf{S}_{1+} \Gamma_1 b_1 = \mathbf{U}_1 \mathbf{A}_1 \Gamma_1 b_1$ and $E(\mathbf{y}_1|\Gamma_1 b_1) = E(\mathbf{H}_{1\perp}^H \mathbf{y}|\Gamma_1 b_1) = \mathbf{H}_{1\perp}^H \mathbf{S}_{1+} \Gamma_1 b_1 = \mathbf{H}_{1\perp}^H \mathbf{H}_1 \mathbf{U}_1 \mathbf{A}_1 \Gamma_1 b_1 = \mathbf{0}$. Notice

that $\mathbf{H}_{1\perp}$, $\mathbf{S}_D$ and $\mathbf{F}_D$ have been used in place of $\mathbf{B}_1^H$, $\mathbf{E}_1$ and $\mathbf{F}_1$, respectively. Similarly the common term in (4.5) can be rewritten into the form of

$$(\mathbf{d}_1 - \boldsymbol{\Upsilon}^H_{\mathbf{y}_1\mathbf{d}_1}\mathbf{R}^{-1}_{\mathbf{y}_1}\mathbf{y}_1) = [\mathbf{H}_1^H - \mathbf{H}_1^H\mathbf{R}\mathbf{H}_{1\perp}(\mathbf{H}_{1\perp}^H\mathbf{R}^{-1}\mathbf{H}_{1\perp})^{-1}\mathbf{H}_{1\perp}^H]\mathbf{y}. \tag{B.5}$$

Using this equation and the definition of $\mathbf{S}_D$ in (4.10) for the evaluation of conditional auto-correlation matrix of the estimation error results in

$$\begin{aligned} &E[(\mathbf{d}_1 - \boldsymbol{\Upsilon}^H_{\mathbf{y}_1\mathbf{d}_1}\mathbf{R}^{-1}_{\mathbf{y}_1}\mathbf{y}_1)(\mathbf{d}_1 - \boldsymbol{\Upsilon}^H_{\mathbf{y}_1\mathbf{d}_1}\mathbf{R}^{-1}_{\mathbf{y}_1}\mathbf{y}_1)^H|\Gamma_1 b_1] \\ &= \mathbf{S}_D - \mathbf{U}_1\mathbf{A}_1^2\mathbf{U}_1^H + \mathbf{U}_1\mathbf{A}_1\Gamma_1\Gamma_1^H\mathbf{A}_1\mathbf{U}_1^H, \end{aligned} \tag{B.6}$$

where we have used the fact that $E(\mathbf{y}\mathbf{y}^H|\Gamma_1 b_1) = \mathbf{R} - \mathbf{S}_{1+}\mathbf{A}_1^2\mathbf{S}_{1+}^H + \mathbf{S}_{1+}\mathbf{A}_1\Gamma_1\Gamma_1^H\mathbf{A}_1\mathbf{S}_{1+}^H$. Multiplying the conditional auto-correlation matrix with the scaling matrices defined for (4.5) directly gives the conditional auto-correlation matrices for each filter bank's output as shown below

$$E(\psi^2_{mmse}|\Gamma_1 b_1) = \Gamma_1^H(\mathbf{M}_S - \mathbf{M}_S^2 + \mathbf{M}_S\Gamma_1\Gamma_1^H\mathbf{M}_S)\Gamma_1 \tag{B.7}$$

$$E(\psi^2_{moe}|\Gamma_1 b_1) = \Gamma_1^H(\mathbf{A}_1\mathbf{U}_1^H\mathbf{S}_D\mathbf{U}_1\mathbf{A}_1 - \mathbf{M}_I^2 + \mathbf{M}_I\Gamma_1\Gamma_1^H\mathbf{M}_I)\Gamma_1 \tag{B.8}$$

$$E(\psi^2_{blue}|\Gamma_1 b_1) = \Gamma_1^H(\mathbf{M}_S^{-1} - \mathbf{I} + \Gamma_1\Gamma_1^H)\Gamma_1 \tag{B.9}$$

$$E(\psi^2_{ml}|\Gamma_1 b_1) = \Gamma_1^H(\mathbf{M}_F + \mathbf{M}_F\Gamma_1\Gamma_1^H\mathbf{M}_F)\Gamma_1, \tag{B.10}$$

where we have defined $\mathbf{M}_S \equiv \mathbf{A}_1\mathbf{U}_1^H\mathbf{S}_D^{-1}\mathbf{U}_1\mathbf{A}_1$, $\mathbf{M}_F \equiv \mathbf{A}_1\mathbf{U}_1^H\mathbf{F}_D^{-1}\mathbf{U}_1\mathbf{A}_1$ and $\mathbf{M}_I \equiv \mathbf{A}_1\mathbf{U}_1^H\mathbf{U}_1\mathbf{A}_1$. The unconditional covariance matrices can be obtained by $Var(\psi|b_1) = E(\psi^2|b_1) - E^2(\psi|b_1)$. Applying (4.18) for computing the fourth moments of Γ_1 for (B.7) $\sim$ (B.10), the variances of the filter banks can be readily shown in the forms

$$\begin{aligned} Var(\psi_{mmse}|b_1) &= tr^2(\mathbf{M}_S) = tr^2(\mathbf{A}_1\mathbf{U}_1^H\mathbf{S}_D^{-1}\mathbf{U}_1\mathbf{A}_1) && \text{(B.11)} \\ Var(\psi_{moe}|b_1) &= tr(\mathbf{A}_1\mathbf{U}_1^H\mathbf{S}_D\mathbf{U}_1\mathbf{A}_1) && \text{(B.12)} \\ Var(\psi_{blue}|b_1) &= tr(\mathbf{M}_S^{-1}) = tr((\mathbf{U}_1\mathbf{A}_1)^{-1}\mathbf{S}_D(\mathbf{U}_1\mathbf{A}_1)^{-H}) && \text{(B.13)} \\ Var(\psi_{ml}|b_1) &= tr(\mathbf{M}_F + \mathbf{M}_F^2) \\ &= tr(\mathbf{A}_1\mathbf{U}_1^H\mathbf{F}_D^{-1}\mathbf{U}_1\mathbf{A}_1 + (\mathbf{A}_1\mathbf{U}_1^H\mathbf{F}_D^{-1}\mathbf{U}_1\mathbf{A}_1)^2). && \text{(B.14)} \end{aligned}$$

Dividing the trace squared of the mean of each filter bank by the corresponding trace of the covariance matrix yields the output SINR.

B.2 Proof of proposition 3

To characterize the performance differences, we introduce a lemma to assist with reducing complexities.

Lemma 1 *For a $N \times M$ matrix $\mathbf{G}$ and two positive diagonal matrices $\Lambda_1^{N\times N}$, $\Lambda_2^{N\times N}$ $> \mathbf{0}$,*

$$tr(\mathbf{G}^H\Lambda_1\mathbf{G})tr(\mathbf{G}^H\Lambda_2\mathbf{G}) \geq tr^2(\mathbf{G}^H\sqrt{\Lambda_1}\sqrt{\Lambda_2}\mathbf{G}). \qquad \text{(B.15)}$$

Proof: Let $\mathbf{G} = [\mathbf{g}_1, \mathbf{g}_2, \cdots \mathbf{g}_M]$ and $\Lambda_i = \text{diag}(\lambda_{i1}, \cdots, \lambda_{iN})$, $i = 1$ or 2, with $\mathbf{g}_i^{N\times 1} = [g_{1i}, \cdots, g_{Ni}]^T$. By the Cauchy inequality,

$$\begin{aligned} tr(\mathbf{G}^H\Lambda_1\mathbf{G})tr(\mathbf{G}^H\Lambda_2\mathbf{G}) &= [\sum_{i=1}^{M}(\lambda_{11}g_{1i}^2 + \cdots + \lambda_{1N}g_{Ni}^2)][\sum_{i=1}^{M}(\lambda_{21}g_{1i}^2 + \cdots + \lambda_{2N}g_{Ni}^2)] \\ &\geq [\sum_{i=1}^{M}(\sqrt{\lambda_{11}\lambda_{21}}g_{1i}^2) + \cdots + \sqrt{\lambda_{1N}\lambda_{2N}}g_{Ni}^2)]^2 \\ &= tr^2(\mathbf{G}^H\sqrt{\Lambda_1}\sqrt{\Lambda_2}\mathbf{G}). \end{aligned} \tag{B.16}$$

The equality holds if $\Lambda_1 = \kappa\Lambda_2, \quad \kappa > 0$. ■

Now, we directly apply this lemma for the proof of Proposition 3.

Proof: The upper bound for the MMSE-based filter banks has already been established in (4.30). Now we investigate the performance differences between the reduced-rank MMSE filter bank and the reduced-rank MOE/BLUE/ML filter banks.

1. Performing eigenvalue decomposition for $\mathbf{S}_D = \mathbf{Q}_S\Lambda_S\mathbf{Q}_S^H$, $\mathbf{S}_D > \mathbf{0}$, yields

$$tr(\mathbf{A}_1\mathbf{U}_1^H\mathbf{S}_D\mathbf{U}_1\mathbf{A}_1) = tr(\mathbf{A}_1\mathbf{U}_1^H\mathbf{Q}_S\Lambda_S\mathbf{Q}_S^H\mathbf{U}_1\mathbf{A}_1). \tag{B.17}$$

Let $\mathbf{G}^H \equiv \mathbf{A}_1\mathbf{U}_1^H\mathbf{Q}_S$. Using Lemma 1, we obtain

$$\begin{aligned} &tr(\mathbf{A}_1\mathbf{U}_1^H\mathbf{Q}_S\Lambda_S^{-1}\mathbf{Q}_S^H\mathbf{U}_1\mathbf{A}_1)tr(\mathbf{A}_1\mathbf{U}_1^H\mathbf{Q}_S\Lambda_S\mathbf{Q}_S^H\mathbf{U}_1\mathbf{A}_1) \\ &= tr(\mathbf{G}^H\Lambda_S^{-1}\mathbf{G})tr(\mathbf{G}^H\Lambda_S\mathbf{G}) \\ &\geq tr^2(\mathbf{G}^H\mathbf{G}) = tr^2(\mathbf{A}_1\mathbf{U}_1^H\mathbf{U}_1\mathbf{A}_1). \end{aligned} \tag{B.18}$$

Dividing both sides by $tr(\mathbf{A}_1\mathbf{U}_1^H\mathbf{Q}_S\Lambda_S\mathbf{Q}_S^H\mathbf{U}_1\mathbf{A}_1)$ yields

$$\begin{aligned} tr(\mathbf{A}_1\mathbf{U}_1^H\mathbf{S}_D^{-1}\mathbf{U}_1\mathbf{A}_1) &\geq \frac{tr^2(\mathbf{A}_1\mathbf{U}_1^H\mathbf{U}_1\mathbf{A}_1)}{tr(\mathbf{A}_1\mathbf{U}_1^H\mathbf{S}_D\mathbf{U}_1\mathbf{A}_1)} \\ \Longrightarrow \quad SINR_{mmse} &\geq SINR_{moe}. \end{aligned} \tag{B.19}$$

The equality holds if $\Lambda_S = \kappa^2\Lambda_S^{-1},\ \kappa > 0$. Then $\Lambda_S = \kappa\mathbf{I}$, *i.e.* $\mathbf{S}_D = \kappa\mathbf{I}$, since $\Lambda_S > \mathbf{0}$. To satisfy the upper bound, $tr(\mathbf{A}_1\mathbf{U}_1^H\mathbf{U}_1\mathbf{A}_1) = tr(\mathbf{U}_1\mathbf{A}_1^2\mathbf{U}_1^H) \leq \kappa L$.

2. Performing eigenvalue decomposition for the kernel matrix of $SINR_{mmse}$ yields

$$\mathbf{A}_1\mathbf{U}_1^H\mathbf{S}_D^{-1}\mathbf{U}_1\mathbf{A}_1 = \mathbf{Q}\Lambda\mathbf{Q}^H. \tag{B.20}$$

Then $tr((\mathbf{U}_1\mathbf{A}_1)^{-1}\mathbf{S}_D(\mathbf{U}_1\mathbf{A}_1)^{-H}) = tr(\mathbf{Q}\Lambda^{-1}\mathbf{Q}^H)$. By Lemma 1,

$$tr(\mathbf{Q}\Lambda\mathbf{Q}^H)tr(\mathbf{Q}\Lambda^{-1}\mathbf{Q}^H) \geq tr^2(\mathbf{Q}\Lambda^{1/2}\Lambda^{-1/2}\mathbf{Q}^H) = tr^2(\mathbf{I}) = L^2. \tag{B.21}$$

Dividing both sides by $tr(\mathbf{Q}\Lambda^{-1}\mathbf{Q}^H)$ establishes the following inequality:

$$\begin{aligned} tr(\mathbf{A}_1\mathbf{U}_1^H\mathbf{S}_D^{-1}\mathbf{U}_1\mathbf{A}_1) &\geq \frac{L^2}{tr((\mathbf{U}_1\mathbf{A}_1)^{-1}\mathbf{S}_D(\mathbf{U}_1\mathbf{A}_1)^{-H})} \\ \Longrightarrow \quad SINR_{mmse} &\geq SINR_{blue}. \end{aligned} \tag{B.22}$$

The equality holds if $\Lambda = \kappa^2\Lambda^{-1},\ \kappa > 0$. Then $\Lambda = \kappa\mathbf{I}$, *i.e.* $\mathbf{A}_1\mathbf{U}_1^H\mathbf{S}_D^{-1}\mathbf{U}_1\mathbf{A}_1 = \kappa\mathbf{I}$. To satisfy the upper bound, $0 \leq \kappa \leq 1$.

3. Let $(\mathbf{U}_1\mathbf{A}_1)^{-1}\mathbf{F}_D(\mathbf{U}_1\mathbf{A}_1)^{-H} \equiv \mathbf{Q}\Lambda_F^{-1}\mathbf{Q}^H$. From (4.11), it is clear that

$$\begin{aligned}
(\mathbf{U}_1\mathbf{A}_1)^{-1}\mathbf{F}_D(\mathbf{U}_1\mathbf{A}_1)^{-H} &= (\mathbf{U}_1\mathbf{A}_1)^{-1}\mathbf{S}_D(\mathbf{U}_1\mathbf{A}_1)^{-H} - \mathbf{I} = \mathbf{Q}(\Lambda^{-1} - \mathbf{I})\mathbf{Q}^H \\
\Lambda_F^{-1} &= \Lambda^{-1} - \mathbf{I} \qquad \text{(B.23)} \\
\Lambda &= \Lambda_F(\Lambda_F + \mathbf{I})^{-1} \qquad \text{(B.24)} \\
\mathbf{A}_1\mathbf{U}_1^H\mathbf{S}_D^{-1}\mathbf{U}_1\mathbf{A}_1 &= (\mathbf{A}_1\mathbf{U}_1^H\mathbf{F}_D^{-1}\mathbf{U}_1\mathbf{A}_1)(\mathbf{A}_1\mathbf{U}_1^H\mathbf{F}_D^{-1}\mathbf{U}_1\mathbf{A}_1 + \mathbf{I})^{-1}. \qquad \text{(B.25)}
\end{aligned}$$

Now the output SINRs of the MMSE and MOE filter banks can be readily expressed in terms of Λ_F as follows

$$\begin{aligned}
SINR_{mmse} &= tr(\Lambda_F(\Lambda_F + \mathbf{I})^{-1}) \qquad \text{(B.26)} \\
SINR_{ml} &= \frac{tr^2(\Lambda_F)}{tr(\Lambda_F) + tr(\Lambda_F^2)}. \qquad \text{(B.27)}
\end{aligned}$$

Let $\Lambda_F = \text{diag}(\lambda_{f_1}, \lambda_{f_2}, \cdots, \lambda_{f_L})$. Subtracting $SINR_{ml}$ from $SINR_{mmse}$, the numerator becomes

$$\left[\sum_{i=1}^{L}\lambda_{f_i}\left(\prod_{j=1,j\neq i}^{L}(1+\lambda_{f_j})\right)\right]\left[\sum_{i=1}^{L}\lambda_{f_i}(\lambda_{f_i}+1)\right] - \left(\sum_{i=1}^{L}\lambda_{f_i}\right)^2\prod_{j=1}^{L}(1+\lambda_{f_j}). \qquad \text{(B.28)}$$

By induction, it can be shown that

$$\begin{aligned}
&SINR_{mmse} - SINR_{ml} = \\
&\frac{\sum_{i=1}^{L-1}\sum_{j=i+1}^{L}\lambda_{f_i}\lambda_{f_j}\left(\prod_{l=1,l\neq i,j}^{L}(\lambda_{f_l}+1)\right)(\lambda_{f_i}-\lambda_{f_j})^2}{\left(\prod_{j=1}^{L}(\lambda_{f_j}+1)\right)\sum_{i=1}^{L}\lambda_{f_i}(\lambda_{f_i}+1)} \geq 0. \qquad \text{(B.29)}
\end{aligned}$$

This follows since $\Lambda_F \geq 0$. The equality holds if and only if $\Lambda_F = \kappa\mathbf{I},\ \kappa > 0$. By (B.24), $\Lambda = \frac{\kappa}{\kappa+1}\mathbf{I} = \mathbf{A}_1\mathbf{U}_1^H\mathbf{S}_D^{-1}\mathbf{U}_1\mathbf{A}_1$, $0 \leq \frac{\kappa}{\kappa+1} \leq 1$.

4. From 2 and 3, if $\Lambda = \kappa\mathbf{I}, 0 \leq \kappa \leq 1$, then $SINR_{mmse} = SINR_{blue} = SINR_{ml}$. From 1, if $\mathbf{S}_D = \kappa_1\mathbf{I}, \kappa_1 \geq \frac{1}{L}tr(\mathbf{U}_1\mathbf{A}_1^2\mathbf{U}_1^H)$, then $SINR_{mmse} = SINR_{moe}$. Let $\mathbf{A}_1\mathbf{U}_1^H\mathbf{S}_D^{-1}\mathbf{U}_1\mathbf{A}_1 = \frac{1}{\kappa_1}\mathbf{A}_1\mathbf{U}_1^H\mathbf{U}_1\mathbf{A}_1 = \kappa\mathbf{I}$, *i.e.* $\mathbf{A}_1\mathbf{U}_1^H\mathbf{U}_1\mathbf{A}_1 = \kappa\kappa_1\mathbf{I} \equiv \kappa_2\mathbf{I}, \kappa_2 \geq 0$, we have the equality $SINR_{mmse} = SINR_{moe} = SINR_{blue} = SINR_{ml}$. Combining the above conditions, the equality holds if $\mathbf{A}_1\mathbf{U}_1^H\mathbf{U}_1\mathbf{A}_1 = \kappa_2\mathbf{I}, \kappa_2 \geq 0$ and $\mathbf{S}_D = \kappa_1\mathbf{I}, \kappa_1 \geq \kappa_2$.

■

B.3 Proof of Theorem 1

To prove the theorem, we need to explore the recursive structure of $\mathbf{E}_i$ in (4.40). For simplicity, we use $\mathbf{A} > \mathbf{0}$ to denote that $\mathbf{A}$ is positive definite (*p.d.*), and use $\mathbf{A}^{M\times M} > \mathbf{B}^{M\times M}$ to denote that for each eigen-pair of Hermitian matrices $\mathbf{A}$ and $\mathbf{B}$, $\lambda_i(\mathbf{A}) > \lambda_i(\mathbf{B}), i = 1\cdots M$. Since $\mathbf{E}_i$ is an error correlation matrix, $\mathbf{E}_i > \mathbf{0}$. Assume the filter's stage is increased from D-1 to D. First, we need to show $\mathbf{U}_{D-1}^H(\mathbf{R}_{d_{D-1}} - \mathbf{U}_D^H\mathbf{R}_{d_D}^{-1}\mathbf{U}_D)^{-1}\mathbf{U}_{D-1} > \mathbf{U}_{D-1}^H\mathbf{R}_{d_{D-1}}^{-1}\mathbf{U}_{D-1}$.

Let $\mathbf{B} \equiv \mathbf{U}_D^H\mathbf{R}_{d_D}^{-1}\mathbf{U}_D$. By matrix inversion lemma,

$$\begin{aligned}(\mathbf{R}_{d_{D-1}} - \mathbf{U}_D^H\mathbf{R}_{d_D}^{-1}\mathbf{U}_D)^{-1} &= \mathbf{R}_{d_{D-1}}^{-1} + \mathbf{R}_{d_{D-1}}^{-1}\mathbf{B}\mathbf{R}_{d_{D-1}}^{-1} + \mathbf{R}_{d_{D-1}}^{-1}\mathbf{B}\mathbf{R}_{d_{D-1}}^{-1}\mathbf{B}\mathbf{R}_{d_{D-1}}^{-1} + \cdots \\ &= \mathbf{R}_{d_{D-1}}^{-1} + \triangle. \end{aligned} \tag{B.30}$$

$\mathbf{B}$ is the congruence transformation of $\mathbf{R}_{d_D}^{-1}$. Since $\mathbf{R}_{d_D} > \mathbf{0}$ and $\mathbf{U}_D$ is non-singular, by Sylvester's *law of inertia*, (see [23]), $\mathbf{B} > \mathbf{0}$. Similarly, $\mathbf{R}_{d_{D-1}}^{-1}$ is non-singular, thus $\mathbf{R}_{d_{D-1}}^{-1}\mathbf{B}\mathbf{R}_{d_{D-1}}^{-1} > \mathbf{0}$. Continuing the same procedure, we have every term on the right hand side being *p.d.*. Now, recall the minimax principle, (see [23]). If matrix $\mathbf{G} > \mathbf{0}$, for any Hermitian matrix $\mathbf{A}$, $\mathbf{A} + \mathbf{G} > \mathbf{A}$. Staring from the second term of (B.30) and recursively applying the minimax principle, we immediately have $\triangle > \mathbf{R}_{d_{D-1}}^{-1}\mathbf{B}\mathbf{R}_{d_{D-1}}^{-1} > \mathbf{0}$. Thus, $\mathbf{U}_{D-1}^H[(\mathbf{R}_{d_{D-1}} - \mathbf{U}_D^H\mathbf{R}_{d_D}^{-1}\mathbf{U}_D)^{-1} - \mathbf{R}_{d_{D-1}}^{-1}]\mathbf{U}_{D-1} > \mathbf{0}$. Similarly, having $\mathbf{A} = \mathbf{U}_{D-1}^H\mathbf{R}_{d_{D-1}}^{-1}\mathbf{U}_{D-1}$ and $\mathbf{G} = \mathbf{U}_{D-1}^H[(\mathbf{R}_{d_{D-1}} - \mathbf{U}_D^H\mathbf{R}_{d_D}^{-1}\mathbf{U}_D)^{-1} - \mathbf{R}_{d_{D-1}}^{-1}]\mathbf{U}_{D-1}$, yields $\mathbf{U}_{D-1}^H(\mathbf{R}_{d_{D-1}} - \mathbf{U}_D^H\mathbf{R}_{d_D}^{-1}\mathbf{U}_D)^{-1}\mathbf{U}_{D-1} > \mathbf{U}_{D-1}^H\mathbf{R}_{d_{D-1}}^{-1}\mathbf{U}_{D-1}$. Let $\mathbf{E}_i^D$ denote $\mathbf{E}_i$ of the D-stage MMSE filter bank. Then we have $\mathbf{U}_{D-1}^H(\mathbf{E}_{D-1}^D)^{-1}\mathbf{U}_{D-1} > \mathbf{U}_{D-1}^H(\mathbf{E}_{D-1}^{D-1})^{-1}\mathbf{U}_{D-1}$ by adding the Dth stage.

Secondly, we need to show that $\mathbf{U}_i^H(\mathbf{E}_i^D)^{-1}\mathbf{U}_i > \mathbf{U}_i^H(\mathbf{E}_i^{D-1})^{-1}\mathbf{U}_i,\ i = 1, \cdots, D-2$, given that $\mathbf{U}_{i+1}^H(\mathbf{E}_{i+1}^D)^{-1}\mathbf{U}_{i+1} > \mathbf{U}_{i+1}^H(\mathbf{E}_{i+1}^{D-1})^{-1}\mathbf{U}_{i+1})$. Recall the recursive structure of $\mathbf{E}_i$ in (4.40). Let $\mathbf{E}_i^D = [\mathbf{R}_{d_i} - \mathbf{U}_{i+1}^H(\mathbf{E}_{i+1}^{D-1})^{-1}\mathbf{U}_{i+1} - \mathbf{B}]$, $\mathbf{B} \equiv \mathbf{U}_{i+1}^H(\mathbf{E}_{i+1}^D)^{-1}\mathbf{U}_{i+1} - \mathbf{U}_{i+1}^H(\mathbf{E}_{i+1}^{D-1})^{-1}\mathbf{U}_{i+1}$, and $\mathbf{E}_i^{D-1} = [\mathbf{R}_{d_i} - \mathbf{U}_{i+1}^H(\mathbf{E}_{i+1}^{D-1})^{-1}\mathbf{U}_{i+1}]$. By matrix inversion lemma,

$$\begin{aligned}(\mathbf{E}_i^D)^{-1} &= (\mathbf{E}_i^{D-1})^{-1} + (\mathbf{E}_i^{D-1})^{-1}\mathbf{B}(\mathbf{E}_i^{D-1})^{-1} + (\mathbf{E}_i^{D-1})^{-1}\mathbf{B}(\mathbf{E}_i^{D-1})^{-1}\mathbf{B}(\mathbf{E}_i^{D-1})^{-1}\cdots \\ &\equiv (\mathbf{E}_i^{D-1})^{-1} + \triangle. \end{aligned} \tag{B.31}$$

Given that $\mathbf{U}_{i+1}^H(\mathbf{E}_{i+1}^D)^{-1}\mathbf{U}_{i+1} > \mathbf{U}_{i+1}^H(\mathbf{E}_{i+1}^{D-1})^{-1}\mathbf{U}_{i+1}$, by the minimax principle, $B > \mathbf{0}$. Since $\mathbf{E}_i^{D-1} > \mathbf{0}$, following the same procedure for (B.30), we have $\triangle > \mathbf{0}$, and thus, $\mathbf{U}_i^H(\mathbf{E}_i^D)^{-1}\mathbf{U}_i > \mathbf{U}_i^H(\mathbf{E}_i^{D-1})^{-1}\mathbf{U}_i$.

Now, starting from the bottom stage, $\mathbf{U}_{D-1}^H(\mathbf{E}_{D-1}^D)^{-1}\mathbf{U}_{D-1} > \mathbf{U}_{D-1}^H(\mathbf{E}_{D-1}^{D-1})^{-1}\mathbf{U}_{D-1}$ results in $\mathbf{U}_{D-2}^H(\mathbf{E}_{D-2}^D)^{-1}\mathbf{U}_{D-2} > \mathbf{U}_{D-2}^H(\mathbf{E}_{D-2}^{D-1})^{-1}\mathbf{U}_{D-2}$, which in terms leaves

$$\mathbf{U}_{D-3}^H(\mathbf{E}_{D-3}^D)^{-1}\mathbf{U}_{D-3} > \mathbf{U}_{D-3}^H(\mathbf{E}_{D-3}^{D-1})^{-1}\mathbf{U}_{D-3}, \cdots.$$

Eventually we have $\mathbf{U}_1^H(\mathbf{E}_1^D)^{-1}\mathbf{U}_1 > \mathbf{U}_1^H(\mathbf{E}_1^{D-1})^{-1}\mathbf{U}_1$. Notice that $\mathbf{E}_1^D$ and $\mathbf{E}_1^{D-1}$ is are another names of $\mathbf{S}_D$ and $\mathbf{S}_{D-1}$, respectively. Thus, $\mathbf{A}_1\mathbf{U}_1^H\mathbf{S}_D^{-1}\mathbf{U}_1\mathbf{A}_1 > \mathbf{A}_1\mathbf{U}_1^H\mathbf{S}_{D-1}^{-1}\mathbf{U}_1\mathbf{A}_1$. This is the proof.

B.4 Derivation of Table 4.1

It is clear from (4.1) $\sim$ (4.4) that the simplifications of $\mathbf{E}_S$ and $\mathbf{E}_O$ tide to that of $\mathbf{R}_T^{-1}$, $\mathbf{C}_T^{-1}$ and $\mathbf{S}_T$. Consider reduced-rank implementations of D stages. By Matrix Inversion Lemma [14], we have

$$(\mathbf{TRT}^H)^{-1} = \left[\begin{array}{c|c} \mathbf{S}_D^{-1} & \triangle \\ \hline \triangle & \triangle \end{array}\right], \quad (\mathbf{TCT}^H)^{-1} = \left[\begin{array}{c|c} \mathbf{F}_D^{-1} & \triangle \\ \hline \triangle & \triangle \end{array}\right], \tag{B.32}$$

and by construction $\mathbf{S}_T = \left[\begin{array}{c} \mathbf{H}_1^H \\ \hline \mathbf{H}_{1\perp}^H \end{array}\right] \mathbf{H}_1\mathbf{U}_1 = \left[\begin{array}{c} \mathbf{I} \\ \hline \mathbf{0} \end{array}\right] \mathbf{U}_1$. Applying the above equations to the simplifications of $\mathbf{E}_S^{\frac{1}{2}} \equiv \omega^H\mathbf{T}\mathbf{S}_{1+}\mathbf{A}_1$ and $\mathbf{E}_O \equiv \omega\mathbf{T}\mathbf{R}\mathbf{T}^H\omega$ for each type of filter bank gives the following results.

MMSE: $\mathbf{E}_S = (\mathbf{A}_1\mathbf{U}_1^H\mathbf{S}_D^{-1}\mathbf{U}_1\mathbf{A}_1)^2$, $\mathbf{E}_O = \mathbf{A}_1\mathbf{U}_1^H\mathbf{S}_D^{-1}\mathbf{U}_1\mathbf{A}_1$

MOE: $\mathbf{E}_S = (\mathbf{A}_1\mathbf{U}_1^H\mathbf{U}_1\mathbf{A}_1)^2$, $\mathbf{E}_O = \mathbf{A}_1\mathbf{U}_1^H\mathbf{S}_D\mathbf{U}_1\mathbf{A}_1$

BLUE: $\mathbf{E}_S = \mathbf{I}$, $\mathbf{E}_O = (\mathbf{A}_1\mathbf{U}_1^H\mathbf{S}_D^{-1}\mathbf{U}_1\mathbf{A}_1)^{-1}$

ML: $\mathbf{E}_S = (\mathbf{A}_1\mathbf{U}_1^H\mathbf{F}_D^{-1}\mathbf{U}_1\mathbf{A}_1)^2$, $\mathbf{E}_O = \mathbf{A}_1\mathbf{U}_1^H\mathbf{F}_D^{-1}\mathbf{U}_1\mathbf{A}_1 + (\mathbf{A}_1\mathbf{U}_1^H\mathbf{F}_D^{-1}\mathbf{U}_1\mathbf{A}_1)^2$.

Substituting these terms back into (4.57) for each filter bank automatically gives the results of $M(s)^{-1}$ in Table 4.1.

B.5 Derivation of (4.58)

Define $\mathbf{R}_1 \equiv E[\mathbf{y}(m)\mathbf{y}(m-1)^H | b_1(m) = b_1(m-1)]$. It is equal to

$$\mathbf{R}_1 = \rho\mathbf{S}_{1+}\mathbf{A}_1^2\mathbf{S}_{1+}^H + \rho\sum_{k=1}^{K}\mathbf{S}_{k-}\mathbf{A}_k^2\mathbf{S}_{k+}^H. \tag{B.33}$$

Since $\mathbf{x} = \left[\mathbf{z}(m)^H\ \mathbf{z}(m-1)^H\right]^H$ and $\mathbf{z}(m) = \omega^H\mathbf{T}\mathbf{y}(m)$,

$$\Phi = E(\mathbf{x}\mathbf{x}^H) = \left[\begin{array}{c|c} \omega^H\mathbf{T}\mathbf{R}\mathbf{T}^H\omega & \omega^H\mathbf{T}\mathbf{R}_1\mathbf{T}^H\omega \\ \hline \omega^H\mathbf{T}\mathbf{R}_1^H\mathbf{T}^H\omega & \omega^H\mathbf{T}\mathbf{R}\mathbf{T}^H\omega \end{array}\right]. \tag{B.34}$$

Substituting Φ into (4.45) gives

$$det[\mathbf{I} + s\mathbf{J}\Phi] = det \left[\begin{array}{c|c} \mathbf{I} + \frac{s}{2}\omega^H \mathbf{T}\mathbf{R}_1^H \mathbf{T}^H \omega & \frac{s}{2}\omega^H \mathbf{T}\mathbf{R}\mathbf{T}^H \omega \\ \hline \frac{s}{2}\omega^H \mathbf{T}\mathbf{R}\mathbf{T}^H \omega & \mathbf{I} + \frac{s}{2}\omega^H \mathbf{T}\mathbf{R}_1 \mathbf{T}^H \omega \end{array} \right]. \tag{B.35}$$

Ignoring the effect of ISI in $\mathbf{R}_1$, which is the second terms in (B.33), leads to $\mathbf{R}_1 = \rho\mathbf{R}_S$. Since $\mathbf{R}_S$ is Hermitian, the matrix of (B.35) becomes Hermitian too. Let $\mathbf{A_{11}} = \mathbf{A_{22}} = \mathbf{A}$ and $\mathbf{B_{12}} = \mathbf{B_{21}} = \mathbf{B}$ in (4.52), it is straightforward to show that

$$det \begin{bmatrix} \mathbf{A} & \mathbf{B} \\ \mathbf{B} & \mathbf{A} \end{bmatrix} = det(\mathbf{A} - \mathbf{B}) det(\mathbf{A} + \mathbf{B}). \tag{B.36}$$

Applying this formula to (B.35) yields

$$det[\mathbf{I} + s\mathbf{J}\Phi] = det[\mathbf{I} - \frac{s}{2}(\mathbf{E}_O - \rho\mathbf{E}_S)] det[\mathbf{I} + \frac{s}{2}(\mathbf{E}_O + \rho\mathbf{E}_S)], \tag{B.37}$$

where $\mathbf{E}_S \equiv \omega^H \mathbf{T}\mathbf{R}_S \mathbf{T}^H \omega$ and $\mathbf{E}_O \equiv \omega^H \mathbf{T}\mathbf{R}\mathbf{T}^H \omega$. Substituting the results of $\mathbf{E}_S$ and $\mathbf{E}_O$ obtained in Appendix C for each receiver gives Table 4.2 of $M(s)^{-1}$.

B.6 Derivations for EGC BLUE-MMSE and BLUE-ML filter banks

For heterogeneous combining schemes, vector $\mathbf{x}^H = [\mathbf{z}_1^H(m) \;\; \mathbf{z}_2^H(m-1)]$. Ignoring ISI

$$\Phi = \left[\begin{array}{c|c} \omega_1^H \mathbf{T}\mathbf{R}\mathbf{T}^H\omega_1 & \rho\omega_1^H \mathbf{T}\mathbf{R}_S\mathbf{T}^H\omega_2 \\ \hline \rho\omega_2^H \mathbf{T}\mathbf{R}_S^H\mathbf{T}^H\omega_1 & \omega_2^H \mathbf{T}\mathbf{R}\mathbf{T}^H\omega_2 \end{array}\right]. \tag{B.38}$$

Directly applying this equation to EGC MMSE-BLUE and ML-BLUE schemes allows us to perform BER analysis for each combining scheme. Before getting into the detail derivations, we define $\mathbf{E}_{S_i}^{\frac{1}{2}} = \omega_i^H \mathbf{T}\mathbf{S}_{1+}\mathbf{A}_1$ and $\mathbf{E}_{O_i} = \omega_i^H \mathbf{T}\mathbf{R}\mathbf{T}^H\omega_i$, $i = 1, 2$. From Appendix C we know that these terms are both Hermitian. So we also redefine $\mathbf{E}_S = \mathbf{E}_{S_1}^{\frac{1}{2}}\mathbf{E}_{S_2}^{\frac{1}{2}}$ and $\mathbf{E}_O = \mathbf{E}_{O_1}^{\frac{1}{2}}\mathbf{E}_{O_2}^{\frac{1}{2}}$ for heterogeneous combining since the contributions now come from two different filters.

- BER for reduced-rank EGC BLUE-MMSE filter banks

In this case, vector $\mathbf{x}^H = [\mathbf{z}_{mmse}^H(m) \;\; \mathbf{z}_{blue}^H(m-1)]$. With the same procedure given in Appendix C, it is not difficult to show that

$$\mathbf{E}_{S_1}^{\frac{1}{2}}\mathbf{E}_{S_2}^{\frac{1}{2}} = \omega_1^H \mathbf{T}\mathbf{R}_S\mathbf{T}^H\omega_2 = \omega_2^H \mathbf{T}\mathbf{R}_S\mathbf{T}^H\omega_1 = \mathbf{A}_1\mathbf{U}_1^H\mathbf{S}_D^{-1}\mathbf{U}_1\mathbf{A}_1 = \mathbf{E}_S \tag{B.39}$$

$$\mathbf{E}_{O_1} = \omega_1^H \mathbf{T}\mathbf{R}\mathbf{T}^H\omega_1 = \mathbf{E}_S \tag{B.40}$$

$$\mathbf{E}_{O_2} = \omega_2^H \mathbf{T}\mathbf{R}\mathbf{T}^H\omega_2 = \mathbf{E_S}^{-1}. \tag{B.41}$$

Thus

$$det(\mathbf{I}+s\mathbf{J}\Phi) \;=\; \left[\begin{array}{c|c} \mathbf{I}+\frac{s}{2}\rho\mathbf{E_S} & \frac{s}{2}\mathbf{E}_{O_2} \\ \hline \frac{s}{2}\mathbf{E}_{O_1} & \mathbf{I}+\frac{s}{2}\rho\mathbf{E_S} \end{array}\right]. \tag{B.42}$$

Let $\mathbf{A}=\mathbf{I}+\frac{s}{2}\rho\mathbf{E_S}$. Applying the lemma of (4.52) gives

$$det[\mathbf{I}+s\mathbf{J}\Phi] = det(\mathbf{A}^2-\frac{s^2}{4}\mathbf{A}\mathbf{E}_{O_1}\mathbf{A}^{-1}\mathbf{E}_{O_2}). \tag{B.43}$$

Since $\mathbf{A}\mathbf{E}_{O_1}=\mathbf{E}_{O_1}\mathbf{A}$ and $\mathbf{E}_{O_1}\mathbf{E}_{O_2}=\mathbf{I}$, it follows

$$\begin{aligned} det[\mathbf{I}+s\mathbf{J}\Phi] &= det(\mathbf{A}^2-\frac{s^2}{4}\mathbf{I}) = det(\mathbf{A}-\frac{s}{2}\mathbf{E}_{O_1}^{\frac{1}{2}}\mathbf{E}_{O_2}^{\frac{1}{2}})det(\mathbf{A}+\frac{s}{2}\mathbf{E}_{O_1}^{\frac{1}{2}}\mathbf{E}_{O_2}^{\frac{1}{2}}) \\ &= det[\mathbf{I}-\frac{s}{2}(\mathbf{E}_O-\rho\mathbf{E}_S)]det[\mathbf{I}+\frac{s}{2}(\mathbf{E}_O+\rho\mathbf{E}_S)] \\ &= det[\mathbf{I}-\frac{s}{2}(\mathbf{I}-\rho\Lambda)]det[\mathbf{I}+\frac{s}{2}(\mathbf{I}+\rho\Lambda)], \end{aligned} \tag{B.44}$$

where $\mathbf{E}_S=\mathbf{A}_1\mathbf{U}_1^H\mathbf{S}_D^{-1}\mathbf{U}_1\mathbf{A}_1=\mathbf{Q}\Lambda\mathbf{Q}^H$.

- BER for reduced-rank EGC BLUE-ML filter banks

In this case, vector $\mathbf{x}^H=[\mathbf{z}_{ml}^H(m)\;\;\mathbf{z}_{blue}^H(m-1)]$. Similarly we obtain

$$\mathbf{E}_{S_1}^{\frac{1}{2}}\mathbf{E}_{S_2}^{\frac{1}{2}}=\omega_1^H\mathbf{T}\mathbf{R}_S\mathbf{T}^H\omega_2 \;=\; \omega_2^H\mathbf{T}\mathbf{R}_S\mathbf{T}^H\omega_1=\mathbf{A}_1\mathbf{U}_1^H\mathbf{F}_D^{-1}\mathbf{U}_1\mathbf{A}_1=\mathbf{E}_S \tag{B.45}$$

$$\begin{aligned} \mathbf{E}_{O_1}=\omega_1^H\mathbf{T}\mathbf{R}\mathbf{T}^H\omega_1 &= \mathbf{A}_1\mathbf{U}_1^H\mathbf{F}_D^{-1}\mathbf{U}_1\mathbf{A}_1+(\mathbf{A}_1\mathbf{U}_1^H\mathbf{F}_D^{-1}\mathbf{U}_1\mathbf{A}_1)^2 \\ &= \mathbf{Q}[\Lambda_F^2(\Lambda_F^{-1}+\mathbf{I})]\mathbf{Q}^H \end{aligned} \tag{B.46}$$

$$\mathbf{E}_{O_2} = \omega_2^H \mathbf{T}\mathbf{R}\mathbf{T}^H \omega_2 = (\mathbf{A}_1\mathbf{U}_1^H\mathbf{S}_D^{-1}\mathbf{U}_1\mathbf{A}_1)^{-1} = (\mathbf{A}_1\mathbf{U}_1^H\mathbf{F}_D^{-1}\mathbf{U}_1\mathbf{A}_1)^{-1} + \mathbf{I}$$
$$= \mathbf{Q}(\Lambda_F^{-1} + \mathbf{I})\mathbf{Q}^H, \tag{B.47}$$

where $\mathbf{E}_S = \mathbf{A}_1\mathbf{U}_1^H\mathbf{F}_D^{-1}\mathbf{U}_1\mathbf{A}_1 = \mathbf{Q}\Lambda_F\mathbf{Q}^H$. Therefore, $\mathbf{E}_O = \mathbf{E}_{O_1}^{\frac{1}{2}}\mathbf{E}_{O_2}^{\frac{1}{2}} = \mathbf{Q}(\mathbf{I} + \Lambda_F)\mathbf{Q}^H = (\mathbf{I} + \mathbf{A}_1\mathbf{U}_1^H\mathbf{F}_D^{-1}\mathbf{U}_1\mathbf{A}_1)$, and thus $\mathbf{E}_{O_1} = \mathbf{E}_S\mathbf{E}_O$ and $\mathbf{E}_{O_2} = \mathbf{E}_S^{-1}\mathbf{E}_O$. Then,

$$det(\mathbf{I} + s\mathbf{J}\Phi) = \left[\begin{array}{c|c} \mathbf{I} + \frac{s}{2}\rho\mathbf{E}_S & \frac{s}{2}\mathbf{E}_S^{-1}\mathbf{E}_O \\ \hline \frac{s}{2}\mathbf{E}_S\mathbf{E}_O & \mathbf{I} + \frac{s}{2}\rho\mathbf{E}_S \end{array}\right]. \tag{B.48}$$

Let $\mathbf{A} = \mathbf{I} + \frac{s}{2}\rho\mathbf{E}_S$ and $\mathbf{B} = \mathbf{E}_S^{-1}\mathbf{E}_O$. Again, using (4.52) followed by some mathematical manipulations, we obtain

$$det[\mathbf{I} + s\mathbf{J}\Phi] = det(\mathbf{A}^2)det(\mathbf{E}_S^2)det(\mathbf{E}_S^{-2} - \frac{s^2}{4}\mathbf{B}\mathbf{A}^{-1}\mathbf{B}\mathbf{A}^{-1}). \tag{B.49}$$

Notice that $\mathbf{E}_S$ and $\mathbf{E}_O$ share common eigenvectors, so do the $\mathbf{A}$ and $\mathbf{B}$. Therefore $\mathbf{E}_S^{-1}\mathbf{B}\mathbf{A}^{-1} = \mathbf{B}\mathbf{A}^{-1}\mathbf{E}_S^{-1}$, since all matrices involved have common eigenvectors [23]. With this property, we have

$$\begin{aligned} det[\mathbf{I} + s\mathbf{J}\Phi] &= det(\mathbf{A} - \frac{s}{2}\mathbf{E}_S\mathbf{B})det(\mathbf{A} + \frac{s}{2}\mathbf{E}_S\mathbf{B}) \\ &= det[\mathbf{I} - \frac{s}{2}(\mathbf{E}_O - \rho\mathbf{E}_S)]det[\mathbf{I} + \frac{s}{2}(\mathbf{E}_O + \rho\mathbf{E}_S)] \\ &= det[\mathbf{I} - \frac{s}{2}(\mathbf{I} + \Lambda_F - \rho\Lambda_F)]det[\mathbf{I} + \frac{s}{2}(\mathbf{I} + \Lambda_F + \rho\Lambda_F)]. \end{aligned} \tag{B.50}$$